

A COMPARATIVE ANALYSIS OF LANDSLIDE MAPPING TECHNIQUES USING EARTH OBSERVATION (EO) DATA



by

Lilian Akudo Akanazu

Under the supervision of

Dr. Stephen Grebby and
Dr. Alessandro Novellino (BGS)

Submitted in Partial Fulfilment of the Requirements for the Degree of Master of
Research

in

Geospatial Data Science

in the

Faculty of Engineering
University of Nottingham

6 January 2025

Declaration of Authorship

I hereby certify that this work is my own, except where otherwise stated, and that it has not been submitted previously for any degree at this, or any other University.

Signed: 
Lilian Akudo Akanazu

Acknowledgements

I would like to express my gratitude to my supervisors, Dr. Stephen Grebby and Dr. Alessandro Novellino for their invaluable guidance and support throughout the course of this research.

This research is funded by the Engineering and Physical Science Research Council (EPSRC) within the Geospatial Systems CDT (EPSRC Reference: EP/S023577/1).

A Comparative Analysis of Landslide Mapping Techniques using Earth Observation (EO) Data

by Lilian Akudo Akanazu

Abstract

Landslides pose significant threats to human life, infrastructure, and the environment. Rapid accurate assessment and identification of these landslides within days to weeks of their occurrence are crucial for timely disaster management and effective emergency response strategies. This study evaluated the performance of freely accessible EO-based tools - HazMapper and Google Earth Engine (GEE), alongside manual delineation technique in the detection and rapid mapping of landslides in Glengyle. Recent landslides which typically leave visible scars on the landscape were primarily considered using two approaches applied by these EO-based tools: pixel-based analysis and SLIP algorithm for change detection. The integration of these methods provides a comprehensive assessment of landslide areas as they consider both changes in vegetation cover and topography. By comparing the pre- and post-event composites of the study area, the landslides were detected based on the NDVI and landslide tracker binary raster image generated by HazMapper and GEE, while the manual technique employed the physical delineation of the landslides using satellite imagery. The performance metrics of these methods identified GEE as the best-performing method with an F1 score of 0.83 over HazMapper and manual technique's 0.81 and 0.79 F1 scores respectively. The kappa value of 0.62 for GEE suggests that the tool's efficacy in rapid landslide mapping performed substantially better than random chance. Replication of the GEE in the secondary (Rest and Be Thankful) and tertiary (Dortyol) study areas further assessed the tools efficacy in mapping other landslide types. With an F1 score of 0.82 and 0.93 for the secondary and tertiary locations, GEE correctly identified a substantial number of landslides in these locations better than random chance. The results suggest that GEE is a robust tool for rapid landslide mapping in emergency situations.

Keywords: Landslides, Earth Observation, Google Earth Engine, HazMapper, Normalised Differential Vegetation Index, SLIP

Table of Contents

Declaration of Authorship	ii
Acknowledgements	iii
Abstract	iv
List of Figures	vii
List of Tables	viii
List of Acronyms	ix
1 Introduction	1
1.1 Background and Rationale	1
1.2 Aim and Objectives	5
1.3 Thesis Structure	5
2 Literature Review	6
2.1 Defining Landslides	6
2.2 Mechanisms of Landslide formation	7
2.2.1 Slope Morphology	8
2.2.2 Geology	9
2.2.3 Soil	9
2.2.4 Moisture Conditions	11
2.3 Triggering factors of Landslide formation	12
2.3.1 Water	12
2.3.2 Seismic activity	13
2.3.3 Volcanic activity	13
2.3.4 Human activity	14
2.4 Landslide based on type of movement	14
2.4.1 Falls	14
2.4.2 Topples	15
2.4.3 Slides	16
2.4.4 Spreads	17
2.4.5 Flows	18
2.5 Landslide mapping approaches	19
2.5.1 Field Surveys	21

2.5.2	Manual Delineation	22
2.5.3	Indexing or Pixel-based technique	23
2.5.4	Object-based Image Analysis (OBIA)	23
2.5.5	Change detection approach	24
2.5.6	Artificial Intelligence (AI)	25
2.6	Google Earth Engine (GEE)	26
2.7	HazMapper	28
2.8	Summary	29
3	Research Methods.	33
3.1	Study Area.	33
3.1.1	Glengyle	33
3.1.2	Rest and Be Thankful	35
3.1.3	Dörtyol	36
3.1.4	Rationale for selection	38
3.2	Data	39
3.2.1	Satellite Imagery	39
3.2.2	Landslide Inventory	40
3.3	Comparison of landslide mapping approaches	41
3.3.1	Manual mapping technique	41
3.3.2	HazMapper	42
3.3.3	Google Earth Engine	44
3.4	Data Processing	46
3.5	Accuracy Assessment	46
3.5.1	Confusion matrix	47
3.5.2	Accuracy	48
3.5.3	Kappa coefficient	48
3.5.4	Precision	50
3.5.5	Recall	50
3.5.6	F1 Score	50
3.5.7	Validation	51
4	Analysis and Results	52
4.1	Glengyle manual mapping results.	52
4.2	Glengyle GEE results	54
4.3	Glengyle HazMapper results	56

4.4 Summary of results	58
4.5 Rest and Be Thankful Valley results	58
4.6 Dortyol results	60
5 Discussion	63
5.1 Objective 1 – Establishing traditional and state-of-the-art EO-based landslide mapping methods	63
5.2 Objective 2 – Investigating free EO-based tools for landslide mapping in Glengyle	64
5.3 Objective 3 – Comparing the efficiency and performance of techniques Applied	65
5.4 Objective 4 – Testing Google Earth Engine on Rest and Be Thankful	67
5.5 Summary of Discussion	68
6 Conclusion	70
7 Future Work	72
Bibliography	73
Appendices	88

List of Figures

2.1	A Schematic of Rockfalls	15
2.2	A Schematic of Topples	16
2.3a	Rotational Landslide	17
2.3b	Translational Landslide	17
2.4	A Schematic of Spread Landslide	18
2.5	A Schematic of Flow Landslide	18
2.6	OBIA demonstration	24
2.7	Global occurrence of Landslides between 2003-2008	30
3.1	Map of Primary and Secondary study areas	34
3.2	Primary and secondary study areas showing landslide susceptibility	35
3.3	Tertiary study area – Dörtüol	37
3.4	Screenshot of the attribute table of landslide inventory	40
3.6	Screenshot of HazMapper interface	44
3.6	A schematic of composite creation in GEE	45
4.1	Manually mapped landslides overlayed on STRM	52
4.2	Manually mapped landslides overlayed on BGS landslide	54
4.3	Google Earth Engine pre- and post-event composite	55
4.4	BGS landslide inventory overlayed on GEE landslide tracker results	55
4.5	HazMapper pre- and post-event composite	57
4.6	HazMapper rdNDVI results showing areas with Vegetation loss	57
4.7	Landslide tracker for Rest and Be Thankful	59
4.8	Landslide tracker image of Dörtüol	61

List of Tables

Table 1	HazMapper input variables, definitions and examples	.	.	29
Table 2	Kappa values explained	.	.	49
Table 3	Confusion matrix for Glengyle manual mapping results	.	.	53
Table 4	Confusion matrix for GEE results	.	.	56
Table 5	HazMapper confusion matrix results	.	.	57
Table 6	Summary of precision metrics for the three methods	.	.	58
Table 7	GEE confusion matrix for Rest and Be Thankful	.	.	59
Table 8	GEE confusion matrix for Dortyol	.	.	60

List of Acronyms

AFAD - Afet ve Acil Durum Yönetimi Başkanlığı (Disaster and Emergency Management Presidency)

BGS – British Geological Survey

CNN – Convolutional Neural Network

DEM – Digital Elevation Model

DRIP – Detecting Real-time Increased Precipitation

DSGSD – Deep-seated Gravitational Slope Deformation

EAFZ - East Anatolian Fault Zone

EM-DAT – Emergency events Database

EO – Earth Observation

GEE – Google Earth Engine

GNSS – Global Navigation Satellite System

GPM – Global Precipitation Measurement

GPS – Global Positioning System

HR – High Resolution

InSAR – Interferometric Synthetic Aperture Radar

LiDAR – Light Detection and Ranging

MODIS – Moderate Resolution Imaging Spectroradiometer

NAFZ - North Anatolian Fault Zone

NDVI – Normalised Difference Vegetation Index

OBIA – Object-based Image Analysis

QGIS – Quantum GIS (Geographic Information System) software

rdNDVI – relative difference Normalised Difference Vegetation Index

SAR - Synthetic Aperture Radar

SLIP – Sudden Landslide Identification Product

SRTM – Shuttle Radar Topography Mission

TDR – Time Domain Reflectometry

VHR – Very High Resolution

1 Introduction

1.1 Background and Rationale

Landslides are among the most frequent natural disasters worldwide that pose severe threat to humans, infrastructures, and the natural environment (Nugroho et al., 2021). They cause significant damage to the landscape, hamper relief efforts in vulnerable locations, and rapidly redistribute sediments across the landscape (Milledge et al., 2021) which in turn result in other secondary hazards like flooding. They are often triggered by several factors which can be classified as either tectonic (e.g. Bennett et al., 2016), climatic (e.g. Moreiras, 2005) and/or human (Petley et al., 2007). In recent years, human influences (e.g. urbanisation) on the natural environment, and exacerbated by climatic conditions, has only but intensified landslide occurrences (Zhu et al., 2023).

Notably, landslide events have severely impeded social developments in societies whether they appear close to inhabited areas, or far from them as seen in countries like China (Dieu Tien et al., 2018; Lin et al., 2021; Zhang et al., 2024), Japan (Ayalew, 2005; Wang et al., 2019; Lusiana, 2022), Greece (Bathrellos et al., 2024), Ethiopia (Shano et al., 2024), Italy (Guzzetti, 2000; Conoscenti et al., 2015; Samia et al., 2017), Turkey (Tan et al., 2011; Demir et al., 2024) and of course the United Kingdom (Winter et al., 2006, 2008; Foster et al., 2011; Gibson et al., 2013; Palamakumbura et al., 2021) amongst others.

Landslide events are a primary contributor to topographic erosion and landscape evolution (Korup et al., 2010). These evolutions result in significant rock-bound and organic (soil and aboveground biomass) carbon modifications (Hilton et al., 2008) causing over 50,000 fatalities between 2004–2016 with billions (USD) in global losses and damaged-infrastructure costs (Froude & Petley, 2018; Emberson et al., 2020; Kirschbaum et al., 2015; Petley, 2012). According to the Global Fatal Landslide Database (GFLD), a total of 55,997 people were killed in 4,862 distinct landslide events between January 2004 and December 2016 (Zhong et al., 2019). In the United States alone, annual losses to mass-wasting events exceed USD 3 billion (Spiker & Gori, 2003) while Sim et al., (2022) estimated landslide-related losses at USD 20 billion annually on a global scale. These consequences to human life and the environment reflects why landslides are considered as natural disasters (Bathrellos et al., 2017).

Relative to other natural disasters, the International Disaster Database (EM-DAT) suggests that landslides account for 4.9% of all natural disaster events, and 1.3% of all natural hazard fatalities between 1990 and 2015 (Froude & Petley, 2018), with 54% of these landslide events

occurring in Asia (Guha-Sapir et al., 2018). However, the effect of landslides on the society has been greatly underestimated in most global databases (Froude & Petley, 2018). For example, Petley (2012) showed that the EM-DAT database underestimated the number of fatal landslide events by ~2000% and fatalities by 430% between 2004 and 2010, whilst Kirschbaum et al. (2015) showed that the EM-DAT database underestimated the number of fatal landslide events by ~1400% and fatalities by 331% between 2007 and 2013. In most cases, this under-reporting of landslide impact is associated with the perception that landslides are secondary hazards, and causes of fatalities are recorded in connection with the primary hazard (e.g. an earthquake rather than a co-seismic landslide) rather than the actual cause of the loss (Froude & Petley, 2018).

Owing to these consequences, a rapid response to landslides is needed to assess the damage caused and to help save lives (Nugroho et al., 2021). A lack of detailed information on the condition or location of the damaged regions immediately following a significant landslide event can disrupt disaster management procedures, resulting in even more fatalities than the actual event (Robinson et al., 2019). In addition to rapid response efforts, it is also essential to create an accurate landslide inventory in the weeks to the following months of landslide events (Froude & Petley, 2018). This detailed inventory helps to identify landslide-prone areas, providing crucial information for pinpointing future hotspots, and implementing preventive measures to reduce the risk of landslides (Nugroho et al., 2021). Even more important it is to create tools with freely available data that can be used to rapidly map these landslides and their levels of damage.

Interest in quantifying landslide risk has developed since the attempt by the International Association of Engineering Geology (IAEG) Commission on Landslides to compile a list of worldwide landslide events for the UNESCO annual summary of information on natural disasters in 1971 (UNESCO,1973; Froude & Petley, 2018). Before now, traditional landslide inventories were generated from expensive time-consuming site visits (e.g. Warburton et al., 2008), severely limiting the number of landslides that could be mapped in scale and size. Although valuable for small scale studies, this method was labour intensive and spatially limited, and therefore inadequate to aid rapid response efforts in emergency situations.

Today, landslide mapping has undergone a transformative evolution with the advent of Earth Observation (EO) technologies, enabling the transition from traditional field-based surveys to more automated and scalable mapping processes. Landslides are now increasingly mapped remotely based on interpretation of satellite or aerial imagery, which enables much larger datasets to be analysed (e.g. Li et al., 2014; Roback et al., 2018). The integration of optical

satellite imagery, Synthetic Aperture Radar (SAR), and multispectral data has provided unparalleled opportunities to monitor and map landslides over large areas with high temporal and spatial resolution. However, these advancements are not without challenges. Cloud cover and dense vegetation, for instance, can obscure optical imagery, making it difficult to detect surface disturbances caused by landslides (Travelletti et al., 2012). On the other hand, SAR technology, while capable of penetrating clouds and vegetation, often struggles to capture rapid landslide events that occur between satellite orbits due to its revisit time, limiting its utility for dynamic processes (Moretto et al., 2021).

Moreover, there are inherent challenges in detecting older or inactive landslides through conventional EO methods, particularly in regions where vegetation has regrown or where surface features indicative of past movement have been eroded or obscured (Zhong et al., 2020). Although not of importance with respect to aiding rapid response efforts, mapping older landslides remains crucial for long-term hazard assessment. Similarly, in arid or semi-arid regions with sparse vegetation cover and minimal observable landscape modification, EO technologies may fail to differentiate landslide scars from other geomorphological features, such as natural erosion or human activities (Piratesh & Li, 2016). These limitations underscore the importance of critically comparing different landslide mapping techniques to evaluate their suitability to rapidly detect and map landslides for diverse terrain conditions and landslide types.

Landslides, though often triggered by specific events such as extreme rainfall or earthquakes, can also be influenced by a range of other factors that reactivate older, seemingly stable slopes. These factors include progressive slope degradation, changes in land use, vegetation loss, and even human activities such as construction or excavation (Zhang et al., 2021a; Zhang et al., 2023). Over time, geological processes like weathering can weaken the structural integrity of slopes, making them susceptible to failure when additional stresses, such as increased pore water pressure from rainfall, are introduced (Zhang et al., 2021b). In regions where landslides have been dormant for decades or centuries, these cumulative effects can bring them back into motion, posing a renewed threat to infrastructure and communities.

In the United Kingdom, for example, many of the landslides recorded in the National Landslide Database (NLD) are ancient and inactive (British Geological Survey - BGS, 2024). However, periods of high rainfall have demonstrated the potential for these slopes to reactivate, as seen during the summers of 2012 and the winters of 2012–2016 (BGS, 2024). These rainfall events triggered numerous landslides across the country, many of which were relatively small in scale but had significant societal impacts. Fatal incidents, such as those in Burton Bradstock and

Beaminster in 2012 and in Looe in 2013, highlight the deadly potential of such occurrences, even when the landslides themselves are not large (BGS, 2024). These examples underscore the need for rapid landslide mapping, particularly during extreme weather events. The ability to quickly identify and monitor these events is crucial for supporting emergency response teams, issuing timely public warnings, and implementing risk mitigation measures. Furthermore, the reactivation of older landslides serves as a reminder that landslide susceptibility is not static but rather evolves over time, influenced by environmental, climatic, and anthropogenic factors (Zhang et al., 2021b). The predominance of relatively small landslides during such periods also raises challenges for traditional mapping methods. Their dispersed nature, temporary visibility, and potential obscuration by cloud cover highlight the importance of advancing EO-based tools for detecting landslides under various conditions and rapidly.

Over the past decade, the availability of free and accessible EO data has revolutionized landslide research and hazard assessment. Satellite missions such as Sentinel-1 and Sentinel-2 (launched by the European Space Agency under the Copernicus program) provide high-resolution optical and radar data at no cost to the user, enabling researchers and practitioners to monitor and analyse large-scale environmental changes in near real-time (Drusch et al., 2012). This abundance of freely available data has catalysed the development of various tools and methodologies for landslide detection and mapping, including Google Earth Engine (GEE), HazMapper, and other cloud-based geospatial platforms that streamline processing and analysis (Gorelick et al., 2017). These tools combine EO data with machine learning, remote sensing indices and terrain analysis to provide automated or semi-automated solutions for landslide mapping, significantly reducing the reliance on time-intensive manual techniques (Mondini et al., 2021). However, while these tools have shown great promise in supporting rapid landslide mapping responses, their performance can vary depending on the input parameters, resolution, and environmental conditions (e.g. vegetation cover, landslide type or landslide trigger).

It is therefore based on this premise that this study seeks to carry out a comparative analysis of rapid landslide mapping techniques using EO methods, by evaluating the strengths and weaknesses of the several methods and to identify the approach that offers consistent performance in a variety of environments. Thus, this study will systematically evaluate and compare the performance of a selection of EO-based tools in accurately detecting landslides across diverse terrains including areas with diverse topography, climate and/or landslide type. The goal is to identify a rapid mapping technique that is universally applicable, adaptable, and

reliable across all terrains. By focusing on rapid mapping techniques to aid emergency response efforts, this study considers the mapping of recent landslides which typically leave visible scars on the environment. Identifying a universal approach would ensure a more timely and effective landslide detection, monitoring, and risk management worldwide, regardless of local constraints.

1.2 Aim and Objectives

The aim of this research is to:

Evaluate and compare the capability of existing Earth Observation (EO) based approaches for rapid and accurate landslide mapping.

To achieve this aim, four objectives have been developed as follows:

1. Establish the traditional and state-of-the-art EO-based approaches to landslide mapping
2. Investigate the application of freely available EO-based approaches to landslide mapping for a case study of Glengyle, Scotland
3. Compare the efficiency and accuracy of these landslide mapping techniques, identifying their strengths and weaknesses
4. Test the most efficient of the compared methods on another landscape to assess its transferability performance on different terrains with different landslide types.

1.3 Thesis Structure

This thesis is structured as follows:

[Section 2](#) is the literature review which discusses literature fundamental to the understanding of this research and a critical analysis of existing landslide mapping methods. [Section 3](#) explains the methods used in this research including descriptions of data and the landslide mapping techniques that were tested. [Section 4](#) discusses the analyses performed and the results therein. [Section 5](#) provides the discussion of the objectives set out in this study and interpretation of the results including their relationship with existing literature and limitations of the research. [Section 6](#) presents the conclusions of the research and how the project addressed the aims and objectives as well as the researcher's thoughts based on the findings from the study. [Section 7](#) presents areas for future work to address the limitations in this research and extended study for research gaps not covered in this study.

2 Literature Review

2.1 Defining Landslides

There is a diversity of definitions for landslides which reflects the complexity of activities associated with the occurrence of this phenomenon, and in most cases, the term is used interchangeably with phrases such as '*slope failures*', '*mudslides*' or '*mass movement*' (Highland & Bobrowsky, 2008). A landslide is a downslope movement of rock or soil, or both, occurring on the surface of rupture—either curved (rotational slide) or planar (translational slide) rupture—in which much of the material often moves as a coherent or semi-coherent mass with little internal deformation (Highland & Bobrowsky, 2008).

Landslide is a general term used to describe the downslope movement of soil, rock, and organic materials under the effects of gravity (Highland & Bobrowsky, 2008). It occurs as gravitational forces exceed the strength of the material in the slope when water builds up in the slope usually due to rain, irrigation, or snow melt (Case, 2001). The water present thus increases the weight of the material on the slope, hydrates and expands the clay minerals that holds the particles together thereby decreasing the strength of the material and weakening the slope (Case, 2001). The result is the yielding of all or part of the slope through downslope movement of materials known as a landslide. In some cases, the pore pressure from ground water can be increased during vibration of large machines, earthquakes or rapid changes of water level, triggering landslides and reactivating dormant landslides when water penetrates old ground cracks (Case, 2001). Vibrations from heavy machinery or seismic activity can disturb the soil structure, allowing groundwater to infiltrate more easily, especially through existing cracks (Case, 2001). Similarly, sudden changes in water levels, such as during heavy rainfall or dam releases, can cause water to rapidly penetrate the ground. This infiltration increases the pore water pressure, which reduces the effective stress that holds soil particles together, decreasing the slope's shear strength (Highland & Bobrowsky, 2008). In dormant landslides, old fractures or cracks provide pathways for water to seep deeper into the soil, reactivating instability and triggering renewed movement. These varying mechanics or triggering factors have informed the classification of landslides into different types based on the type of movement and materials involved (Highland & Bobrowsky, 2008).

2.2 Mechanisms of landslide formation

Landslide formation is a complex and dynamic process influenced by a wide range of geological, hydrological, environmental, and anthropogenic factors (Li et al., 2020). At its core, a landslide occurs when the forces driving material downslope—primarily the force of gravity—exceed the resisting forces that maintain the slope's stability, such as the material's shear strength and internal cohesion (Petley, 2012). However, while gravity is the fundamental force behind all landslides, the processes that destabilize slopes and trigger failures are highly variable and depend on site-specific conditions (Fidan et al., 2024). These mechanisms include long-term processes, such as weathering and progressive slope degradation, and short-term triggers, such as heavy rainfall, earthquakes, volcanic activity, or human disturbances (Fidan et al., 2024).

As previously mentioned, water plays a particularly critical role in landslide formation, as it can both increase the weight of slope materials and reduce their shear strength through the buildup of pore water pressure (Polemio & Petrucci, 2000). Similarly, seismic activity can weaken slope stability by inducing ground shaking and disrupting the internal structure of the mass of substrate (Gariano & Guzzetti, 2016). Also, erosion, whether caused by rivers, waves, or human activities, often undercuts slopes, removing material that supports the overburden, creating conditions that are prone to failure (Malamud et al., 2004). Anthropogenic factors, such as deforestation, construction and excavation, further exacerbate these natural processes, altering the delicate balance of forces on a slope (Vasantha & Bhagavanulu, 2008). The mechanisms leading to landslides often interact in complex ways. For example, prolonged weathering can weaken a slope over decades, while a single intense rainfall event or earthquake may act as the immediate trigger for failure (Calcaterra & Parise, 2010). In some cases, the absence of vegetation, whether due to natural processes like wildfires or human-induced deforestation, removes the root systems that help bind soil and reduce erosion, leaving slopes more vulnerable to sliding (Vasantha & Bhagavanulu, 2008). Understanding these mechanisms is essential not only for predicting when and where landslides might occur but also for developing targeted mitigation strategies that address both long-term susceptibility and short-term triggers.

Landslides are generally controlled by the slope morphology, geology, soils, and moisture conditions (Ohlmacher, 2000). These specific factors contribute to landslide formation and interconnected with the hydrology, topography, vegetation, climate, and

seismology of each location, they play pivotal roles in influencing not only where landslides are likely to occur but also their frequency, magnitude, and potential impact (Malamud et al., 2004).

2.2.1 Slope morphology

Slope is the gradient or steepness of the land surface typically referring to the inclination of land or terrain relative to a horizontal plane (Harist et al., 2018). Slope morphology refers to the shape, structure, and configuration of a slope, including its angle, curvature, and overall profile (Wang et al., 2020). The combination of slope angle, shape, and aspect, slope morphology plays a primary role in landslide occurrence.

Steeper slopes are inherently more prone to landslides due to the gravitational force acting on slope materials, which increases with angle (Turel & Frost, 2011). A steep slope demonstrates how large the shear stress is and how low the security factor is for slope (Nourani, et al., 2014). This is because as slope increases, tangential stress increases in the residual or consolidated soil covering, axial tension decreases and stability deteriorates (Çellek, 2020). Thus, with the increase of the slope, the block-creation potential of the material increases, and this leads to the increase in the weight of rock blocks at the top of the mass. As a result, slope does not only affect stress distribution within masses but also affects the magnitude of shear and normal stress on shear surfaces (Çellek, 2020).

Slopes with angles exceeding the material's angle of repose (e.g. typically 25–45° for loose debris) are particularly unstable (Zhuang et al., 2016). The shape of the slope also influences landslide susceptibility. Concave slopes tend to accumulate water and loose sediments, creating zones of high stress that are more prone to failure (Turel & Frost, 2011). Conversely, convex slopes may shed water and sediment more easily but are vulnerable to surface erosion that could destabilize them. Aspect, or the direction a slope faces, determines exposure to climatic factors like sunlight and wind. South-facing slopes in the Northern Hemisphere, for instance, often experience greater weathering and vegetation loss due to higher solar radiation, potentially reducing stability (Çellek, 2020). In addition, terrain irregularities such as ridges, cliffs, and overhangs can create localized stress concentrations, further influencing slope stability (Çellek, 2020).

2.2.2 Geology

Geology, which includes the composition, structure, and physical properties of Earth materials, is a critical factor influencing landslide susceptibility (Lee et al., 2002). The type of rock and soil in an area determines its mechanical strength, weathering potential, and ability to resist external forces (Ohlmacher, 2020). Variations in geological characteristics can significantly alter the stability of slopes, making an understanding of geology essential for landslide risk assessment and management (Lee et al., 2002). The type of rock present on a slope plays a fundamental role in its stability. Hard rocks such as granite and basalt are generally strong and resistant to deformation (Stead & Wolter, 2015). However, when these rocks are heavily fractured or weathered, their strength diminishes, making them more prone to failure (Stead & Wolter, 2015). In contrast, softer rocks like shale, siltstone and sandstone are weaker and more susceptible to landslides, especially under conditions of prolonged weathering and erosion (Guzzetti et al, 1996). Shale is more vulnerable due to its fine laminations, which allows it to break easily along bedding planes (Stead, 2015; Rosly et al., 2022). Unconsolidated materials, including volcanic ash and glacial till, lack cohesive strength and are especially vulnerable to failure when saturated with water, making them common contributors to landslide events (Guzzetti et al, 1996).

Geological structures such as faults, joints, and bedding planes create inherent weaknesses within the rock mass, often serving as sliding surfaces during slope failures (Guerriero et al., 2021). Fault zones are particularly hazardous because they contain fractured and weakened rocks, which allow water infiltration that reduces slope stability (Lee et al., 2002). Joints and fractures similarly act as conduits for water, promoting chemical weathering and further destabilizing the slope (Stead & Wolter, 2015). Bedding planes in sedimentary rocks are especially significant when they dip parallel to the slope, as they provide a natural surface along which sliding can occur (Guerriero et al., 2021). Structural features such as folds also influence stability, with anticlines creating zones of tension and synclines accumulating water that can weaken the slope materials (Rosly et al., 2022).

2.2.3 Soil

Soil plays a critical role in determining slope stability and is a key factor influencing the occurrence and characteristics of landslides. The properties of soil, including its composition, structure, and hydrological behaviour, significantly impact how slopes respond to external stresses such as rainfall, seismic activity, or human intervention (Iverson et al., 2000). Different

soil types exhibit varying levels of shear strength and cohesion, making some soils more prone to landslides than others. The composition and texture of soil are fundamental in controlling its stability. Soils with a high proportion of clay are particularly susceptible to landslides due to their unique mineralogical properties (Mugagga et al., 2012). Clay minerals have a plate-like structure that allows them to absorb water, causing swelling and a reduction in shear strength (Yalcin, 2007). When saturated, clay-rich soils can transform into a viscous mass, leading to rapid slope failure (Yalcin, 2007). In contrast, sandy soils which are more granular exhibit higher permeability and allow water to drain more easily (Acharya et al., 2009). However, sandy soils may also lose stability during intense rainfall events or under high pore water pressure, especially if they are poorly compacted (Acharya et al., 2009). Loamy soils, which consist of a mixture of sand, silt and clay, tend to have intermediate stability, but their behaviour under stress varies depending on the relative proportions of these components (Temme, 2021).

Soil structure, or the arrangement of soil particles and pores, is another critical determinant of slope stability (Chen & Martin, 2002). Well-structured soils with stable aggregates are more resistant to erosion and mass wasting, while poorly structured soils are prone to collapse under stress (Chen & Martin, 2002). Soils with a high degree of porosity can absorb and retain significant amounts of water, which may increase their weight and decrease their strength during heavy rainfall or flooding (Temme, 2021). Conversely, compacted soils with low porosity may shed water more rapidly but can also become destabilized when underlying layers become saturated, leading to shallow landslides or debris flows (Sunbul et al., 2021). Organic content within soils also influences their stability. Soils rich in organic matter, such as peat, tend to have low bulk density and high water-holding capacity (Błońska et al., 2018). While this can support vegetation and reduce erosion, it also makes the soil prone to instability when saturated. Peaty soils, common in certain high-altitude and wetland environments, are particularly prone to landslides due to their compressibility and weak structure when wet. In contrast, mineral-rich soils often exhibit higher strength but are more susceptible to weathering and erosion over time (Cerri et al., 2020).

The hydrological properties of soil, including its permeability and drainage capacity, are key factors in landslide formation. Permeable soils, such as sandy or gravelly soils, allow water to infiltrate rapidly, reducing surface runoff but increasing the risk of subsurface instability (Chen & Martin, 2002). On the other hand, impermeable soils, such as those rich in clay, can trap water near the surface, creating perched water tables that add weight to the slope and reduce its stability. The interaction between soil layers of differing permeability, known as

stratification, can also exacerbate instability by concentrating water flow along specific horizons, leading to increased pore water pressure and slope failure (Chen & Martin, 2002).

2.2.4 Moisture conditions

Moisture conditions influence landslide susceptibility by altering the mechanical properties of soil and rock, directly impacting slope stability. The presence of water within slope materials can either enhance or diminish stability, depending on the extent and distribution of moisture. In moderate amounts, water can provide cohesion in granular soils like sands through surface tension, which helps particles bind together (Wicki et al., 2020). However, when water levels increase significantly, such as during prolonged rainfall or snowmelt, saturation occurs. Saturation reduces the frictional resistance between particles and increases the weight of slope materials, creating conditions that favour slope failure (Whiteley et al., 2019). This dual role of water makes it one of the most influential factors in landslide initiation.

A critical mechanism through which moisture destabilizes slopes is the increase in pore water pressure. Pore water pressure refers to the pressure exerted by water within the void spaces of soil or rock (Matsuura et al., 2008). When water infiltrates a slope and fills the pores, it effectively "floats" the particles, reducing their ability to interlock and resist shear forces (Matsuura et al., 2008). As a result, the shear strength of the material decreases, making it more prone to failure. This phenomenon is particularly severe in fine-grained soils, such as clays or silts, which are less permeable and retain water for longer periods (Błońska et al., 2018). In contrast, coarse-grained soils like sands or gravels drain more effectively, reducing the likelihood of prolonged waterlogging but remaining susceptible to rapid failures during extreme rainfall events (Acharya et al., 2009).

The interaction between moisture conditions and geological or topographical factors further amplifies landslide risks. In layered soils or rock formations, differences in permeability can lead to water accumulation along less permeable layers, creating perched water tables and zones of high pore water pressure (Matsuura et al., 2008). Additionally, slopes undercut by rivers, waves, or human activities are particularly vulnerable, as water infiltration further destabilizes the already weakened base (Matsuura et al., 2008). Moisture also contributes to the weathering of slope materials, as repeated cycles of wetting and drying weaken soil and rock over time. These processes underscore the complex relationship between moisture conditions and landslides, emphasizing the need for careful monitoring and management of water dynamics in landslide-prone areas (Whiteley et al., 2019).

2.3 Triggering factors to landslide formation

The triggering factors of landslide formation refer to the immediate conditions or events that initiate the movement of soil, rock, or debris down a slope. While the inherent instability of a slope may result from predisposing factors such as geology, topography or soil properties, a triggering factor acts as the catalyst that converts potential instability into active failure (Jaafari, 2024). These triggers can be natural, such as intense rainfall, rapid snowmelt, earthquakes, or volcanic activity; or anthropogenic, including construction activities, deforestation, or changes in drainage patterns. Often, a combination of these factors work together to overwhelm the stability of a slope, particularly in areas already susceptible to landslides. Highland and Bobrowsky (2008) identified two primary categories of factors that trigger landslide formation as being natural and human factors, and in some cases, a combination of both factors. These factors typically act on slopes already predisposed to instability due to their geological, morphological, or hydrological characteristics. However, human activities, including construction, deforestation, and land-use changes, increasingly contribute to landslide occurrences by accelerating or compounding natural processes.

2.3.1 Water

Water is a primary cause of landslides through slope saturation which can occur in the form of intense rainfall, snowmelt, changes in ground-water levels, and surface-water level changes along coastlines, earth dams, etc. (Polemio & Petrucci, 2000). Intense or prolonged rainfall increases the water content in soil and rock, leading to saturation and a rise in pore water pressure (Polemio & Petrucci, 2000). This process reduces the shear strength of the landmass, destabilizes slopes causing shallow landslides or debris flows. Similarly, rapid snowmelt introduces large volumes of water into the subsurface, saturating the soil and triggering landslides in high-altitude regions or during spring thaw (Moreiras et al., 2012). Water's erosive power also undermines slope stability by scouring riverbanks, coastal cliffs, and road cuttings, removing support at the base of slopes and initiating failures. The role of water is particularly significant in tropical regions, where monsoons or cyclonic storms can dump large volumes of rain in a short time, overwhelming natural drainage systems and leading to catastrophic landslides (Amarasinghe et al., 2024).

2.3.2 Seismic activity

Many mountainous areas that are vulnerable to landslides have also experienced at least moderate rates of earthquake activity in recorded times ([Lenti & Martino, 2012](#)). Earthquakes in steep terrain greatly increase the likelihood that landslides will occur due to ground shaking, liquefaction of susceptible sediments, or shaking-induced dilation of soil materials, which allows rapid infiltration of water ([Keefer, 2002](#)). However, the relationship between earthquakes and landslides depends on several factors, including the magnitude of the earthquake, the distance from the epicentre, geological conditions, topography, and weather conditions prior to the event ([Lenti & Martino, 2012](#)). For instance, the 1964 Great Alaska earthquake in the United States caused widespread landsliding and other ground failure, which led to most of the monetary loss attributed to the earthquake ([Plafker, 1965](#); [Page, 1968](#)). Also, the 2018 Hokkaido Eastern Iwate Earthquake (magnitude 6.6) triggered over 6,000 landslides, primarily in Atsuma town. The event was notable for its devastating impact, killing over 40 people and causing widespread infrastructure damage ([Wang et al., 2019](#)). In Nepal, the 2015 Gorkha Earthquake (magnitude 7.8) triggered thousands of landslides across central Nepal, severely impacting rural communities ([Goda et al., 2015](#)).

Seismic activity thus remains a primary trigger for landslides in tectonically active regions because of the unique ability of earthquakes to destabilize slopes through intense ground shaking ([Keefer, 2002](#)). This destabilization emphasizes the need for rapid landslide mapping by quickly identifying the affected areas which is crucial for guiding emergency response, allocating resources effectively, and planning relief efforts. Timely mapping also helps rescue teams access impacted zones, prevents further casualties by identifying secondary hazards, and supports long-term recovery by informing stabilization and rebuilding efforts.

2.3.3 Volcanic activity

Landslides due to volcanic activity represent some of the most devastating types of failures. Volcanic lava may melt snow rapidly, which can form a mass of rock, soil, ash, and water that accelerates rapidly on the steep slopes of volcanoes, devastating everything in its path ([Barbano et al., 2014](#)). These volcanic debris flows can reach great distances after they leave the flanks of the volcano and can also damage structures in flat areas surrounding the volcanoes ([Korup et al., 2019](#)). Volcanic edifices are young, unconsolidated, and geologically weak structures that in many cases can collapse and cause rockslides, landslides, and debris avalanches ([Blahůt et al., 2019](#)). Many islands of volcanic origin experience periodic failure of their perimeter

areas (due to the weak volcanic surface deposits), and masses of soil and rock slide into the ocean or other water bodies, such as inlets (Blahůt et al., 2019). Such collapses may create massive sub-marine landslides that may also rapidly displace water, subsequently creating deadly tsunamis that can travel and do damage at great distances, as well as locally (Pistolesi et al., 2020).

2.3.4 Human activities

Human activities have increasingly emerged as significant contributors to landslide initiation, often exacerbating natural triggers (Li et al., 2020; Sun et al., 2021). Deforestation, for instance, removes vegetation that stabilizes slopes by anchoring soil and intercepting rainfall. Without this protective cover, soil becomes exposed to erosion, infiltration, and weathering, dramatically increasing landslide susceptibility (Vasanth & Bhagavanulu, 2008). Similarly, construction activities, including road building, mining, and urban expansion, alter the natural slope profile, reduce material strength, and add extra load to slopes (Salmi et al., 2017). These modifications often disturb the equilibrium of slopes, making them more vulnerable to external triggers such as heavy rainfall or seismic events. Improper drainage systems, often associated with poorly planned infrastructure, can lead to water accumulation and localized slope failures (Kazmi et al., 2016). In agricultural areas, over-irrigation or poor land management practices can also saturate soils, destabilizing slopes and leading to landslides (Lacroix et al., 2020).

The interaction between natural and human factors often creates a compounded effect, amplifying landslide risks. For instance, deforestation in mountainous regions can lead to increased runoff during heavy rainfall (Vasanth & Bhagavanulu, 2008), while poorly managed construction on unstable slopes can trigger landslides during earthquakes (Wang et al., 2014). The increasing impact of climate change further complicates these dynamics, as more intense and frequent rainfall, rising temperatures, and melting glaciers are expected to intensify landslide activity worldwide (Li et al., 2020). Understanding the complex interplay between these natural and human triggers is crucial for developing effective strategies to mitigate landslide risks and protect vulnerable communities.

2.4 Landslides based on type of movement

2.4.1 Falls

A fall usually begins with the detachment of soil or rock, or both, from a steep slope along a surface on which little or no shear displacement of the material has occurred (Highland &

Bobrowsky, 2008). The detached material subsequently descends mainly by falling, rolling, or bouncing, depending on the type of material for example rockfalls. The primary feature of this type of landslide is the absence of interaction between the detached material and any other material on the landscape as the detached material falls freely (Parise, 2001). This type of landslide is usually common on very steep or vertical slopes such as along coastal areas, with differing velocity depending on the slope steepness (Case, 2001). In most cases, it is the result of a progressive crack or detachment of the material from underneath the slope either by natural processes such as streams or rivers, or by human activities such as excavation (Highland & Bobrowsky, 2008). Rock falls however, particularly those involving small volumes, have received less attention than many other types of landslides (Parise, 2001), as focus is primarily dedicated to catastrophic rockfall avalanches. Moreover, rock falls are the most abundant type of landslide triggered by earthquakes, as shown by historical worldwide earthquake-induced landslide data compiled by Keefer (1984), and by numerous landslide inventories from post-earthquake investigations (e.g. Keefer, 2000). A schematic of rockfalls has been illustrated in Figure 2.1.

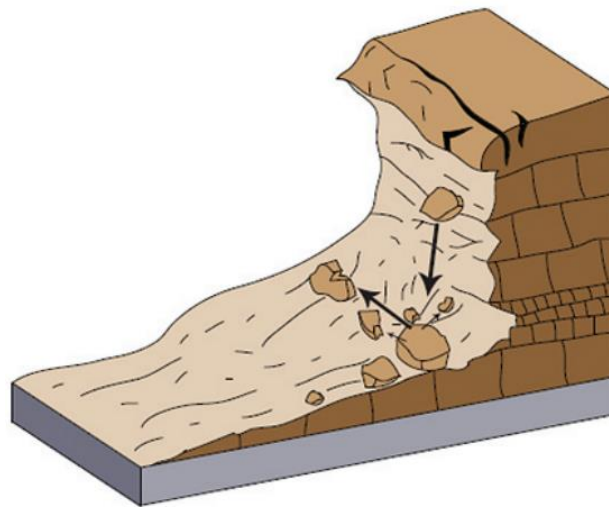


Figure 2.1: A schematic of a rockfall. Credit: (Highland & Bobrowsky, 2008)

2.4.2 Topples

Topples are recognized as the forward rotation out of slope of a mass of soil or rock around a point or axis below the centre of gravity of the displaced mass (Highland & Bobrowsky, 2008). The primary feature of this landslide type is that the material tilts or tips over before falling. Toppling is sometimes driven by gravity exerted by the weight of material upslope from the displaced mass (Parise, 2001). Geological and structural landscapes which are the most prone

to toppling failures are also highly susceptible to rock falls and, topples generally lead to falls of the displaced mass (de Freitas & Watters, 1973; Caine, 1982). Sometimes toppling is due to water or ice in cracks in the mass and can consist of rock, debris (coarse material), or earth materials (fine-grained material) (Highland & Bobrowsky, 2008). They are known to occur globally and prevalent in columnar-jointed volcanic terrain, as well as along stream and river courses where the banks are steep (Highland & Bobrowsky, 2008). Their velocity varies from extremely slow to extremely rapid, sometimes accelerating throughout the movement depending on distance of travel (Parise, 2001). A schematic of topples is provided in Figure 2.2.

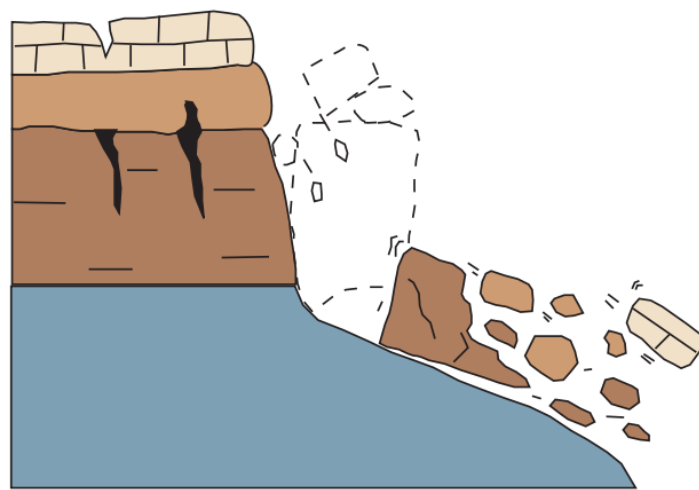


Figure 2.2: A schematic of Topples. Credit: (Highland & Bobrowsky, 2008).

2.4.3 Slides

A slide is a downslope movement of a soil or rock mass occurring on surfaces of rupture or on relatively thin zones of intense shear strain (Highland & Bobrowsky, 2008). The mass movement does not initially occur simultaneously over the whole of what eventually becomes the surface of rupture, as the volume of displacing material enlarges from an area of local failure (Xie et al., 2020). Slides are generally classified as rotational or translational, depending on the surface of rupture. Rotational landslides (slumps) occur most frequently in homogeneous materials found in fills (Highland & Bobrowsky, 2008), with the surface of rupture curved upward (spoon-shaped) and the slide movement rotational about an axis that is parallel to the contour of the slope (Xie et al., 2020). In translational landslides, the mass moves out, or down and outward, along a relatively planar surface with little rotational movement or backward tilting (Highland & Bobrowsky, 2008). This type of slide may progress over considerable

distances if the surface of rupture is sufficiently inclined, in contrast to rotational slides, which tend to restore the slide equilibrium (Xie, et al., 2020). The material in the slide may range from loose, unconsolidated soils to extensive slabs of rock, or both. Translational slides commonly fail along geologic discontinuities such as faults, joints, bedding surfaces, or the contact between rock and soil (Highland & Bobrowsky, 2008). A schematic of rotational and translational landslides has been presented in Figure 2.3a and Figure 2.3b.

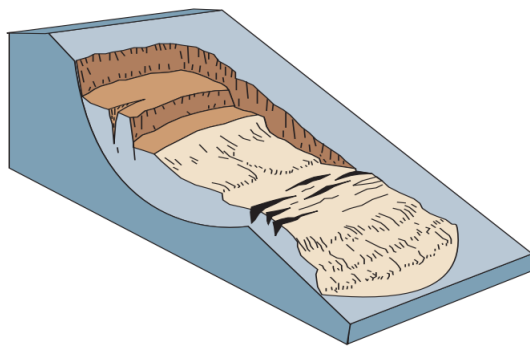


Figure 2.3a: Rotational Landslide
Credit: (Highland and Bobrowsky, 2008)

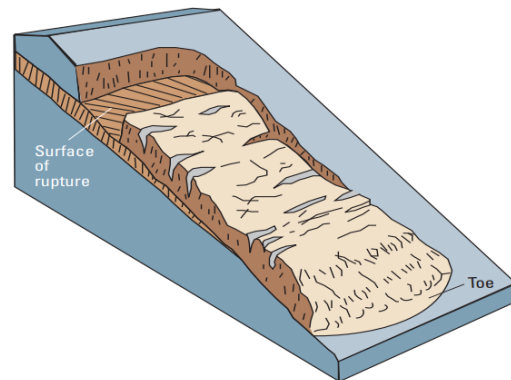


Figure 2.3b: Translational Landslide

2.4.4 Spreads

Usually occurring on very gentle slopes, spreads are an extension of a cohesive soil or rock mass combined with the general subsidence of the fractured mass of cohesive material into softer underlying material (Highland and Bobrowsky, 2008) often in association with liquefaction or weakened soils. They are characterized by the lateral extension and movement of large masses of soil or rock across a horizontal or gently sloping surface (Figure 2.4) usually less than 6° (Chung et al., 2014). Spread landslides often occur near river valleys or coastal areas where sediments are loosely compacted, and groundwater or tidal forces may contribute to weakening the soil (Highland and Bobrowsky, 2008).

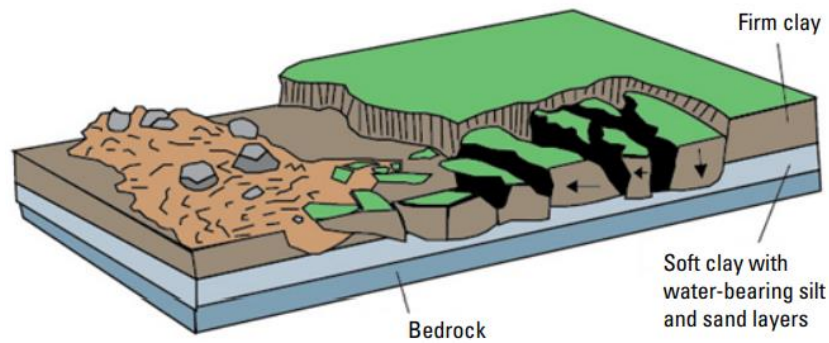


Figure 2.4: A schematic of spread landslide. (Credit: Highland and Bobrowsky, 2008).

2.4.5 Flows

A flow (see Figure 2.5) is a spatially continuous movement in which the surfaces of shear are short-lived, closely spaced, and usually not preserved (Highland and Bobrowsky, 2008). It often begins as a slide forming on a surface of rupture, but then continues moving over a long distance (Hungr et al., 2001). Often, there is a gradation of change from slides to flows, depending on the water content of the material and mobility, (Highland and Bobrowsky, 2008) causing the component velocities in the displacing mass of a flow resemble those in a viscous liquid. Occasionally, as a rotational or translational slide gains velocity and the internal mass loses cohesion or gains water, it may evolve into a flow. Hence, they have been informally and inappropriately called “mudslides” due to the large quantity of fine material that may be present in the flow (Highland and Bobrowsky, 2008).

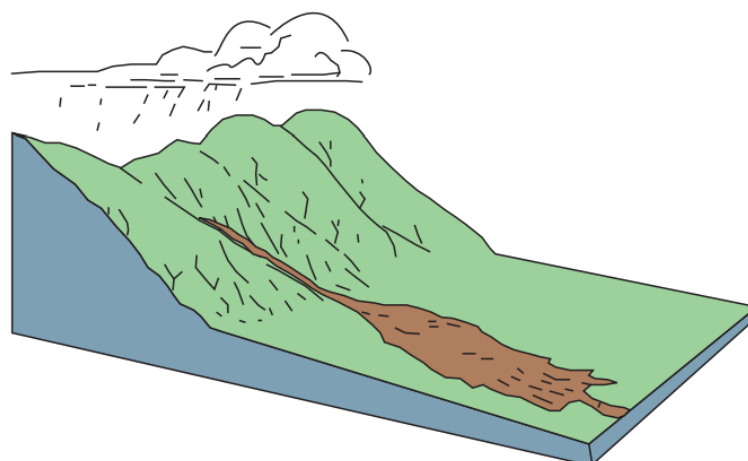


Figure 2.5: A schematic of flow landslide. Credit: (Highland and Bobrowsky, 2008).

2.5 Landslide mapping approaches

Systematic reviews of the literatures on landslide detection and mapping techniques have been published over the last 20 years, considering several input materials and mapping techniques such as geomorphological mapping, topographic maps, and aerial photography (Parise, 2001). Similarly, reviews of the application of spaceborne, airborne, and terrestrial remote sensing technologies (Guzzetti et al., 2012), Synthetic Aperture Radar (SAR; Modini et al., 2021) and multitemporal interferometric SAR (Schlögl et al., 2022; Novellino et al., 2024) have also been conducted. Landslide mapping has also been commonly implemented using several methodologies such as post-event aerial photo analysis and plotting (Cardinali et al., 2000), manual or automatic identification based on the use of high-resolution digital elevation models (DEMs) obtained from airborne lidar surveys conducted after the event (Avanzi et al., 2015; Giordan et al., 2018) or traditional geomorphological field surveys (Pepe et al., 2019). Traditionally, landslide mapping relied on field surveys where geologists visited affected sites, manually identify landslide features, and recorded their characteristics (Warburton et al., 2008). With the advent of remote sensing technology, landslide mapping began to incorporate aerial photography and satellite imagery (Giordan et al., 2018). These methods allowed for broader coverage and identification of landslides in areas that were previously inaccessible.

With the increase in satellite images in recent years, even shallow landslides have been detected (Lu et al., 2019; Martha, 2010), thanks to the robust improvement of satellite resolution which enabled more accurate and widespread landslide detection. Techniques such as the Normalized Difference Vegetation Index (NDVI), change detection analysis, and machine learning algorithms have further enhanced the ability to detect and predict landslides on a large scale (Guzzetti et al., 2012). Tools like Google Earth Engine (GEE) and HazMapper now allow researchers to process vast amounts of EO data quickly for the whole planet, providing near real-time monitoring and mapping capabilities, making them crucial for rapid response efforts. Generally, there are two widely used remote sensing techniques for landslide mapping broadly classified into active and passive systems based on how they collect data from the Earth's surface. Passive sensors rely on natural energy, primarily sunlight, to detect and measure reflected or emitted radiation from the Earth's surface. These sensors capture data in the visible, near-infrared, shortwave infrared, and thermal infrared portions of the electromagnetic spectrum; examples include optical sensors on satellites like Sentinel-2, Landsat, and MODIS (Stumpf, 2013). Optical remote sensing involves the use of satellite or airborne sensors to capture images of the Earth's surface in various bands of the electromagnetic spectrum,

primarily in the visible, near-infrared (NIR), and shortwave infrared (SWIR) (Stumpf, 2013). Image processing techniques for the analyses of optical data comprise image classification, feature and change detection, which in principle allow rapid landslide mapping.

The capabilities of optical remote sensing systems are determined by features of the sensors, the supporting platforms and the image analysis techniques used to extract information (Pradhan & Lee, 2007). It begins with the capture of multispectral or hyperspectral images of the Earth's surface by optical sensing platforms such as Sentinel-2, Landsat, or commercial satellites like WorldView or SPOT (Pradhan & Lee, 2007). The image is pre-processed by atmospheric correction, georeferenced, and cloud-masked to removed cloud-covered areas (Stumpf, 2013). In cases where multiple images cover the region of interest, a composite of the image is generated by combining the images to create a single image of the region of interest. An inherent limitation of optical imaging is its dependence on direct sight contact with the targeted object which does in general limit the investigating of landslides under dense vegetation and limits the frequency of spaceborne observations in high latitudes and the tropics where cloud cover is more persistent throughout the year (Stumpf, 2013).

Active sensors, in contrast, generate their own energy to illuminate the target area and measure the reflected or backscattered signal. Examples include Synthetic Aperture Radar (SAR), Light Detection and Ranging (LiDAR), and radar altimeters (Mondini et al., 2021). SAR remote sensing from airborne and satellite platforms exploits active emissions of electromagnetic radiation in the microwave spectral range (Mondini et al., 2021). SAR operates by emitting radar waves from an orbiting satellite or aircraft and measuring the reflected signals to generate high-resolution images of the Earth's surface (Meyer, 2019). The systems capture images by emitting radar signals that bounce off the Earth's surface as echoes. The strength of the echo depends on the properties of the scattering ground surface in relation to the radiation frequency (e.g., the dielectric constant, the terrain roughness), the distance between the antenna and the ground, and the satellite view angle (Mondini et al., 2021), and it is recorded in the “amplitude” of the electromagnetic wave (Meyer, 2019).

The time it takes for the signal to return is recorded, and from this, high-resolution images are generated (Mondini et al., 2021) by calculating the distance between the satellite and the Earth's surface at each point, allowing for precise mapping of surface features and terrain deformations (Meyer, 2019). Since active radar sensors do not require illumination from the sun, and microwaves penetrate the clouds, SAR imagery can – in principle – capture the occurrence (or recurrence) of landslides all day long, even in areas where clouds obstruct optical sensors

(European Space Agency, 2020). This makes SAR imagery a potentially ideal solution for the detection and mapping of landslides compared to passive optical remote sensing techniques. Some studies have applied SAR technology in landslide detection and mapping (Burrows et al., 2020; Rodriguez et al., 2002; Herrera et al., 2009), but notable constraints have been highlighted by Maconi (2019) when used for operational monitoring and anomaly detection over regional scales. Since SAR relies greatly on the amplitude of return of signals, there is the risk of misdetection when applied in mountainous regions. Thus, SAR is often paired with interferometric techniques (InSAR), which allows for the measurement of ground displacement between two or more SAR images taken at different times (Mondini et al., 2021). The following sub-sections explore both the traditional and widely used modern earth observation-based techniques for landslide mapping.

2.5.1 Field Surveys

Field surveys are one of the earliest and most direct methods of landslide mapping. Field survey relies heavily on the use of various close observation and measurement equipment, such as clinometers, displacement metres, stress metres, water level gauges, global navigation satellite system (GNSS) receivers, and Time Domain Reflectometry (TDR) (Zhong et al., 2019). This approach involves on-site investigations where experts physically assess the affected area, documenting landslide features such as scarp faces, debris flow paths, and deposits. During these surveys, tools like Global Positioning Systems (GPS), drones, or total stations are often used to map landslide boundaries and measure slope angles, elevations, and distances (Zhong et al., 2019). However, this approach is inefficient for mapping landslides over a large area since it requires considerable time, materials, and labour; and it is impossible to identify all the parts of a landslide (e.g. the scarp face, boundary, and deposits) accurately where the topography is hummocky and/or the vegetation is tall or dense (Santangelo et al., 2010). Even though the results of spectral analysis with high resolution imageries are preferable when mapping landslides over large areas (Dou et al., 2015), field work is still conducted when it is necessary to map single landslides in detail for a specific event, or to validate maps prepared using remote sensing techniques (Santangelo et al., 2010). The difficulty of this method stems from several causes, including: (i) the size of the landslide, often too large to be seen completely in the field, (ii) the viewpoint of the investigator, often inadequate to see all parts of a landslide (e.g., the scarp, lateral edges, deposit, toe) with the same detail, and (iii) the fact that old landslides are often partially or totally covered by forest, or have been partly dismantled by

other landslides, erosion processes, and human actions, including agricultural and forest practices (Guzzetti et al., 2012). This technique however is more efficient in mapping a single landslide or small group of landslides triggered by a specific event (e.g. Santangelo et al., 2010), or to validate inventory maps prepared using other techniques.

2.5.2 Manual delineation

Traditionally, manual visual image interpretation for landslide recognition has been based on aerial photographs and recently extended to high resolution (HR) and very high resolution (VHR) optical satellite imagery (e.g., WorldView-2/3, QuickBird) (Scaioni et al., 2014) and is still the most widely used method for landslide detection and inventory preparation (Holbling et al., 2017). This remains widely adopted because a trained geomorphologist can readily recognize and map landslides on the aerial photographs, aided by the vertical exaggeration introduced by stereoscopic vision (illusion of depth) (Guzzetti et al., 2012). However, unlike automated or semi-automated approaches, manual mapping relies on human expertise to detect landslide features based on knowledge of terrain, vegetation patterns, and changes in landscape morphology such as those described in section 2.2.1 (Scaioni et al., 2014). The first step in manual landslide mapping is the selection of the appropriate high-resolution satellite or aerial imagery (Holbling et al., 2017), that covers both pre-event and post-event time frames to allow for comparison. Using GIS software like QGIS, the manual mapping process involves visually inspecting the satellite images for specific indicators of landslides like visible vegetation loss, scar faces or terrain disruption (Scaioni et al., 2014). Once these features are identified, the next step is to manually digitize or draw polygons around the landslide areas. Even though it allows for a detailed, high-accuracy representation of landslide events, manual delineation is time-consuming and labour-intensive, making it unsuitable for large-scale mapping projects. Also, due to the large variability of landslide phenomena, not all landslides are clearly and easily recognizable in the field, from the aerial photographs or the satellite images (Guzzetti et al., 2012). Thus, this method is best applied immediately after a landslide event when individual landslides are “fresh” and usually clearly recognizable as the boundaries between the failure areas (i.e., depletion, transport and deposition areas) and the unaffected terrain are usually distinct, making it relatively simple for the geomorphologist to identify and map the landslide. This is particularly true for small, shallow landslides, such as soil slides or debris flows (Guzzetti et al., 2012).

2.5.3 Indexing or Pixel-based technique

This approach identifies landslides based on thresholds applied to individual pixels of remotely sensed imagery. These thresholds can be determined either manually (supervised) or automatically (unsupervised) and are designed to classify pixels as belonging to landslides or not (Novellino et al., 2024). The core assumption of these techniques is that landslides are more likely to occur under conditions that mirror past events. For instance, areas with similar vegetation loss, topographic characteristics, or soil moisture changes are flagged as susceptible to landslides (Novellino et al., 2024). This makes these methods particularly useful in areas where the triggering conditions for landslides are well understood.

Common parameters used in pixel-based mapping include indices such as the Normalized Difference Vegetation Index (NDVI), which helps detect vegetation loss often associated with landslides, as noted by Fiorucci et al. (2019). Additionally, topographic parameters such as slope, aspect, and curvature, as described by Scheip and Wegmann (2021), are critical in identifying unstable terrain. SAR data, specifically backscatter values, are also utilized for detecting changes in surface roughness and soil moisture, as highlighted by Burrows et al. (2020). These parameters are widely available in remote sensing datasets, making the pixel-based approach versatile and applicable across different landscapes.

Despite its advantages, pixel-based techniques involve significant human intervention, particularly in selecting the parameters and defining the threshold values. This introduces a level of subjectivity, which can influence the accuracy and reproducibility of the results. Furthermore, these methods often struggle with the “salt-and-pepper effect”, where individual pixels are classified as landslides in isolation, leading to a scattered or noisy output (Holbling et al., 2017). Although post-processing filters can reduce this effect, it remains a limitation, especially in areas with heterogeneous landscapes.

2.5.4 Object-based Image Analysis (OBIA)

While the pixel-based method uses the spectral information of single pixels and has been successfully used to map landslides (Mondini et al., 2017, 2011; Nichol and Wong, 2005), OBIA uses segmentation to convert homogenous pixels into objects (Amatya et al., 2021). These objects are defined by their shared spectral, textural, morphological, and topographical characteristics. By moving away from artificial square cells, segmentation provides a more realistic representation of landscape features, addressing one of the key limitations of pixel-based methods (Novellino et al., 2024). Landslide detection using OBIA consists of two

important steps - segmentation and classification (Amatya et al., 2019). The main challenge in implementing a segmentation algorithm is determining the segmentation parameters that defines the size of the objects (Martha et al., 2012). The goal of image segmentation is to produce objects that are internally homogenous and externally heterogenous from its neighbours (Espindola et al., 2006). OBIA divides the image into segments or "objects" based on their spectral, spatial, and textural characteristics, such as colour, shape, size, and texture. These segments represent homogeneous areas in the imagery, which could either be parts of a landslide or a stable terrain (Martha et al., 2012). After the segmentation, the algorithm is trained to classify the objects into different land cover types or features (Figure 2.6).

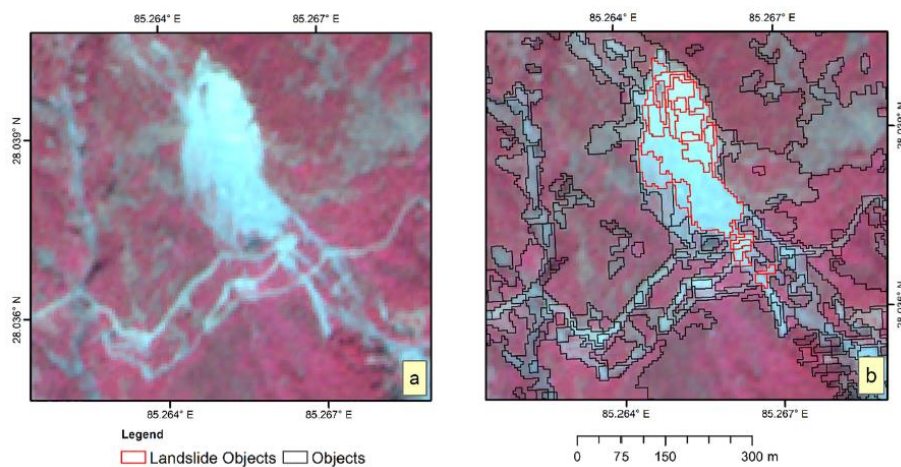


Figure 2.6: a) landslide in study area b) segmented objects (Credit: Amatya et al., 2021)

For landslide mapping, it can distinguish between landslide-affected areas and stable terrain by analysing the features of the objects, such as slope, soil texture, and surface roughness (Martha et al., 2012). The segmentation rulesets are then developed using site-specific characteristics and manual thresholding of diagnostic features such as slope and elevation (Novellino et al., 2024). Various studies have applied OBIA in mapping landslides around the world, e.g. Amatya et al. (2019, 2021) Martha et al. (2012, 2016), Rau et al. (2014) and Sun et al. (2017). However, Stumpf and Kerle (2011) tested various landslide diagnostic features in different part of the world and found it to be site specific. Thus, various features must be segmented for each site studied as rule-based approaches like the OBIA provide very limited transferability.

2.5.5 Change detection approach

This approach relies on fundamental principles of image interpretation to identify and map landslide events by comparing imagery from before and after a triggering event, such as heavy

rainfall or seismic activity (Novellino et al., 2024). The mapping is performed manually or automatically using advanced tools like Google Earth Engine, where analysts look for distinctive geomorphological features associated with landslides, such as scarps, trenches, bulging toes, and double ridges, which indicate slope failures and subsequent ground displacement (Psomiadis et al., 2020). Typically, this method involves the use of pre- and post-event imagery to detect and map changes caused by landslides. For example, an analyst might compare satellite or aerial images from before a heavy rainfall event with those captured afterward to locate newly formed landslides (Novellino et al., 2024). The differences in terrain, surface features, or vegetation patterns between the two time points help identify areas affected by slope failures. Studies such as Psomiadis et al. (2020), have demonstrated the effectiveness of this approach for detailed landslide mapping in specific areas. However, while the change detection approach was widely adopted during the 2000s and early 2010s, particularly when high-resolution imagery became more accessible, it has notable limitations (Novellino et al., 2024). Specifically, the process is time-consuming and labour-intensive, making it unsuitable for mapping landslides across large spatial extents or regions with frequent or widespread landslide activity. Additionally, the accuracy of this approach depends on the availability of high-resolution imagery, as coarse-resolution images may not capture the fine-scale change features necessary for identifying landslides (Novellino et al., 2024). Furthermore, the method involves a degree of subjectivity since it relies on human interpretation, which can vary depending on the analyst's experience and expertise.

2.5.6 Artificial Intelligence (AI)

The rise of AI in this domain is largely attributed to the growing availability of satellite data over recent years. AI-based approaches leverage this abundance of data to train models capable of automatically identifying landslides by learning patterns from a combination of diverse features. These features include both the causes and effects of landslides, such as scarps, vegetation loss, geological factors, slope steepness, weather conditions, and satellite imagery (Novellino et al., 2024). By analyzing these features together, AI models can effectively map landslides without requiring predefined physical or numerical models.

The AI training process is fundamentally data-driven, relying on relationships learnt between existing landslide inventories and derived features (Novellino et al., 2024). This adaptability eliminates the need for strict physical equations or rules, allowing AI systems to generalize based on patterns present in the data. Studies, such as Prakash et al. (2020), have shown that

AI-based techniques offer better accuracy compared to traditional methods, making them one of the most promising approaches for landslide detection. Since 2020, AI has become the dominant technique in landslide mapping, demonstrating significant advancements in both precision and efficiency (Novellino et al., 2024).

While earlier data-driven algorithms like principal component analysis (Đurić et al., 2017) and maximum likelihood classification (Modini et al., 2017) have been applied to landslide mapping, there has been a notable shift toward deep learning models such as the U-Net Convolutional Neural Network (CNN). U-Net, in particular, has gained prominence for its ability to perform automatic image segmentation by classifying individual pixels as either landslide or non-landslide (Novellino et al., 2024). Unlike traditional neural networks, U-Net is highly flexible and can work with both small datasets (e.g., hundreds of landslide events) and large-scale datasets, making it ideal for diverse applications. By extracting the most effective features from input imagery, U-Net models provide highly accurate results for landslide mapping (Amankwah et al., 2022). Despite their potential, AI methods do have limitations. Most AI techniques, including U-Net, require large, high-quality training datasets to achieve optimal performance. Additionally, the computational power needed for training and processing deep learning models can be significant, which may limit their accessibility for some users or regions (Novellino et al., 2024).

The following sections discuss two main tools that have been used in the application of these techniques in landslide mapping. These tools are freely accessible and are particularly valuable for rapid landslide mapping, playing a critical role in supporting swift disaster response efforts. By providing timely and accurate information, these tools enable emergency teams to identify hazardous areas, prioritize rescue operations, and allocate resources effectively, ultimately reducing the impact of landslide disasters on affected communities.

2.6 Google Earth Engine (GEE)

Google Earth Engine (GEE) is a cloud-based platform designed for planetary-scale geospatial analysis. It allows users to access large collections of satellite imagery and real-time environmental data without the need for local computing resources (Notti et al., 2023). This platform supports a range of data formats, including optical, radar, and elevation data, making it particularly suitable for multi-sensor landslide mapping (Handwerger et al., 2022). It amplifies geospatial analyses by improving the accessing and processing of geospatial data. GEE provides instant access to 37 years of satellite images, with many publicly available

geospatial datasets, including optical image collections (e.g., MODIS, Landsat, and Sentinel-2), SAR data from Sentinel-1, land cover classifications, and precipitation data (Notti et al., 2023).

A commonly used landslide mapping technique in GEE is the change detection approach, using multi-temporal images to create composites of the landscape (Notti et al., 2023). The advantage of multi-temporal images for change detection is that they reduce noise, compared with bi-temporal images, thus allowing for clearer visualisation of changes on the earth's surface (Handwerger et al., 2022). It also allows for the generation of a pre- and post-event image of the landscape, using different parameters peculiar for change analysis in each location (Nowak et al., 2021) to detect landslides. As landslides result in vegetation loss, GEE uses the Normalised Difference Vegetation Index (NDVI) for landslide detection and mapping. Thus, for optical images, it applies the greenest-pixel method which selects the maximum value NDVI pixel within the stack to produce an aggregate image (Notti et al., 2023). This effectively removes cloudy pixels and smoothens over temporarily reduced NDVI signals from agricultural activity.

For landslides, images showing the relative difference in the normalised difference vegetation index (rdNDVI) calculated from cloud-free composites using Sentinel-2 or Landsat images can be used to map landslides (Lindsay et al., 2022). The versatility of this platform in geospatial analysis and monitoring landscape changes makes it a more preferred choice in landslide mapping as evident in various research e.g. Nowak et al. (2021), Notti et al. (2023) and Lindsay et al. (2022) among others. These studies indicate that manual or automated landslide detection could be significantly improved with multi-temporal image composites using freely available earth observation images from GEE (Lindsay et al., 2022), as it allows the replication of this method in new areas, which can be helpful for reducing spatial bias in landslide databases.

In GEE, two other commonly used algorithms for landslide detection are the SLIP (Sudden Landslide Identification Product) and the DRIP (Detecting Real-Time Increased Precipitation) models (Fayne et al., 2019). These algorithms work together to identify landslides leveraging a range of geospatial datasets to provide accurate and reproducible results. SLIP utilizes optical data from the Landsat-8 Operational Land Imager sensor, elevation data from the Shuttle Radar Topography Mission (SRTM), and precipitation data from the Global Precipitation Measurement (GPM) mission (Fayne et al., 2019). It applies change detection algorithms to identify where landslides may have occurred based on vegetation loss, which is a key indicator of slope failures in vegetated regions. SLIP's ability to integrate multiple data sources makes it

a spatially customizable tool for landslide identification, providing reproducible results tailored to specific study areas.

DRIP, on the other hand, complements SLIP by identifying the timing of potential landslide events. It uses near-real-time precipitation data to detect extreme rainfall events and correlates them with SLIP's spatial landslide detections (Fayne et al., 2019). This model provides suggested dates for landslide occurrences, helping refine the temporal accuracy of SLIP detections. Additionally, DRIP's capability to identify extreme rainfall in near-real time enhances its utility in forecasting and disaster management by suggesting where potential landslide-prone areas may be located (Fayne et al., 2019).

Together, SLIP and DRIP form a powerful combination for landslide detection, combining spatial and temporal analysis to improve the accuracy and reliability of landslide mapping efforts. These models showcase the potential of GEE in integrating multi-sensor datasets for hazard detection and monitoring.

2.7 HazMapper

HazMapper (Hazard Mapper) is an open-access application developed in Google Earth Engine for the rapid characterization of natural disasters (Scheip & Wegmann, 2021). It allows users to derive map and GIS-based products from Sentinel or Landsat datasets without the time and cost-intensive resources required for traditional analysis. While the underlying mathematics are not novel, HazMapper applies multi-spectral satellite data processing for the evaluation of natural hazards by leveraging the accessibility and computational power of Google Earth Engine (Scheip & Wegmann, 2021). HazMapper is useful for monitoring landscape changes that results in the removal or recovery of terrestrial vegetation associated with a natural disaster or human activities. Thus, the platform is not currently suitable for use in non-vegetated environments (e.g., polar, high-altitude, or desert regions).

The source code for HazMapper initiates data processing on remote servers without requiring any specialized or licensed software and can be performed on any internet-connected device (Scheip & Wegmann, 2021), allowing users to quickly evaluate spatially expansive hazards by panning or zooming without downloading any data. The user can modify some variables such as the dataset type (Landsat 7, Landsat 8, Sentinel-2), the event date (known date of the hazard occurrence), the pre-event and post-event time windows, maximum cloud cover for analysis, and the slope thresholds according to landscape type (Table 1).

Table 1: HazMapper input variables, definitions and examples. (Source: [Scheip & Wegmann, 2021](#)).

Input variables	Definition	Example
Dataset	Dataset to use for analysis, currently Landsat 7, Landsat 8, or Sentinel-2	Sentinel-2 (10 m) 2015+
Event date	Date of storm, earthquake, weather event, etc.	9 December 2016
Pre-event window	The number of months to use for observing the greenest pixel-by-pixel conditions prior to the event	12
Post-event window	The number of months to use for observing the greenest pixel-by-pixel conditions following the event	3
Maximum cloud cover	The maximum percentage of a scene obscured by clouds and still used in the analysis; the cloud-cover percent is embedded in the metadata for each Landsat or Sentinel scene	30
Slope threshold	A minimum topographic slope value in degrees, less than which will be omitted from the data visualization; this is helpful to remove water bodies like lakes and adjacent oceans in coastal regions	0.01

The layers on the interface can be toggled on/off and their transparency modified with a slider to help with visualization ([Scheip & Wegmann, 2021](#)). The data download function allows for the further analysis of processing results, including incorporation into emergency operation mapping platforms and advanced scientific analysis or visualization. The user can download the (1) rdNDVI image, (2) pre-event and (3) post-event greenest-pixel composite images, (4) elevation and hill shade images derived from the global 30m SRTM dataset, and/or (5) any user-digitized geometries delineating points or areas of interest ([Scheip & Wegmann, 2021](#)). These layers are downloaded as raster files or .kml for further analysis on Google Earth or GIS environment.

2.8 Summary

Landslides can occur in different ways whether they fall, flow, slide, spread, or topple depending on the terrain and what triggers them, like heavy rain, earthquakes, or even human activities. Each type behaves differently, but they all share one thing in common: they can cause serious damage to both the environment and infrastructure. All landslides, no matter how they occur, are a threat, thus understanding and mapping them correctly is crucial for minimizing their impact on the environment. Landslides also occur in a variety of environments ([Figure. 2.7](#)), characterized by either steep or gentle slope gradients, from mountain ranges to coastal cliffs, and even underwater ([Kirschbaum et al., 2010](#)).

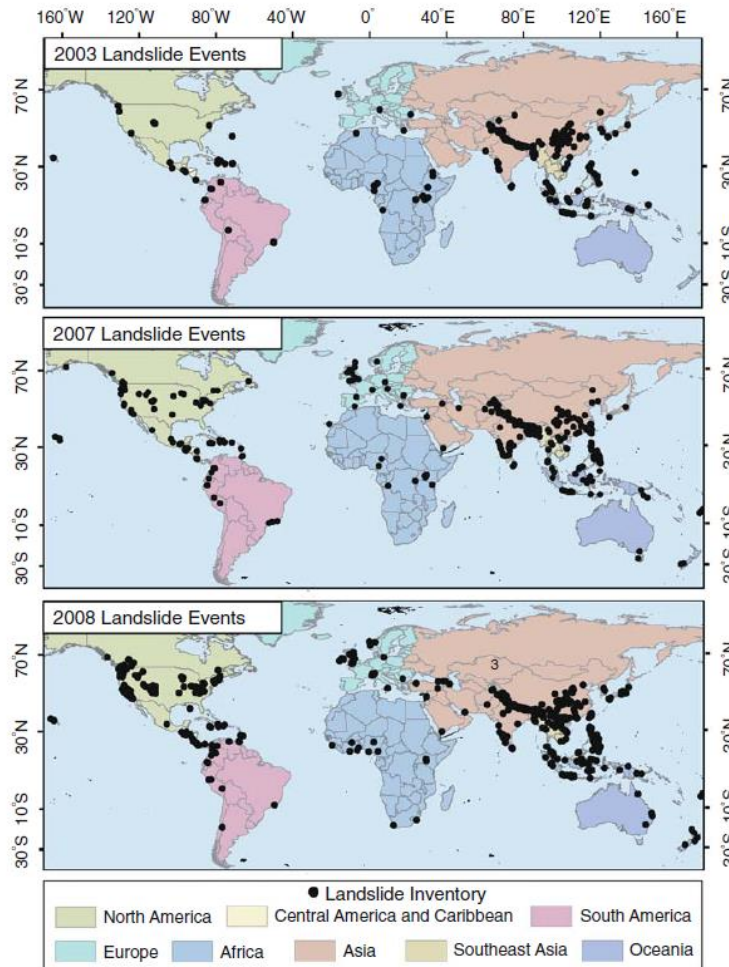


Figure 2.7: Global distribution of landslide occurrence between 2003-2008. (Credit: Kirschbaum et al., 2010)

Geologically, weathered rock, sheared, fissured, or jointed rock material, contrasting earth materials, and the low adhesiveness of the rock are known causes of landslides (Alexander, 1992). Morphologically, all forms of erosion, such as fluvial, wave, and glacial, along a slope may cause landslides and other types of flows, while deposition and weathering are also major triggers of landslides (Lee, 2007). In general, gravity has been known to be the primary driving force for a landslide (Kirschbaum et al., 2010). In many cases, the landslide is triggered by a specific event such as a heavy rainfall, an earthquake, a volcanic eruption, a slope cut to build a road, or other human activities exposing the surface of the earth (Zhong et al., 2019). However, one factor is commonly present in all landslide occurrence – the presence of moisture on the landscape (Lee, 2007).

Given the widespread occurrence of landslides across different regions and terrains, it becomes essential to develop effective ways to understand and monitor them. In some cases, landslides may not have distinguishable spectral, spatial, or temporal characteristics, as they may be

covered by other land cover types (Amatya et al. 2019). Also, the surface features of a landslide can vary greatly, affected by the different geological, geomorphological, and hydrological factors as well as weather conditions, and other factors. These differences in the surface features are often remarkable and non-negligible, and thus it is difficult to identify a landslide with only a few simple criteria (Martha et al., 2012).

Thus, satellite imagery is considered as one viable tool for landslide detection and mapping using primarily aerial and satellite optical imagery interpreted visually or processed by semi-automatic or automatic procedures or algorithms (Mondini et al., 2021). While previous methods discussed above have demonstrated effectiveness, they also present certain limitations in mapping landslides. Comparisons have also been made between different satellite products and their ability to detect landslides. In a study conducted by Mondini et al. (2021), 48% of the case studies in 58 articles across 32 nations used SAR imagery to detect landslides in most geological settings. This is without limitation though as Nugroho et al. (2021) asserted that utilising SAR requires large amounts of data downloaded to the local system to be processed on a local computer. In their comparison between Sentinel-1 SAR and Sentinel-2 optical imagery using the Google Earth Engine (GEE) cloud-based computing system, Nugroho et al. (2021) concluded that Sentinel-2 imagery performed better in landslide detection compared to Sentinel-1.

Despite the robustness of satellite imagery in landslide mapping, slides and flows have been noted to be the most common landslide type analysed using EO data (Novellino et al., 2024). In a review comparing landslide mapping using EO data from 40 different satellites, Novellino et al. (2024) identified that slides and flows were analysed using 30 satellites, falls 6 satellites, complex landslides 3, and deep-seated gravitational slope deformation (DSGSD) one. This is because flows and slides remain the easiest types of landslides to detect from space mainly due to their size and characteristic shape of the landscape area affected (Novellino et al., 2024). Falls and topples are more challenging to identify unless high-resolution satellite data is available. This is due to their small footprint on the environment and tendency to occur on steep slopes which might be in the shadow of the satellite line of sight (Novellino et al., 2024). Conversely, DSGSD despite being large events are usually very slow and do not leave visible markers in the environment as vegetation can quickly cover the unstable area (Novellino et al., 2024).

Based on these findings and the limitations posed by certain landslide mapping techniques, landslide types, and the goal of this study to assess freely accessible EO-based tools for

landslide mapping, this study will evaluate three freely accessible rapid landslide mapping approaches, focusing on their accuracy and replicability across different regions in terms of topography and landslide types. This comparative analysis of the selected techniques will not only assess their performance in mapping landslides but also emphasize their potential applicability in regions with diverse environmental conditions and landslide types. Moreover, because the focus of this study is on rapid landslide mapping approaches to aid emergency disaster response strategies within days to weeks following a landslide event, newer landslides with visible scars on the landscape will be primarily considered.

3 Research Methods

3.1 Study area

This study employs a three-tiered approach to evaluate and validate rapid landslide mapping techniques across different landscapes using three distinct study areas – primary, secondary and tertiary, to ensure the comprehensive evaluation and robustness of the results. These distinct study areas were selected because of the difference in terrain types and landslides present in these areas, to satisfy the goal of this research which as stated earlier, is to identify a rapid landslide mapping technique using EO data, that is universally acceptable, adaptable, and reliable across all terrains, thereby ensuring more effective landslide detection regardless of local constraints.

3.1.1 Glengyle

The primary study area of this research is Glengyle, a low valley plain in Western Stirling, Scotland, United Kingdom precisely at 56° 17' 9.09" N and 4° 40' 58.25" ([Figure 3.1](#)). It lies in the northwest shore of the Loch Katrine, a freshwater lake that plays significant role in the supply of drinking water to Glasgow and the Glengyle distillery ([Gilen, 2013](#)). Situated in the Scottish Highlands, a region renowned for its complex geological history shaped by tectonic movement, volcanic activity and glaciation ([Ballantyne & Gordon, 2021](#)), it is said to be prominently dominated by slopes of the Silurian formation ([Gilen, 2013](#)). This area lies near the Highland boundary fault which demarcates the transition between the ancient metamorphic rocks of the highlands and the ancient sedimentary rocks of the lowlands ([Ballantyne & Gordon, 2021](#)).

The general landscape of Britain has been classified into a series of Quaternary Domains that reflects a combination of the landscape morphology, assemblages of superficial sediment and the range of Quaternary geological processes that has shaped its formation ([Booth et al., 2015](#)). Glengyle falls within the ‘mountain and valley’ sub-domain in the glaciated province which refers to landscapes that have been modified by successive glaciations and accelerated paraglacial processes ([Ballantyne, 2002](#)). Landscapes in the mountain and valley domain comprises deeply dissected mountains and extensive upland plateaus, precipitous slopes, and glaciated troughs with lower slopes and valley bottoms filled with superficial sediments, variously reworked by river and slope processes ([Booth et al., 2015](#)). The valley bottom and

lower slope deposits consist of till, moraine and glaciofluvial sands and gravels (65%) that are highly variable, compact and commonly fissile (in areas of schist and slate bedrock) (Booth et al., 2015). Formed as a result of series of glaciated events, the high energy inputs from the very steep antecedent relief to the high precipitation and the powerful physical processes operating over the higher ground in this domain, a number of geomorphological processes are active and result in rock topples, severe debris flow activity, flash flood events landslips and other gravitational mass movement (Booth et al., 2015). Thus, these areas have been mapped as ‘*significantly susceptible*’ to landslides according to the BGS GeoSure landslide database of the United Kingdom (Figure 3.2).

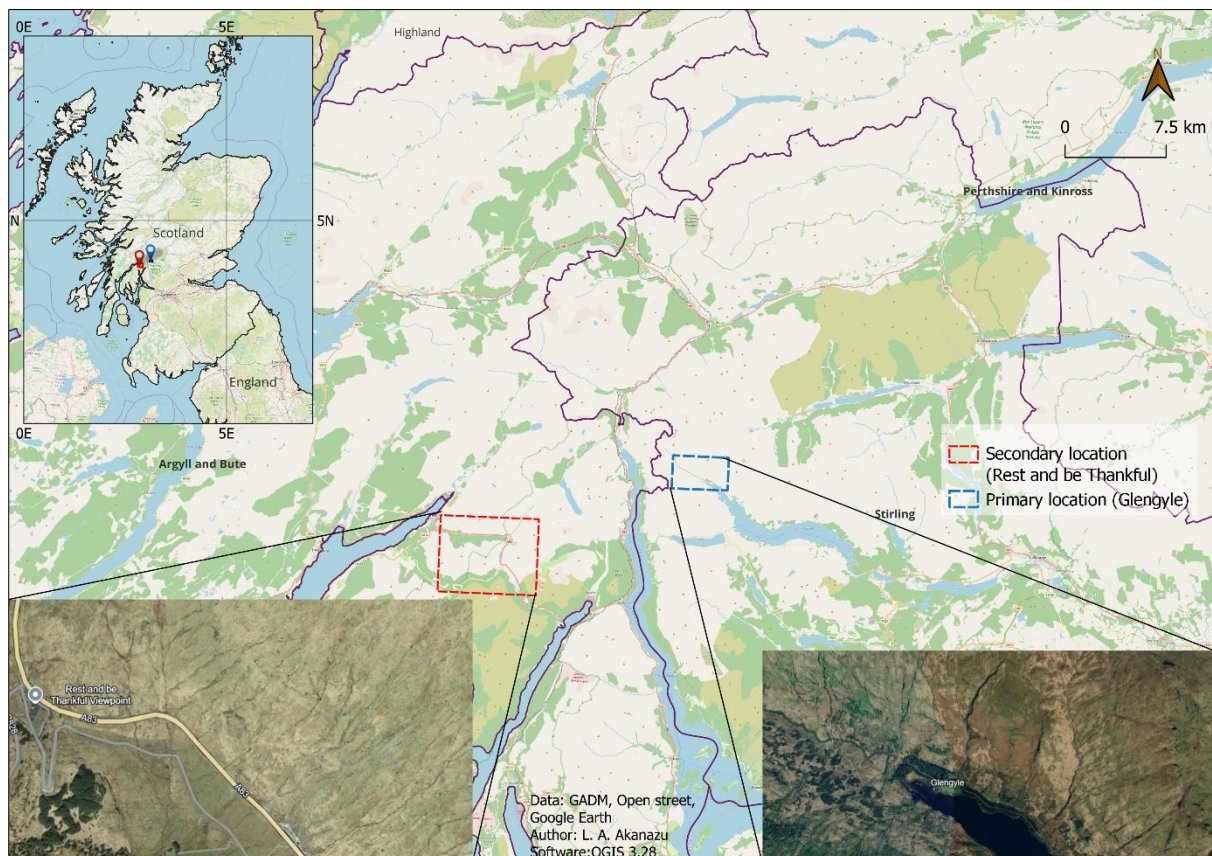


Figure 3.1: Map of Primary and Secondary study areas

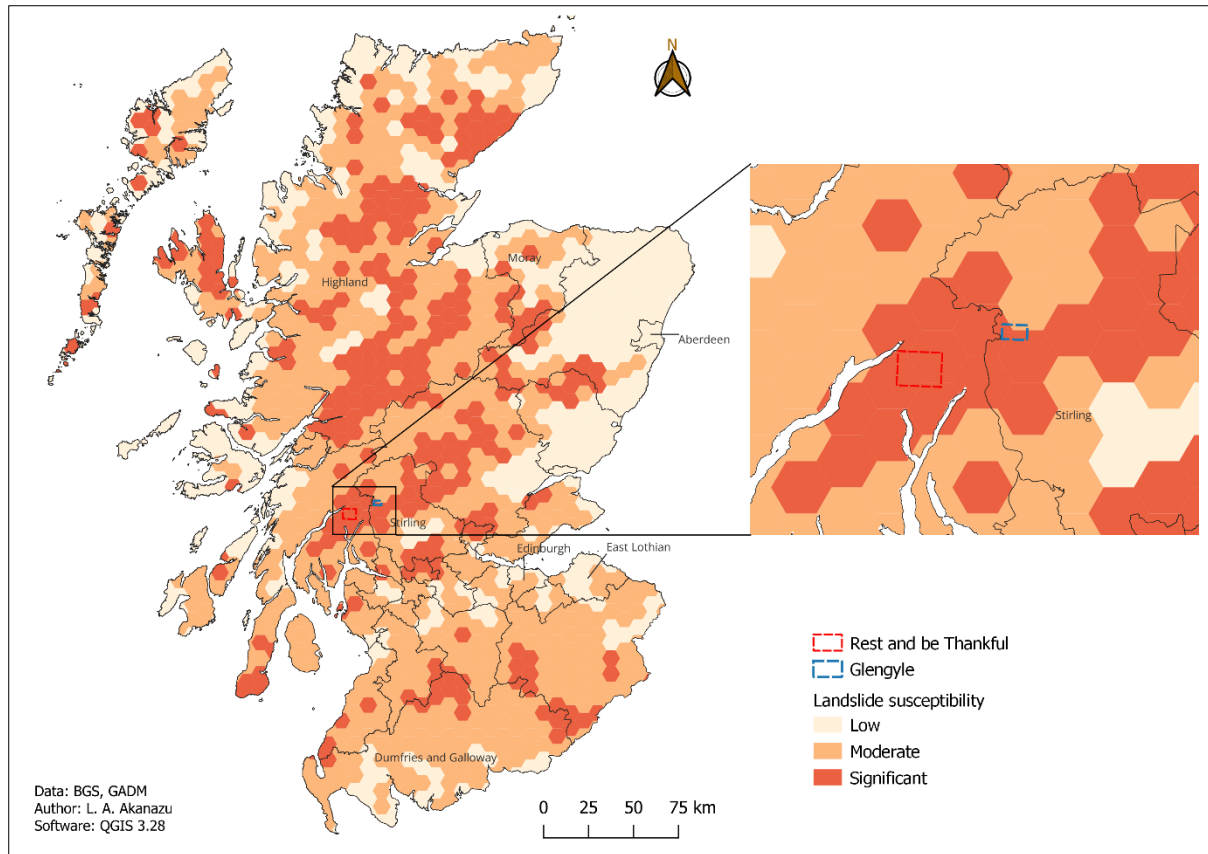


Figure 3.2: Primary and secondary study areas showing landslide susceptibility

Characterised by steep narrow U-shaped valleys carved by glaciers, Glengyle’s topography is often unstable and, when combined with heavy rainfall, can become prone to slope failure (Ballantyne & Gordon, 2021). Glengyle experiences a temperate maritime climate with high annual rainfall due to its location in the highlands, which acts as a barrier to moisture-laden winds from the Atlantic Ocean (Ballantyne, 2019). The frequent and intense rainfall significantly increases the likelihood of rainfall-triggered landslides, as water infiltrates the soil and rock, reducing slope stability (Palamakumbura et al., 2021). This vulnerability and the high occurrence of landslides made this location a compelling choice for this study.

3.1.2 Rest and be Thankful

Deriving its name from travellers who would stop, rest and be thankful for reaching the top of their climb, the secondary study area Rest and Be Thankful valley is located on the A83 in Argyll and Bute, between Arrochar and Inveraray (Figure 3.1). The stretch of road is over 240 metres above sea level and passes through Glen Croe (BEAR Scotland, 2020). The main slope at the Rest and be Thankful sits at a gradient of 32°–33° with some slope regions towards the top of the slope more than 40° (Sparkes et al., 2017). The underlying slope is comprised

principally of fine-grained schists such as perlite, with an overlying cover of glaciogenic sediment and soil up to several metres in thickness (Sparkes et al., 2017). Some exposures of schist on the slope appear to be highly weathered and extremely degraded and therefore represent a likely source of progressive pedogenesis, therefore altering the hydraulic transmissivity of the soil over time and contributing towards reductions in shear strength, termed ‘ripening’ by Nettleton et al. (2004). The cross profile of the landscape plotted by Sparkes et al., (2017) shows a large concavity which characterises the top of the slope. This topographic depression appears to concentrate drainage towards the centre of the slope, as opposed to the convex margins where bedrock outcrops are more common. Such convergence of hydrogeological flow would explain the greater propensity of slope failures in this location as discussed in section 2.2.1 above.

It has also been classified in the ‘mountain and valley’ sub-domain but with slightly higher slope angles consisting of glacially eroded troughs scouring the valley bottom to form U-shaped valleys (Winter et al., 2024). The UK National Landslide Database (NLD) (Foster et al., 2012) also indicates that although the ‘Mountain and Valley’ domain is five times larger than the ‘Ice-scoured Montane’ domain, it contains almost 30 times more recorded debris flows events. Due to its location in the landslide active sub-domain, around 20 debris flows have been recorded at the Rest and be Thankful since 2007, resulting in around 11 road closures, equating to an average of roughly one road closure per year (Sparkes et al., 2017). More so, Argyll & Bute is one of the wettest areas of the UK, thus contributing significantly to the rate of slope activity in this location (Sparkes et al., 2017).

3.1.3 Dörtyol

The third study area is Dörtyol, located in the South of Türkiye at the northern edge of the province Hatay, some 80km north of Antakya (Figure 3.3). Bounded by the Amanos Mountains to the East and the Mediterranean Sea to the West, the plain elevations range from 0 to 200 m above sea level, but a 20m high vertical step interrupts the smooth plain close to the southwest coast (Brehme et al., 2011). This area comprises of two major geological sections - the Precambrian to Mesozoic units of the Amanos Mountains and the quaternary deposits on the coastal plain (Brehme et al., 2011). The oldest units are elastic rocks from Precambrian and Palaeozoic while the Mesozoic units are mostly limestones (Brehme et al., 2011). The transition zone to the coastal plain is composed of serpentinites while a cross-section through the plain

shows tertiary conglomerates underlying the quaternary alluvium (Turkmen et al., 1974), with the coastal plain characterised by seasonal and perennial marsh (Brehme et al., 2011).

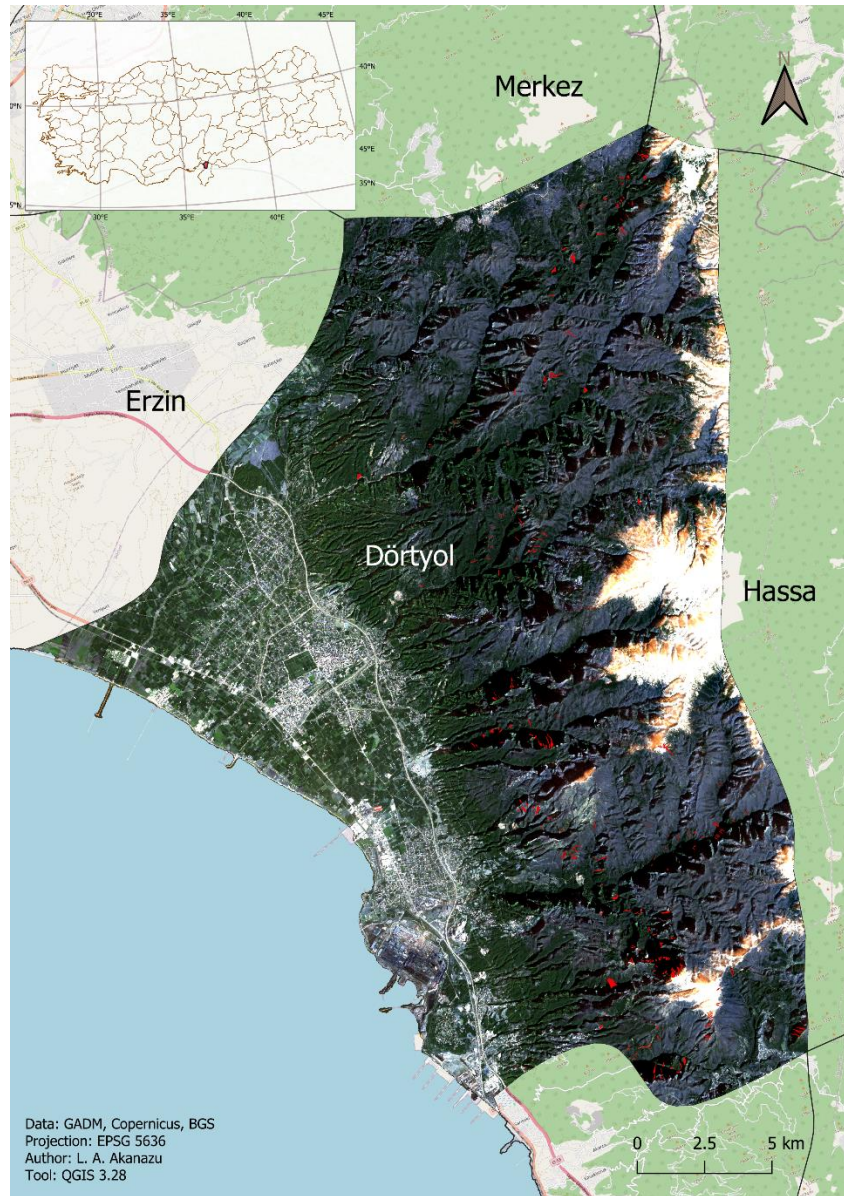


Figure 3.3 Tertiary study area – Dörtyol with landslides shown in red polygons

Türkiye and its surroundings, which are exposed to compressional tectonic processes under the influence of the Eurasian, Arabian and African plates, are located on the highly seismically active Anatolian plate, where major earthquakes have occurred throughout history (McKenzie 1972; Şengör and Yilmaz 1981). The most crucial fault zones in the Anatolian region are The North Anatolian Fault Zone (NAFZ) and the East Anatolian Fault Zone (EAFZ), which show strike-slip characteristics (Brehme et al., 2011). These fault zones cause the movement of the Anatolian plate to the West in a counterclockwise direction, and as a result of this activity,

destructive earthquakes have occurred in Anatolia and its immediate surroundings (Barka and Kadinsky-Cade 1988; Duman and Emre 2013). According to the records of the Disaster and Emergency Presidency of Türkiye (AFAD), on February 6, 2023, two earthquakes with magnitudes of 7.7 (focal depth=8.6 km) and 7.6 (focal depth=7 km) occurred at 04:17 (GMT+3) and approximately 9 hours later at 13:24, respectively. As a result of the earthquakes, damages were experienced in the provinces and districts of Kahramanmaraş, Hatay, Gaziantep, Adiyaman, Malatya, Kilis, Adana, Diyarbakir, Osmaniye, Elazig, and Sanliurfa affecting a total population of more than 15 million people (AFAD 2023). Between these two severe earthquakes, one more aftershock with a moment magnitude of 6.6 occurred at the epicentre of Nurdagi District of Gaziantep. That aftershock has been the largest recorded in the region. Afterward, another aftershock with a magnitude of 6.4 occurred in Yayladagi district of Hatay province on February 20, 2023, at 20:04 (GMT+3) (AFAD 2023) which triggered several co-seismic landslides in Hatay.

This site was chosen in Turkey because the province of Hatay where this location lies had the most landslides (according to the BGS landslide inventory) totalling 275 pre- and co-seismic landslides, the most recorded in a single location. Due to its unique topography comprising of low plains in the West and elevated plateau to the East, most of the landslide occurrence in this region typically occur in the East (Appendix I) with the most common landslide types being slides and rockfalls (AFAD 2023). The complexities of these landslides make this location suitable to assess the performance of the best performing method in landslide mapping, to confirm if other types of landslides such as topples and rockfalls present in this region can be mapped even in complex terrains different from the primary study area.

3.1.4 Rationale for selection

The selection of the three locations for this study was designed to systematically evaluate the performance, consistency, and generalizability of rapid landslide mapping methods under varying geological and environmental conditions. Owing to its high concentration of mapped debris flows, the primary area serves as the baseline for testing the methods to identify the optimum rapid landslide mapping approach. The secondary area, Rest and Be Thankful, was selected to evaluate the consistency of the best-performing method when applied to a new location with slightly different geology. This location experiences regular debris flow events triggered by seasonal rainfall, making it an ideal site to test the transferability of the detection thresholds and workflow derived from the primary area. This dual testing approach allows for

an evaluation of whether the selected method can consistently detect the same landslide type (debris flow) across locations with minor geological variations. By controlling for landslide type, the focus remains on testing the method's ability to adapt to differences in terrain geology and hydrology without introducing additional complexity. Successful detection in both areas demonstrates the robustness of the method for debris flows in diverse but related environments.

The tertiary study area was selected to evaluate the generalizability of the best-performing method to identifying different landslide types under different geological conditions. Unlike the primary and secondary areas, the tertiary area includes a range of landslide types (e.g., rock falls and slides) a different climate setting (temperate with dry and hot summers) and is characterized by distinct geological formations and triggering mechanisms (e.g., tectonic activity, rainfall, and anthropogenic disturbances). By applying the method to different landslide types, this phase evaluates whether the selected technique is capable of detecting other morphologies beyond debris flows, addressing its applicability to diverse landslide types. The geological differences between the tertiary area and the other study areas allow for an assessment of the method's potential for universal application in regions with varying terrain and environmental conditions. Success in this area indicates that the method is not overly specialized to specific conditions but has the versatility needed for broader usage. This strategy of progressing from controlled to diverse environments ensures a rigorous assessment of the best-performing method, ensuring that the findings are not limited to a single landslide type or geological setting, providing insights into the method's performance under real-world complexities, and its potential for widespread adoption.

3.2 Data

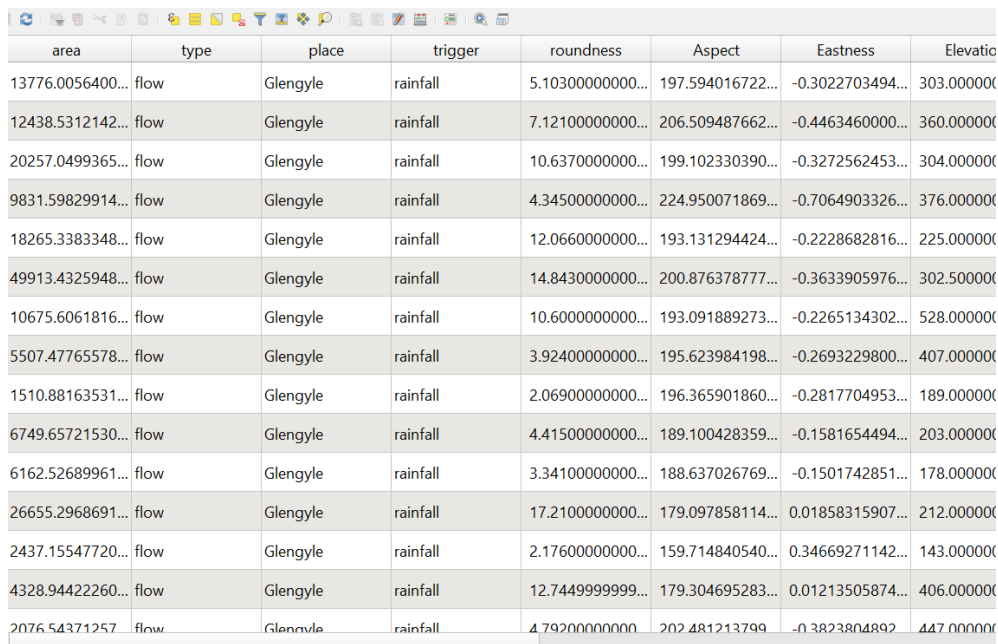
3.2.1 Satellite imagery

This study uses Sentinel-2 harmonized imagery from the Copernicus constellation. Sentinel-2 has a high visit frequency of every 5 days across the equator, enabling the monitoring of dynamic events such as landslides, through observing changes before and after events. With a spatial resolution of 10m, it allows for the detailed mapping of subtle land changes, such as vegetation cover (Fayne et al., 2019) that might indicate a potential landslide event on the landscape. The harmonized data from the Sentinel-2 in GEE was used because it is pre-processed with atmospheric correction which ensures consistency across different dates, in this case, before and after a landslide event. It also ensures consistency in data quality and accuracy, which is vital for comparative analyses across different time periods and regions. The Sentinel-

2 satellite imagery was also used in the manual mapping technique ([Appendix II](#)) to delineate the landslide polygons following the visible scars on the landscape. This consistency is particularly important in validating the findings of this research and assessing the performance of different landslide mapping techniques.

3.2.2 Landslide inventory

The landslide inventory compiled manually by BGS provides a comprehensive dataset of landslide occurrences across various locations, including our study areas. This shapefile, consisting of polygons representing individual landslides, has attributes such as landslide type, triggering factors, slope angle, elevation, geographic location, and the area of coverage ([Figure 3.4](#)). These details make the inventory particularly useful for our study, as they offer valuable ground truth data for validating the performance and accuracy of the landslide mapping techniques compared in this study.



area	type	place	trigger	roundness	Aspect	Eastness	Elevatic
13776.0056400...	flow	Glengyle	rainfall	5.10300000000...	197.594016722...	-0.3022703494...	303.000000
12438.5312142...	flow	Glengyle	rainfall	7.12100000000...	206.509487662...	-0.4463460000...	360.000000
20257.0499365...	flow	Glengyle	rainfall	10.63700000000...	199.102330390...	-0.3272562453...	304.000000
9831.59829914...	flow	Glengyle	rainfall	4.34500000000...	224.950071869...	-0.7064903326...	376.000000
18265.3383348...	flow	Glengyle	rainfall	12.06600000000...	193.131294424...	-0.2228682816...	225.000000
49913.4325948...	flow	Glengyle	rainfall	14.84300000000...	200.876378777...	-0.3633905976...	302.500000
10675.6061816...	flow	Glengyle	rainfall	10.60000000000...	193.091889273...	-0.2265134302...	528.000000
5507.47765578...	flow	Glengyle	rainfall	3.92400000000...	195.623984198...	-0.2693229800...	407.000000
1510.88163531...	flow	Glengyle	rainfall	2.06900000000...	196.365901860...	-0.2817704953...	189.000000
6749.65721530...	flow	Glengyle	rainfall	4.41500000000...	189.100428359...	-0.1581654494...	203.000000
6162.52689961...	flow	Glengyle	rainfall	3.34100000000...	188.637026769...	-0.1501742851...	178.000000
26655.2968691...	flow	Glengyle	rainfall	17.21000000000...	179.097858114...	0.01858315907...	212.000000
2437.15547720...	flow	Glengyle	rainfall	2.17600000000...	159.714840540...	0.34669271142...	143.000000
4328.94422260...	flow	Glengyle	rainfall	12.7449999999...	179.304695283...	0.01213505874...	406.000000
2076.54371257...	flow	Glengyle	rainfall	4.79200000000...	202.481213799...	-0.3823804892...	447.000000

Figure 3.4: Screenshot of the attribute table of the landslide inventory

The inventory's broad coverage and thorough documentation ensure that a diverse range of landslide events is captured, giving us a strong foundation to compare our results with. The fact that this inventory was manually mapped by BGS adds an additional layer of reliability, as human experts carefully identified and outlined landslide boundaries. This inventory for the three study locations chosen for this study was provided by BGS. The relevant data for the study areas was extracted using QGIS by filtering the relevant place names for e.g. 'Glengyle', utilizing it as a benchmark for evaluating our methods. This dataset enabled the assessment of

how well each technique, particularly the automated ones, performed in replicating or identifying the same landslides, ensuring that the accuracy of the research could be cross validated. Important to note is that the landslide type observed in the primary study area Glengyle is confirmed to be debris flow as seen in the landslide inventory (Figure 3.4). However, in the inventory for the tertiary study area Dorthyol, the landslide types were only classified as either pre-seismic or co-seismic slides (Appendix III) with no further differentiation between the landslide types (e.g. rockfalls or slides). The unavailability of this information limited the further analysis on this landscape to assess the performance of the optimal method in identifying specific types of landslides, and if some types are better identified than the others using this method. The only basis for the conclusion whether the method will identify other landslide types or not, is the knowledge according to AFAD (2023) that the common types of landslides in this location are slides and rockfalls.

3.3 Comparison of landslide mapping approaches

3.3.1 Manual Mapping technique

First, a manual mapping technique was employed using Sentinel-2 satellite imagery and Google Earth to detect and delineate landslides. This approach allowed for a more direct and detailed identification of landslides based on visual inspection of the landscape, capturing changes such as vegetation loss, scar faces, and other signs of terrain disruption typically associated with landslides. This method was considered particularly useful because the primary study area is on a small scale, and it is of interest to compare the efficiency of traditional mapping technique in landslide mapping. Creating a manual landslide inventory was necessary to evaluate the performance and limitations of traditional mapping techniques in comparison to automated methods in the study area. While the BGS inventory provided a reliable validation dataset, it was essential to develop a separate inventory to simulate a manual mapping workflow and assess its feasibility, accuracy, and efficiency when applied to the same region.

The Sentinel-2 satellite imagery with a spatial resolution of 10m was downloaded from the Copernicus website, capturing the region after a significant landslide event. The date range to access the data was set from August 6 2019, to October 30 2019 for an event date of August 5 2019. This window period was selected because of the limited availability of cloud-free images for the study area when the window period was constrained to just one month (August 2019). In QGIS software, the imagery was carefully analysed for visible indicators of landslides. The primary signs included large areas of vegetation loss, which was evident in the satellite data

where vibrant green areas turned to shades of brown or grey, indicating where the landscape had been stripped of vegetation. The visible landslide scars were delineated by creating polygons of landslides using QGIS tools.

To delineate the landslides, a threshold-based approach was used based on changes to vegetation. Using the identify tool in QGIS, pixels with values greater than 0.2 were selected as the value of the image pixels ranged from 0 (no vegetation loss) to 0.69 (severe vegetation loss). These represented areas where significant vegetation loss had occurred, corresponding to potential landslide zones. These pixels were manually digitized on QGIS to create polygons of landslides in the study area. To improve the mapping accuracy, the results were cross-referenced using Google Earth imagery. Google Earth allowed for a closer inspection of the terrain, providing a high-resolution, near-ground view of the areas identified as landslides in the Sentinel-2 imagery. This comparison helped verify that the changes detected in the satellite images, such as bare slopes or scar faces, were indeed associated with landslide events. The combination of both tools provided a more comprehensive validation, ensuring that the manual delineation was both precise and accurate.

The spatial distribution of the landslides, concentrated along steeper slopes, was further validated using SRTM imagery, which provided topographic data to confirm the correlation between landslides and slope steepness. This demonstrated the significant influence of terrain on landslide occurrence, highlighting that steep slope, particularly those with gradients above 15 degrees, were most susceptible to slope failures.

3.3.2 HazMapper

Traditional remote sensing landslide mapping is performed by observing changes in aerial photographs (e.g., [Malamud et al., 2004](#)) which relies on a single pre- and post-event scenes that could be hampered when unfavourable atmospheric conditions exists ([Scheip & Wegmann, 2021](#)) for example rainfall triggering mass wasting or volcanic eruptions. To overcome this challenge caused by atmospheric conditions, HazMapper capitalizes on a technique within Google Earth Engine to generate and perform calculations on a greenest-pixel composite. This compositing method utilizes data from many images, reducing noise present from clouds and other aerosol particles in a given single image. The greenest-pixel composite is a single composite or tiled image generated from all images within the user-defined pre- and post-event window that records the pixel with the highest NDVI result, or the “greenest” pixel ([Eq. 1](#)).

$$NDVI = \left(\frac{NIR - Red}{NIR + Red} \right), \quad (1)$$

where NIR is the near-infrared response and Red is the visible red band.

HazMapper relies on a relative difference in the NDVI technique (rdNDVI, Eq. 2). Instead of differencing true colour composites (i.e., red, green, and blue bands), HazMapper exploits changes in surface vegetation by developing and differencing an NDVI band from the greenest-pixel composite images:

$$rdNDVI = \left(\frac{NDVI_{post} - NDVI_{pre}}{\sqrt{NDVI_{pre} + NDVI_{post}}} \right) \times 100, \quad (2)$$

where $NDVI_{pre}$ and $NDVI_{post}$ are the NDVI images of the pre- and post-event greenest-pixel composites, respectively. The results of the processing routine indicate a normalized percentage of the NDVI gained or lost. The result is an illustration of the areas on the landscape that have either gained (increase in NDVI pixel values) or lost (decrease in NDVI pixel values) vegetation across the event as constrained by the pre-event window and post-event window date ranges. The three resulting data layers (greenest-pixel composite from pre- and post-event and rdNDVI) and SRTM-derived 30m resolution hill shade layer are added to the standard layer pane.

Recognizing that in forested areas landslides denude the landscape of vegetation, NDVI change detection methods have been used for identifying landslides in many mid-latitude regions (Huang et al., 2020; Tsai et al., 2010; Mondini et al., 2011; Lu et al., 2019; Yang et al., 2013). This approach was applied in this study using the NDVI to assess areas that have been affected by landslides. The landslide mapping process using HazMapper began by focusing on a known landslide event in Glengyle that occurred after a heavy rainfall on August 5, 2019, as reported by the [Daily Mail](#) on August 7, 2019. This event was chosen because it coincided with significant landslide activity in the study area. The satellite imagery window covered a period of 3 months before and after the event, allowing for a comprehensive analysis of the landscape before and after the rainfall-induced landslides.

To ensure clarity in the satellite data, the imagery used was filtered to have a maximum cloud cover of 10%, reducing the interference from clouds and providing a clearer view of the land surface. In addition, a slope threshold of 15° was applied during the mapping process. This specific slope angle was chosen based on research by Fan et al. (2017), which indicated that

landslides occurring in the Silurian layer (as found in our study area) are typically found on slopes with angles between 15° and 35°. The 15° threshold ensured that the focus remained on accounting for all areas with susceptibility to slope failure. Once these parameters were set, the HazMapper tool was used to identify potential landslide areas as revealed by vegetation loss according to the rdNDVI (Figure 3.5).

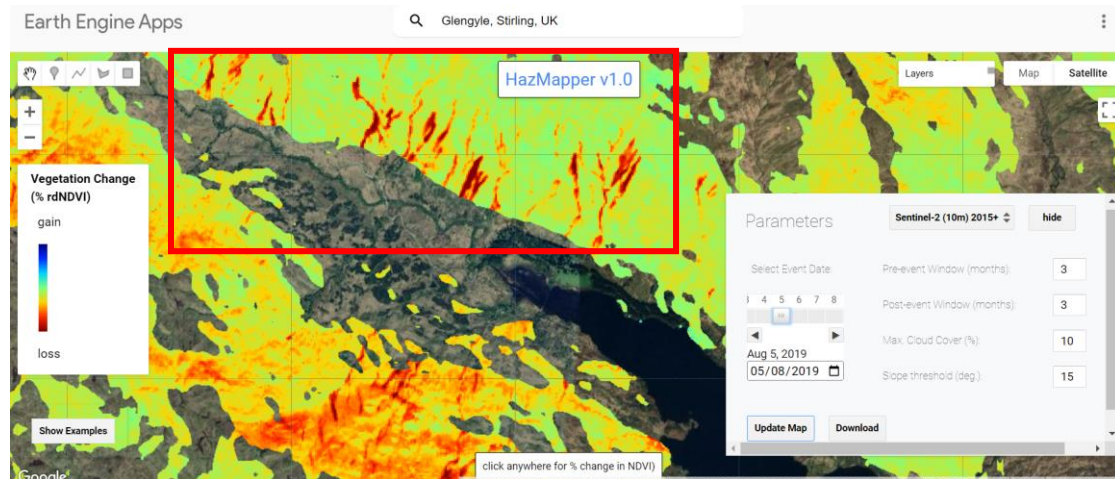


Figure 3.5 – Screenshot of HazMapper interface showing rdNDVI panel, visible landslide scar and panel to adjust parameters according to landscape.

The focus is on the visible landslide scars in Figure 3.5, showing obvious downslope movement materials. The output from HazMapper was downloaded as a raster image and imported into QGIS for further analysis, where it was overlaid with additional data to refine the landslide identification. The use of QGIS allowed for a more detailed analysis, including comparison with topographic data and other mapping layers, to ensure the identified landslides were accurately captured.

3.3.3 Google Earth Engine

The process of monitoring landslides using GEE involved a series of detailed steps, beginning with the acquisition and analysis of Sentinel-2 satellite imagery. In this study, the SLIP algorithm (discussed in section 2.6) was applied as it represents an important first attempt at developing an automated framework for medium-resolution regional landslide detection. An earth engine code developed by the BGS using the SLIP algorithm for landslide detection was adapted and modified to fit the specific study area. First, separate pre- and post-event image collections were produced by filtering the entire Sentinel-2 level 2A harmonised collection, by location and date. Next, the NDVI bands were added to all images in the filtered collection.

Then, ‘greenest pixel’ pre- and post-event composite images were created by taking the maximum NDVI value for each pixel, within the image collection, using the quality mosaic function. Finally, a difference image (rdNDVI) was produced by subtracting the pre-event composite from the post-event composite. For the event date of August 4 2019, four sets of dates were chosen for the satellite imagery to provide a robust temporal analysis: two dates for the start and end before the landslide event, and two dates for the start and end after the event. This allowed for a comparison of the landscape before and after the landslide occurred. These images were then processed into median composites, a method where multiple satellite images taken over a specific time period are combined (Figure 3.6). In each composite, the value of each pixel is determined by calculating the median reflectance value from all corresponding pixels across the images. This helps to reduce noise, such as temporary cloud cover, and provides a clearer image of the land surface both before and after the landslide.

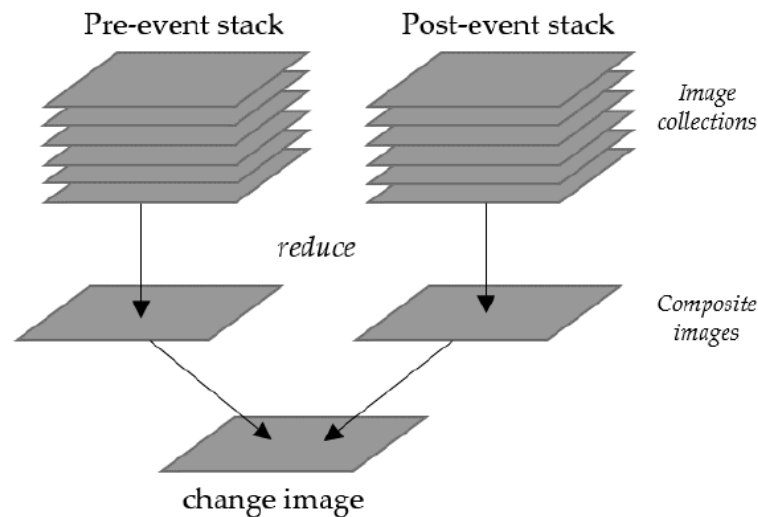


Figure 3.6 A schematic of composite image creation in GEE (Credit: [Lindsay et al., 2022](#))

A Digital Elevation Model (DEM) of the study area was added to the Sentinel-2 baseline collections, which were split into two sets: pre-event and post-event. This elevation data helped enhance the analysis by highlighting the slopes and terrain variations that could affect landslide occurrence. The median composites of these collections were used to identify significant changes in the landscape, particularly in areas where vegetation loss or soil disturbance was apparent. By assessing reflectance changes, the composites revealed the effects of the landslide event on the landscape, particularly in regions with steep slopes or altered vegetation cover.

To further refine the analysis, a landslide tracker image was generated. This tracker focused on key parameters such as vegetation loss, soil moisture, and slope angles—all crucial factors in

detecting and mapping landslides. By evaluating these variables, areas with significant changes were highlighted, indicating potential landslide occurrences. The resulting imagery provided a clear visualization of landslide-prone zones and areas where the event had the most substantial impact. Once the analysis was complete, the images and results were downloaded for further analysis in QGIS. This allowed for a detailed comparison of the identified landslide areas with other data, including manual delineations and ground-truth information, helping to verify the accuracy and completeness of the GEE mapping technique.

3.4 Data Pre-processing

The initial step in data processing involved creating a bounding box for the region of interest (ROI) by obtaining the coordinates for the study area using the *'bbox'* online tool to draw a rectangle around the areas of interest. Using a python code, the coordinates derived from the bounding box were converted into a shapefile of the study area to facilitate further analysis.

In GEE, the study area shapefile was added as the region of interest (roi) together with the SRTM data from the US Geological Survey. The SRTM was clipped to the roi, and the imagery filtered by selecting dates corresponding to pre- and post-event periods of landslide activity. A cloud-masking algorithm was applied to eliminate cloudy pixels, ensuring that only clear satellite data was used. Bands corresponding to the NDVI (red and NIR) were extracted, followed by the calculation of red reflectance changes, soil moisture variation, and NDVI changes. The resulting data were then binarized, classifying the landscape into areas of likely landslide occurrence and non-landslide zones.

3.5 Accuracy assessment

The accuracy of the three landslide mapping approaches—GEE, HazMapper, and manual delineation—was systematically evaluated by comparing their performance in identifying landslide occurrences using the landslide inventory of BGS. First, the results from all three methods were overlaid in QGIS for a visual comparison. This allowed for a side-by-side analysis of the spatial distribution of landslides identified by each method, providing an initial sense of how well they aligned.

To further quantify the differences between the methods, a differential analysis was performed. This involved subtracting the landslide image from the landslide inventory to highlight areas where their results did not match. Mismatched pixels—those representing landslides in one method but not in another—were visually inspected to understand where the method fell short

in detecting landslides. Furthermore, statistical matrices were generated to test the performance of each method in mapping landslides accurately.

3.5.1 Confusion Matrix

This matrix compared the predicted landslide occurrences against the actual occurrences recorded in the BGS landslide inventory. The confusion matrix was generated by converting the BGS landslide inventory to binary raster of 1 and 0, with every pixel outside the landslide polygon assigned the value 0, signifying no landslide occurrence. Because the manual technique had the landslides in vector format, these landslide polygons were also converted to raster pixels to enable the extraction of landslides from the BGS binary raster.

To polygonise the GEE landslide raster imageries to vector for overlay analysis, the values of the pixels in the areas with high vegetation loss were examined using the identify tool in QGIS, comparing the values between the areas of high and low vegetation loss. The raster value ranged between 0-255 so a threshold of 70 was chosen such that from 0-69 was reclassified to 0 (no landslide) while 70-255 was reclassified as 1 (landslide). For the HazMapper raster image, the value of the after-event raster image showed values ranging from -66 to 43, reflecting the changes in vegetation cover. To focus on potential landslide areas, the data was filtered and pixels with values between -23 and -66 were selected and classified as 1, indicating landslide occurrence, while all other values were set to 0. This filtering process allowed the isolation of areas where significant vegetation loss had occurred, pointing to slope failure.

The confusion matrix was calculated using the raster calculator to subtract the landslide values of the GEE/Manual/HazMapper raster from the BGS landslide raster in the following format:

True Positive (TP) = ("Model binary raster = 1") AND ("BGS binary raster = 1")

False Positive (FP) = ("Model binary raster = 1") AND ("BGS binary raster = 0")

True Negative (TN) = ("Model binary raster = 0") AND ("BGS binary raster = 0")

False Negative (FN) = ("Model binary raster = 0") AND ("BGS binary raster = 1")

The matrix helped in calculating key metrics such as true positives (correctly identified landslides), false positives (non-landslide areas identified as landslides), true negatives, and false negatives. Using the values from the confusion matrix, the accuracy and precision of each method were calculated, providing a detailed performance assessment.

3.5.2 Accuracy

Accuracy is a simple and widely used metric that provides an overall measure of the correctness of a classification model. In this context, accuracy helps determine how well each method identifies landslide events and distinguishes them from non-landslide areas, providing a baseline for comparing different techniques. Ranging between 0 and 1, higher accuracy generally indicates that the method is more reliable, but it should be interpreted alongside other metrics, especially in cases where the dataset is imbalanced (e.g., when non-landslide areas dominate the region). It is calculated with the formula:

$$\text{Accuracy} = \frac{\text{TP} + \text{TN}}{\text{TP} + \text{TN} + \text{FP} + \text{FN}} \quad (3)$$

where:

TP (True Positive): Correctly identified landslides (pixels correctly classified as landslides).

TN (True Negative): Correctly identified non-landslides (pixels correctly classified as non-landslides).

FP (False Positive): Non-landslides incorrectly classified as landslides.

FN (False Negative): Landslides incorrectly classified as non-landslides.

3.5.3 Kappa Coefficient

To assess whether the results of the mapping technique happened by chance (randomly) or due to the efficacy of the method applied, the Cohen's Kappa coefficient was calculated. This statistic measures the agreement between the detected landslide and the actual landslide beyond what would be expected by chance. In this case, the Kappa values were used to evaluate the agreement between the landslide areas and the ground-truth BGS landslide inventory. It is calculated using equation 3 below:

$$k = P_o - P_c / 1 - P_c \quad (4)$$

where:

P_o is proportion of correctly classified instances calculated as $\text{TP} + \text{TN} / N$; where N is the number of observations and TP and TN defined above.

P_c is the expected agreement that could occur by chance, calculated based on the marginal probabilities of the actual and predicted classes as;

$$P_c = ((TP+FN)*(TP+FP))/N^2 + ((FP+TN)*(FN+TN))/N^2$$

where:

(TP+FN) is the total number of actual positives.

(FP+TN) is the total number of actual negatives.

(TP+FP) is the total number of predicted positives.

(FN+TN) is the total number of predicted negatives.

These values were substituted in the Kappa's formula above to derive the Kappa value of each method applied in landslide mapping. The results usually range from 0 – 1 with 0 representing poor agreement between the method and the actual observation (indicating more occurrence by chance and not due to the method's efficacy), and 1 indicating stronger agreement reflecting the reliability of the mapping technique. Kappa values can therefore be interpreted as:

Table 2: Kappa values explained (Sim & Wright, 2005)

Kappa value	Interpretation
< 0.00	Poor agreement (worse than random chance)
0.00–0.20	Slight agreement
0.21–0.40	Fair agreement
0.41–0.60	Moderate agreement
0.61–0.80	Substantial agreement
0.81–1.00	Almost perfect agreement

However, Kappa has limitations which includes its sensitivity to class imbalance. For example, if non-landslide areas are more abundant in the binary raster, the Kappa value would be low even if the landslide areas have been correctly classified. This would result in a biased interpretation of the method's performance as low Kappa values indicates random performance due to chance and does not reflect the actual performance of the method. To overcome this potential bias, complementary statistics like the precision and the recall were further calculated to provide further evaluation to the methods' performance.

3.5.4 Precision

This metric measures the accuracy of the positive predictions made by the method by quantifying the proportion of the correctly predicted positive cases (landslides) out of all cases classified as positive by the method. It is calculated with the formula:

$$\text{Precision} = \frac{\text{TP}}{\text{TP} + \text{FP}} \quad (5)$$

Precision is a very important metric in this analysis especially as false positives carry significant consequences. In which case, a false positive may mean that areas mapped as landslides may not necessarily be at risk resulting in false alarm and waste of resources. The value of precision ranges between 0 and 1 with 1 indicating a perfect performance by the method in correctly identifying landslides. For example, a precision value of 0.7 means that the method's positive predictions are correct 70% of the time.

3.5.5 Recall

Recall measures how well the methods identify all positive cases, in this case, actual landslides. It does this by calculating the proportion of correctly identified landslides out of all the actual landslides both correctly and incorrectly classified. Ranging from 0-1, it estimates the correctness of the method in identifying actual landslides such that a recall value of 0.8 for example, means that method correctly identified 80% of actual landslides. It is calculated as:

$$\text{Recall} = \frac{\text{TP}}{\text{TP} + \text{FN}} \quad (6)$$

This metric is particularly useful in this case particularly as missed landslides could result in significant consequences, as it ensures that vulnerable areas are properly identified. Recall could be traded off with precision in some instances and the choice to choose between precision and recall depends on the application of the model. However, high recall is important in applications involving safety, but in this case, we aim to strike a balance between both metrics by calculating the F1 score to get a single measure that considers both aspects of each method's performance.

3.5.6 F1 Score

The F1 score is a performance metric for binary classification models as is evident in this study for landslides occurrence, that combines both the precision and recall of the model or method,

into one single metric. Used in situations where the costs of false alarms (false positives and false negatives) are not equal, this metric is best fit in this scenario as it helps us to determine the strength of each method tested. For the purpose of coherence and to identify the best performing method without bias, we assessed these methods using a single metric - the F1 score, rather than choosing between precision and recall or to trade off one for the other. By balancing precision and recall, the F1 score provides a comprehensive measure of model performance, ensuring fair evaluation in complex and imbalanced classification problems. The F1 score is calculated using the formula below:

$$\text{F1 Score} = 2 \times \frac{\text{precision} \times \text{recall}}{\text{precision} + \text{recall}} \quad (7)$$

The F1 score ranges between 0 and 1, with 1 ranked as the best possible score suggesting that the model performs well in identifying positive cases while minimizing both false positives and false negatives.

3.5.7 Validation

The comparison between the three methods provided a baseline to assess the accuracy of each method in detecting actual landslide occurrences. Following from the accuracy assessments by comparing the results from the GEE, manual delineation, and HazMapper methods, the results of these methods were validated using the BGS landslide inventory for the location. The method with the best performance (highest metric) was then applied to the secondary and tertiary study area to evaluate its effectiveness across a different landscape. Following the replication of the best performing method in the other landscapes, the performance metric of the method was also derived to compare the method's performance in these new landscapes, to ensure its robustness in terrain application and replicability. These subsequent replications on the secondary and tertiary landscapes were also validated using the BGS landslide inventory for these locations to compare the performance of the method in mapping landslide in these new locations.

4. Analysis and Results

4.1 Glengyle manual mapping results

From the manual mapping technique, a total of 54 landslides primarily debris flows were identified in the study area. These landslides were observed to run from the top to the bottom of the slopes in seemingly parallel lines, indicating a consistent downslope movement of material. This pattern is typical of gravity-driven landslide processes, where steeper gradients increase the likelihood of slope failure. When compared with SRTM imagery (Figure 4.1), the spatial distribution of the 54 landslides identified displayed a clear pattern along slopes with angles greater than 15°. The SRTM data, which provided detailed elevation information, confirmed that the majority of the detected landslides occurred in areas with significant topographic variation. The combination of steep slopes and the parallel arrangement of the landslide paths suggests that these areas are highly susceptible to slope failure due to gravitational forces acting on the loose or unstable material.

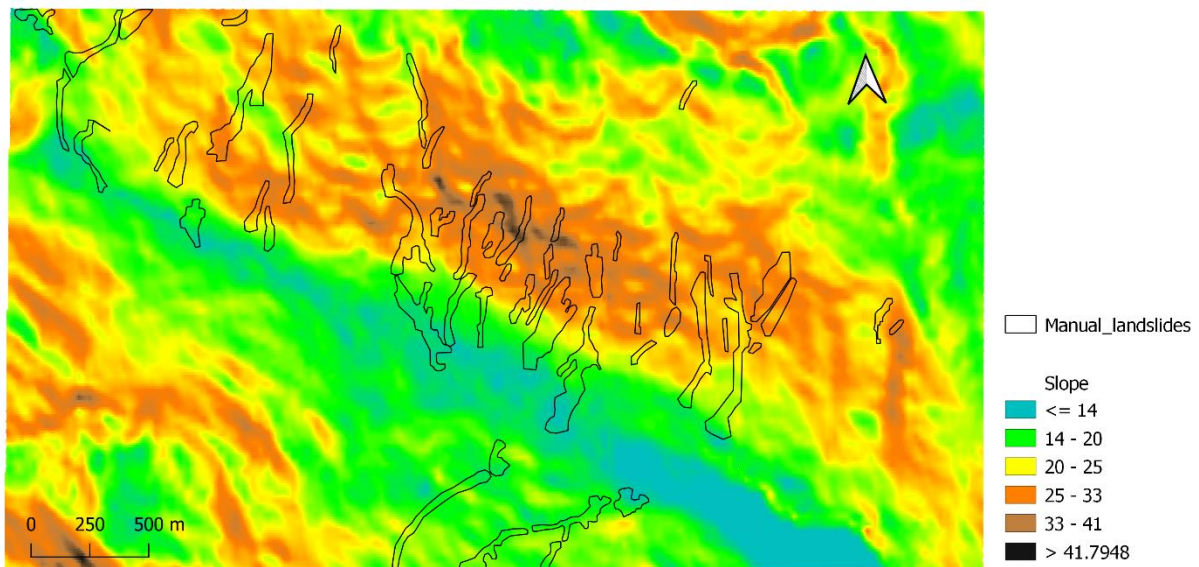


Figure 4.1 – Manually mapped landslides overlaid on SRTM imagery

The confusion matrix was generated for this method (Table 3) using the rasterised image of the manually delineated landslides.

Table 3: Confusion matrix for Glengyle manual mapping results

	Predicted landslide	Predicted no landslide
Actual landslide	0.53	0.18
Actual no landslide	0.09	0.20

From the confusion matrix, the metrics of accuracy for this method (Accuracy, Kappa value, precision, recall and F1 scores) were determined using equations 3, 4, 5, 6 and 7 above.

With an overall **accuracy of 0.73**, the manual method was able to correctly classify over half of the total observed landslides. This indicates that while some areas were successfully mapped, a significant portion of landslides went undetected, which highlights the need for more robust methods or improvements in manual mapping. On the other hand, the **precision** of the manual delineation method was **0.85**. This relatively good precision highlights the method's reliability in avoiding false positives, particularly as the false negatives were the least at 0.09. However, this level of precision may also suggest a degree of conservatism in the technique, as it might have missed mapping less obvious landslide features which were not visibly distinct from other areas in the landscape, contributing low false positive rates.

The **recall** calculated at **0.74** indicates that using the manual technique, 74% of the actual landslides in the study area were correctly identified, while the **F1 score** calculated at **0.79** indicates a good balance in this method's performance in identifying actual landslides and avoiding no landslide areas (false alarms). The **kappa value** was calculated at **0.399**. Using the Kappa value interpretation in Table 2 above, this indicates that there is a fair agreement between the method's prediction of landslides and their true classifications. This means that the method performed better than random chance but could be better improved as it still has misclassified areas.

The manually mapped landslides were further compared with the BGS landslide inventory and a clear difference in the total mapped area is observed in Figure 4.2 below.

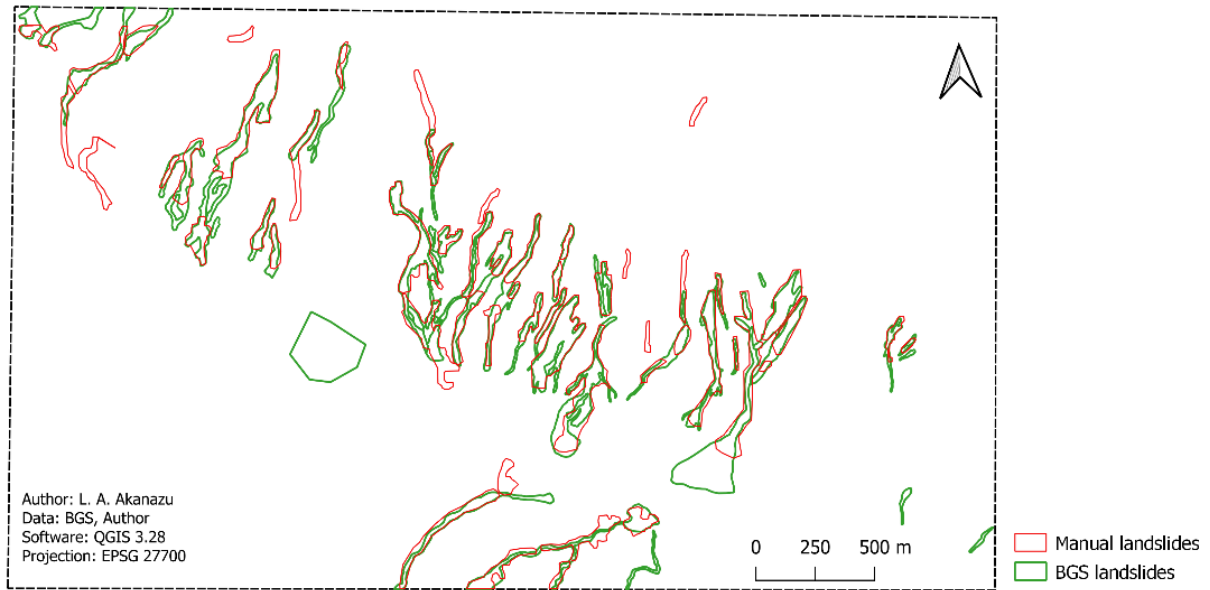


Figure 4.2 – Manually mapped landslides overlaid with BGS landslide inventory

The manually mapped landslides covered an area of 0.356 km², whereas the BGS landslide inventory identified a total area of 0.569 km². This discrepancy highlighted a significant difference of 0.432 km², suggesting that the manual delineation method missed or failed to capture a considerable portion of the landslide-affected area. However, it is important to note that the area of discrepancy accounted for the total area where both datasets (BGS inventory and manual landslides) do not match. Thus, the combination of both areas of mismatches (Figure 4.2) amounted to 0.432km² instead of 0.213km² when calculated mathematically (that is, 0.569 – 0.356).

4.2 Glengyle GEE results

The median composite of the study area from Google Earth Engine analysis revealed significant changes in the landscape before and after the landslide event. The composite imagery clearly displayed areas where vegetation loss occurred, indicated by stark scar faces in the terrain (Figure 4.3) where the land had shifted. These scar faces, typically visible after landslides, pointed to regions of significant instability and material displacement.

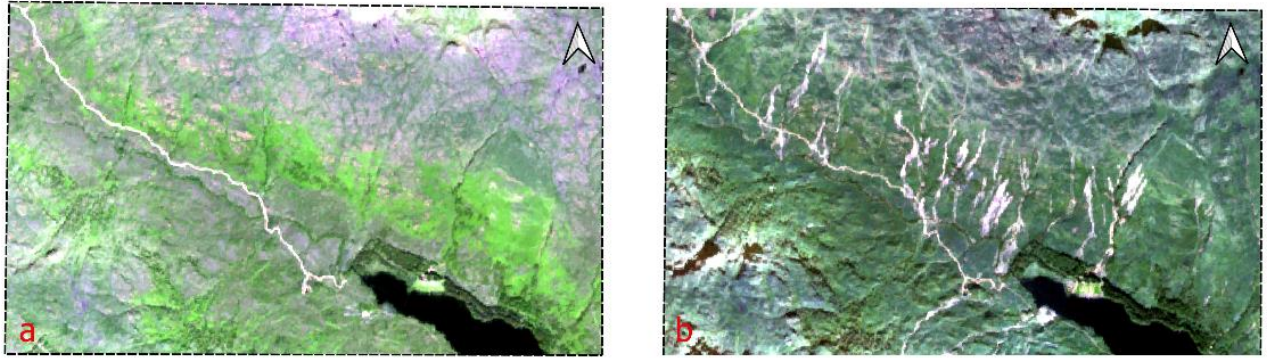


Figure 4.3: a) pre-event composite b) post-event composite

By analysing the temporal imagery, distinct differences between the pre-event and post-event conditions were identified, with the most notable feature being the exposed soil surfaces in the affected areas, typically associated with debris flow landslides. As landslides often involve the sudden removal of topsoil and vegetation, leaving behind exposed soil and rock, and this was evident in the scarred terrain observed in the post-event images. These scar faces offered direct visual evidence of the slope failure.

Along with the composite imagery, a landslide tracker image was produced, providing a binary classification with pixel values of 1 and 0 representing landslide and no landslide, respectively. This layer allowed for a more refined analysis, enabling clear identification of where the landslides occurred. The binary classification helped validate the areas of vegetation loss by comparing them with the BGS landslide inventory for the study area (Fig 4.4).

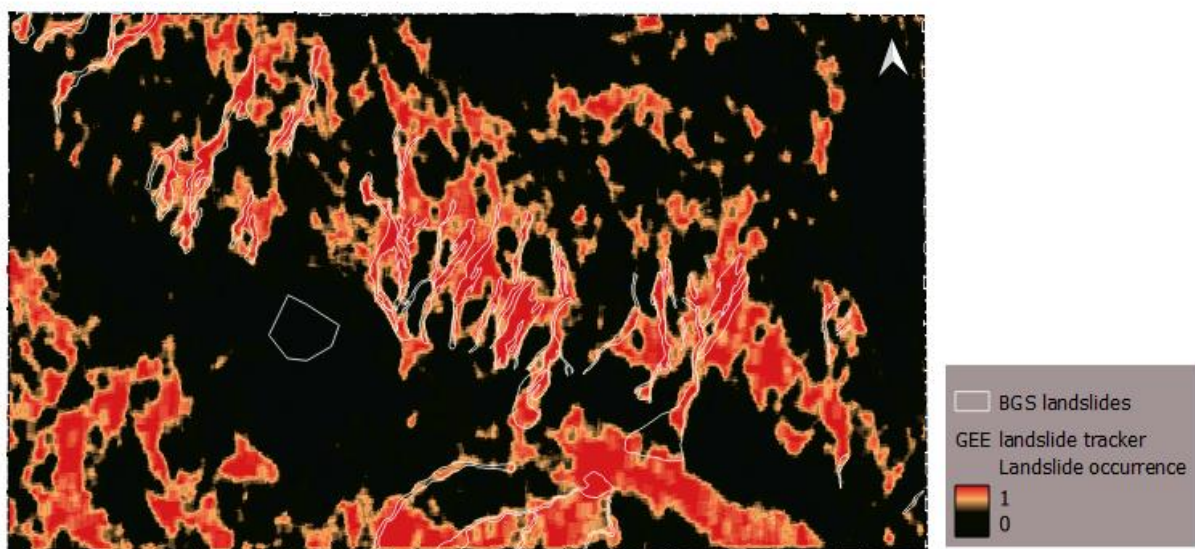


Figure 4.4: BGS landslide inventory overlaid on GEE landslide tracker results

The results from the confusion matrix allowed for the calculation of precision and accuracy of the GEE method (Table 4). The **accuracy** was determined to be **0.81**, meaning that the GEE method correctly classified 81% of all observations, whether they were landslides or non-landslide areas. Essentially, four out of five observations made by the GEE method were correctly identified.

Table 4: Confusion matrix of GEE landslide mapping results

	Predicted landslide	Predicted no landslide
Actual landslide	0.52	0.02
Actual no landslide	0.19	0.37

On the other hand, the **precision** was calculated at **0.73**, which represents the method's ability to correctly classify landslides when it predicted a landslide. In other words, 73% of the areas that GEE identified as landslides were actually landslides, while the remaining 26.8% were falsely classified. The **recall** calculated at **0.96** and the **F1 score at 0.83** indicates that this technique correctly identified 96% of all the landslides and has a very good balance between correctly classifying landslides and avoiding errors. Nonetheless, some false classifications were still made. This highlights some limitations of the GEE method in differentiating actual landslides from non-landslide features, especially in areas where the landscape may share similar characteristics. Finally, the **kappa value** was calculated at **0.620** indicates a substantial level of agreement between this technique's predictions and the ground truth, beyond what would be expected by chance.

4.3 Glengyle HazMapper results

The pre- and post-event composites of the location generated with HazMapper (Figure 4.5) revealed visible scars on the landscape relating to downslope movement of materials due to mass wasting. The rdNDVI (Figure 4.6) image on the other hand shows severe vegetation loss in the areas where these parallel scars are located on the landscape. This image was further used to calculate the confusion matrix of the method (Table 5) to test the method's performance in mapping landslides.

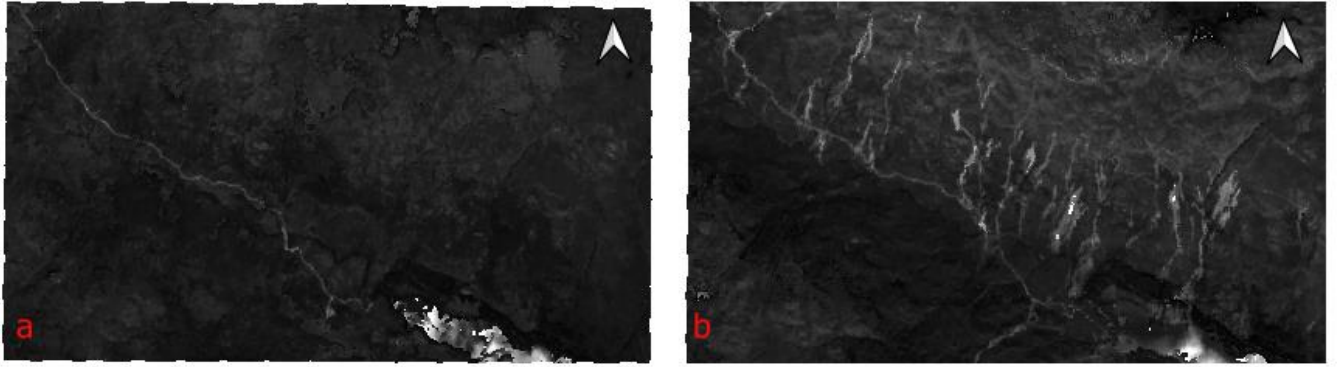


Figure 4.5: a) pre-event composite b) post-event composite

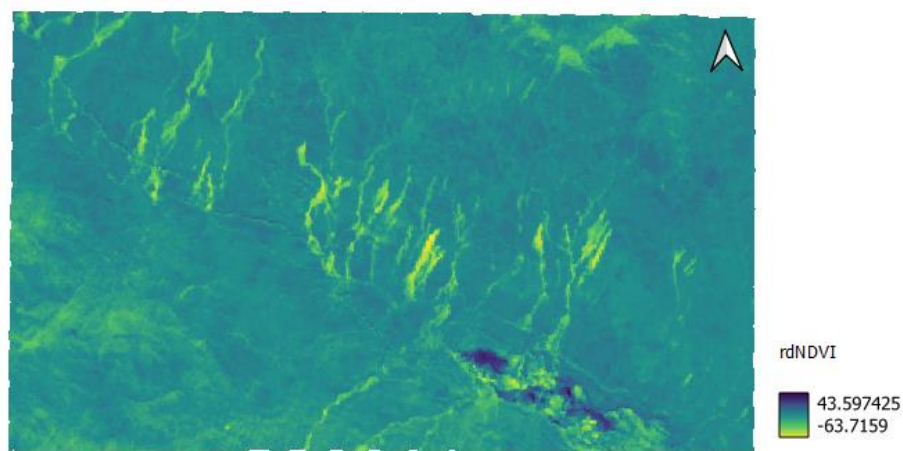


Figure 4.6: HazMapper rdNDVI results showing areas with vegetation loss

The confusion matrix for this method is presented in the table below.

Table 5: HazMapper confusion matrix results

	Predicted landslide	Predicted no landslide
Actual landslide	0.55	0.09
Actual no landslide	0.17	0.19

The results from the confusion matrix allowed for the calculation of precision and accuracy of the method. The **accuracy** was determined to be **0.74**, this means that the HazMapper tool correctly classified 74% of all observations whether they were landslides or non-landslide areas. Also, the **precision** was calculated at **0.76**, which represents the tool's ability to correctly classify landslides when it predicted a landslide. The **recall and F1 score** were calculated at **0.85 and 0.81 respectively**. This indicates that HazMapper successfully identified 85% of all

the actual landslides in the study area and had a good balance in avoiding errors (non-landslide areas). The **kappa value of 0.407** suggests that this technique had a moderate agreement between its performance in mapping landslides and the actual landslides present in the location.

4.4 Summary of Results

From the analysis and results presented above, the three landslide mapping methods have been applied to assess their performance in landslide mapping in the primary study area, Glengyle. For clarity of purpose and easy comparison, the performance metrics of the three methods are summarised in the table below:

Table 6: Summary of performance metrics for the three methods

Method	Accuracy	Precision	Recall	Kappa value	F1 Score
Manual	0.73	0.85	0.74	0.399	0.79
GEE	0.81	0.73	0.96	0.620	0.83
HazMapper	0.74	0.76	0.859	0.407	0.81

The manual mapping technique had greater precision compared with the other two methods, because the pixels were carefully selected using the identify tool during digitisation. However, it had the lowest F1 score which relates to the balance between the accuracy and precision of the method. The change-adjusted kappa values of 0.399, 0.620 and 0.407 shows that the performance of these three methods varies. With GEE scoring the highest, this highlights the superiority of GEE in landslide mapping over the other two methods that is, the landslides mapped using this technique are less likely to be detected randomly by chance. Also, with the GEE having the highest F1 score showing a good balance both in identifying the landslides and avoiding errors more than the other methods, GEE was further applied in the secondary and tertiary study areas – Rest and Be Thankful valley and Dortyol, Turkey – to assess its performance for different locations and landslide types, respectively.

4.5 Rest and Be Thankful valley results

The GEE method was applied in Rest and Be Thankful valley using the same GEE procedure, adjusting the parameters to fit the study area. Similar results were obtained for further analysis such as the pre- and post-event composites and in particular the landslide tracker image (Figure 4.7), which shows a binary classification of debris flow landslides in the study area. The binary raster was also used to calculate the confusion matrix, which provides a comprehensive

overview of the predictive performance of the mapping technique in this new study area (Table 7).

Table 7: GEE confusion matrix for Rest and Be Thankful

	Predicted landslide	Predicted no landslide
Actual landslide	0.53	0.03
Actual no landslide	0.20	0.23

From this matrix, the calculated the **precision and accuracy** of the method was found to be **0.726 and 0.767 respectively**. The precision of 0.726 indicates that out of all the areas predicted as landslides, about 72.6% were correctly identified as actual landslides. This result shows that while this method can reasonably map landslides accurately, there is a moderate rate of false positives (20%), meaning that a significant number of areas were incorrectly classified as landslides. With the **recall** calculated at **0.94**, it indicates that 94% of the actual landslides were identified by GEE in this new location with only a small proportion missed (5.36%). **The F1 score at 0.82** suggests that GEE had a good balance between correctly identifying landslides and avoiding error in Rest and Be Thankful. Albeit the lower precision indicates that some areas were misclassified as landslides. The **kappa value** was calculated at **0.504**. This indicates a moderate agreement between the mapped landslide and the actual landslides observed in the study area.

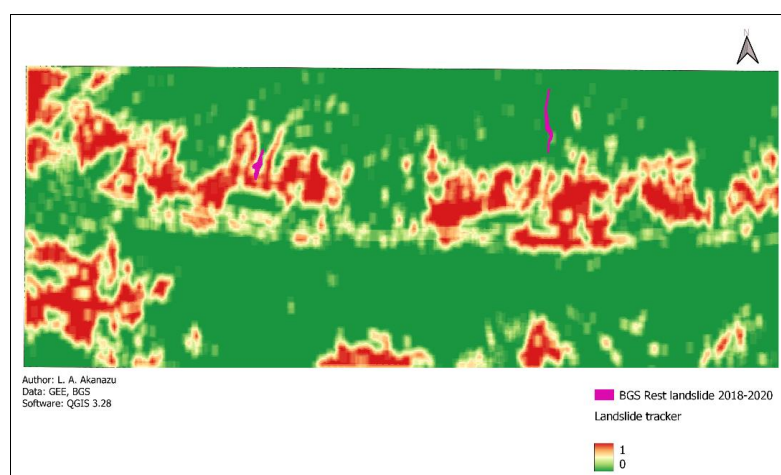


Figure 4.7 – Landslide tracker for Rest and Be Thankful valley

From the figure above, visible vegetation loss signifying potential landslides can be seen in bright red colours, showing more landslides than the BGS inventory. This is because the BGS inventory are mapped manually based on reported landslides, therefore, since GEE results are compared with the reported landslides mapped in the BGS inventory and not all the landslide occurring in the location, this explains why the GEE has more landslides than the inventory resulting in low performance in the metrics for this location (See [Appendix IV](#)).

4.6 Dortyol results

GEE was also applied to the tertiary study area using the same GEE code and procedure and adjusting the parameters to fit the study area, to evaluate the tool's ability to rapidly detect and map other landslide types. The pre- and post-event composites and the landslide tracker image which shows a binary classification of the landslides in the study area was generated ([Figure 4.8](#)). The landslide tracker raster image was used to calculate the confusion matrix of the method in this study area to evaluate the methods performance in landslide mapping in this new location ([Table 8](#)).

Table 8: GEE Confusion matrix for Dortyol

	Predicted landslide	Predicted no landslide
Actual landslide	0.68	0.02
Actual no landslide	0.08	0.22

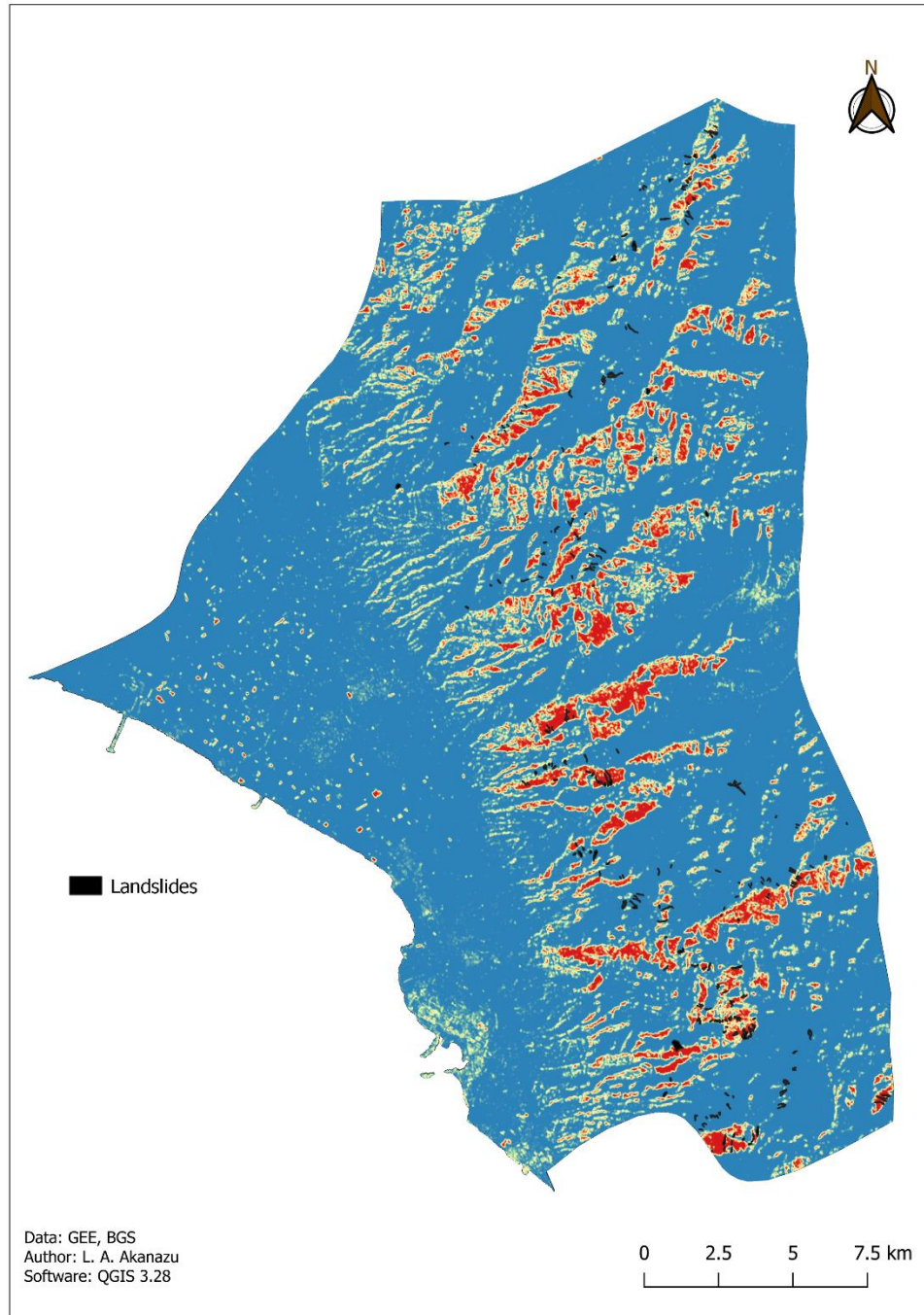


Figure 4.8 - Landslide tracker image of Dortyol showing identified landslides overlaid with BGS landslides

Using the confusion matrix, further metrics such as the precision, accuracy, recall and F1 score were also calculated. The **accuracy and precision** were calculated at **0.9 and 0.894 respectively**. This indicates that GEE identified 90% of all landslides present in this location, and of all the landslides identified, 89% of them were correctly classified. The **recall** calculated at **0.971** demonstrates that GEE identified almost all the actual landslides present in this

location missing out a small proportion of 2.86%. With the precision at 89% and the recall at 97%, the **F1 score** calculated as **0.93** suggests a great balance by the method in correctly identifying landslides and avoiding errors. However, with the lower precision value, some areas were misclassified as landslides with suggests for possible improvement. The **kappa value of 0.74** indicates substantial agreement between the model's predictions and the actual data, even after accounting for chance agreement. This value shows that the model is not only accurate due to the distribution of class labels but is making meaningful predictions that align closely with the observed ground truth. While there is still some room for improvement, this Kappa value signifies that the model is fairly consistent in mapping the landslides beyond what would have been mapped by chance.

Moreso, since it has been previously established in [section 3.2.2](#) that the landslides common in this location are slides and rockfalls, the performance of GEE to correctly identify 90% of the landslides in this location suggests that GEE can be applied in the identification and mapping of other landslide types besides debris flows.

5 Discussion

5.1 Objective 1 – Establishing the traditional and state-of-the-art landslide mapping methods:

The first objective of this research was to establish a clear understanding of both traditional and state-of-the-art Earth Observation (EO) methods for landslide mapping. Through an extensive literature review showing practical application of these methods, this objective has been successfully achieved, highlighting the evolution of landslide detection techniques from manual field-based approaches to cutting-edge, automated methods. Historically, manual mapping and field surveys have been the foundation of landslide detection. These methods involve direct observation and on-the-ground analysis by experts, making them highly accurate in local contexts. However, despite their reliability in specific areas, these approaches are inherently time-consuming, labour-intensive, and limited in scale. Manual methods also introduce a level of subjectivity, with the quality of the output dependent on the surveyor's expertise and the visibility of landslide evidence in the field.

The introduction of optical remote sensing marked the first major shift towards broader and more efficient landslide detection. Using satellite-based imagery, such as that from the Landsat and Sentinel missions, researchers were able to monitor changes in land cover associated with landslides across larger areas. However, these optical methods are not without limitations, most notably their susceptibility to cloud cover, which restricts their applicability in many regions which in turn has driven the development of more advanced EO techniques. The review further highlighted the transition from optical remote sensing technologies to more sophisticated platforms such as SAR and InSAR, which have expanded the possibilities for large-scale, real-time monitoring of landslides.

This study also identified and discussed different techniques that can be used in mapping various landslide types as well as the state-of-the-art methods in landslide detection, specifically OBIA and machine learning and other tools such as GEE and HazMapper which represent the future of rapid landslide mapping. These methods go beyond the limitations of earlier approaches by leveraging automation, object-based segmentation, and predictive modelling to enhance detection accuracy, especially in complex and diverse terrains. The ability of machine learning models to integrate various environmental variables and learn from

historical events makes them particularly valuable for future landslide monitoring and prediction.

5.2 Objective 2 – Investigating free EO-based tools for landslide mapping in Glengyle:

The second objective of this research was to investigate the efficacy of free Earth Observation (EO)-based tools for landslide mapping in the study area of Glengyle. With this research focusing on debris flow mapping as prevalent in the study area, vegetation loss was considered a key indicator of landslide occurrence in the study area thus, techniques that can detect vegetation loss using the NDVI index were primarily considered. This objective has been successfully achieved by testing two widely used free EO platforms—Google Earth Engine (GEE) and HazMapper— applying mainly change detection and pixel-based analysis techniques and comparing their results with those of traditional manual mapping methods. Through this process, the research has provided valuable insights into the strengths and limitations of each approach, particularly in the context of a smaller study area like Glengyle. Google Earth Engine (GEE) and HazMapper were employed to detect landslides in Glengyle, leveraging their free access to multi-temporal satellite imagery and automated processing capabilities.

GEE, with its extensive datasets and advanced analytical tools, allowed us to apply indices such as the Normalized Difference Vegetation Index (NDVI) and assess soil moisture changes, which are important indicators of landslide activity. The analysis successfully detected landslides in the study area, and GEE proved to be an efficient and scalable tool for landslide mapping. HazMapper, another EO-based tool designed specifically for hazard mapping, also performed well in detecting landslides. By using NDVI values and slope as key parameters, HazMapper identified areas likely to have experienced landslides. However, similar to GEE, HazMapper displayed limitations when applied to a smaller study area like Glengyle. Its reliance on slope as a primary factor led to instances of over-prediction, where steep, non-landslide zones were mistakenly classified as landslide-affected areas. This reflects the tool's automated nature, which, while effective on a larger scale, may lack the fine-tuned precision needed for small, complex landscapes.

In addition to the EO-based tools, manual mapping was tested to determine whether it could provide more precise results in a smaller area like Glengyle. The manual mapping method, while precise, did not outperform the EO-based tools in terms of discovering additional

landslides. However, it did contribute to mapping more landslides than those included in the pre-existing landslide inventory by using satellite imagery as a base. This suggests that while manual methods offer a valuable complement to EO-based approaches, the efficiency and scalability of tools like GEE and HazMapper make them highly suitable for both small and large-scale studies.

5.3 Objective 3 – Comparing the efficiency and accuracy of these techniques applied to identify their strengths and weaknesses:

The third objective of this research was to evaluate the performance and accuracy of the selected landslide mapping methods in the context of our study area. This involved assessing the ability of each method to detect landslides, comparing the accuracy of their results against an existing landslide inventory provided by the British Geological Survey (BGS), and analysing their performance using statistical metrics such as precision, accuracy, and confusion matrices. The aim was to provide a comprehensive understanding of how well these methods function in detecting landslides and identifying potential limitations in their application.

Following from the results presented in [Table 5](#) above, GEE performed better than the other two methods, producing an accuracy of 0.81, a precision of 0.73, and an F1 score of 0.83 indicating a reasonably strong performance. The precision of 0.73 reflects this method's ability to correctly identify landslides among its predictions, while the 0.81 accuracy showed that a significant portion of both landslides and non-landslide areas were classified correctly. These values underscore GEE's effectiveness in integrating soil moisture and vegetation indices (such as NDVI) to detect landslides. GEE's kappa value of 0.620 also indicates that the method performed substantially well in mapping landslides, better than random occurrence.

These results of the other methods reflect on their limitation in landslide mapping, particularly in comparison to GEE. HazMapper, while a valuable tool for assessing landslide susceptibility, has limitations that affected its overall performance compared to the GEE, one of which is its reliance on predefined algorithms and models that may not capture the full complexity of landslide events ([Scheip et al., 2021](#)). Also, HazMapper utilises only slope as a consideration factor in determining landslide occurrence, which, in reality, is not the only determinant of landslide occurrence especially for spreads, where the slope angle is very low ([Roush, 2024](#)). While slope is an important factor in landslide susceptibility, relying solely on it can result in significant overestimation of landslide-affected areas. The simplicity of this approach limits HazMapper's ability to account for other critical factors influencing landslides, which may

contribute to its lower accuracy compared to GEE which incorporates additional factors such as soil moisture and vegetation indices.

The manual mapping technique on the other hand is primarily constrained by time and resource. It is labour-intensive, requiring experts to analyse satellite imagery visually, which can lead to human error and subjectivity in identifying landslides (Warburton et al., 2008). This method often results in incomplete inventories, as it may miss smaller or less obvious landslides due to the subjective nature of human interpretation (Warburton et al., 2008). Additionally, manual mapping is less scalable; as the area of interest increases, the feasibility of conducting thorough manual analyses diminishes (Scaioni et al., 2014). The reliance on expert judgment can also introduce variability in results, as different analysts may have differing thresholds for identifying landslides (Guzzetti et al., 2012). Remarkably, 85% of the landslides identified through the manual mapping process matched those already recorded in the inventory. This high level of agreement demonstrates the reliability of the manual detection process (Holbling et al., 2017), affirming that most of the significant landslide events were captured accurately.

However, despite this high match rate, some landslides recorded in the inventory were not identified during the manual mapping process. This could be due to several factors, such as the limitations of the 10-meter spatial resolution of the Sentinel-2 imagery, which might not capture smaller or more subtle landslide events. Additionally, manual methods are inherently subjective (Holbling et al., 2017), and the reliance on visible indicators like vegetation loss or scar faces may have led to the omission of landslides that either did not exhibit these features prominently or were masked by other landscape elements.

These discrepancies highlight the need for a complementary approach that combines manual inspection with automated methods to ensure a more exhaustive landslide detection process. The difference in the mapped areas indicates the challenges of manual identification methods, where subtle or less visible landslides may be easily overlooked. The Maximum Difference of 0.058 km² between individual landslide polygons further emphasizes this challenge, as some landslide events may be substantially under- or over-estimated during manual digitization, compared to the more comprehensive BGS inventory.

It is important to note that the BGS landslide inventory was mapped manually and some of the polygons mapped as landslides in the inventory were not actual landslides but landcover change (Appendix II). This is an evident limitation of the manual delineation technique and explains the significant disparity in the difference analysis between the manual delineation and BGS

inventory discussed in [section 4.1](#) above. These differences can be attributed to the limitations of the manual process, such as the reliance on visual interpretation, the resolution of the satellite imagery used, and the subjectivity of the operator in delineating landslide boundaries. Also, because the BGS inventory was mapped based on reported landslides, landslides that were not reported were not accounted for. This comparison underlines the importance of integrating multiple methods, such as combining manual techniques with automated tools like HazMapper or GEE, to improve the accuracy and comprehensiveness of landslide mapping efforts. The substantial difference in the total area covered suggests that manual mapping alone may not be sufficient for capturing the full extent of landslide hazards in a region.

Finally, besides having the best F1 score, GEE also incorporated other factors such as slope and soil moisture, that play key roles in determining landslides. Apparently, since not all vegetation loss means the presence of landslides, the incorporation of soil moisture gives more context to the cause of vegetation loss, that is the presence of moisture, relating it to possible landslide occurrence. This explains why GEE mapped more landslides than the BGS inventory and HazMapper, and also performed better than the two methods as it accounted for the change in soil moisture within the landscape.

5.4 Objective 4 – Testing the most efficient method on other landscapes:

The fourth objective of this research aimed to test the most efficient landslide detection method identified GEE on a different landscape to evaluate its performance in varying terrain conditions. After proving effective in the primary study area of Glengyle, the GEE approach was applied to a secondary location, the Rest and Be Thankful valley, known for its recurring landslide events particularly during winter, and Dortyol which experienced severe landslides after an earthquake event in 2023. This step was crucial in assessing the transferability and robustness of the method across different landscapes, particularly those with different slope angles and different environmental conditions. When tested in the Rest and Be Thankful valley, the GEE method showed a slight decrease in performance. The accuracy dropped to 0.77 while the precision was consistent at 0.73. While the overall performance remained relatively strong, the decrease in accuracy indicates that this method encountered some challenges in this new terrain. This difference could be attributed to the specific characteristics of the Rest and Be Thankful valley, such as the unique topography or the lack of cloudless imagery during the period under analysis, which limited the temporal resolution of the study.

Also, the kappa value reduced from 0.62 in Glengyle to 0.50 in Rest and be Thankful which may be attributed to the difference in slope angles and topography. Moreso, the BGS landslide inventory was more robust for Glengyle than for Rest and be Thankful, which allowed for better comparison in Glengyle. This lack of sufficient ground truth data for the latter landscape may create a limitation in the number of pixels with which the confusion matrix was generated for this region, thereby reducing the performance of the method in this region.

Similar patterns were observed in Dortyol with GEE correctly identifying 90% of all landslides present in the location with a precision of 89%. This location features different types of landslides, such as rock falls and topples, highlighting the tool's ability to detect various landslide mechanisms accurately. This was the highest recorded so far in a single location which affirms the importance of well-documented landslide inventory for validation purposes (Guzzetti et al., 2012). However, despite these strong results, the lower precision value suggests that some non-landslide areas were incorrectly classified as landslides, indicating a potential area for improvement in future analysis.

5.5 Summary of Discussion

EO-based rapid landslide mapping approaches such as those considered in this study has proven to be a powerful tool in disaster management, providing critical insights for emergency relief efforts. Current capabilities, such as those offered by Sentinel-2 with its 10-meter resolution and 5-day revisit cycle, enable timely identification of landslide-affected areas, allowing rescue teams to prioritize responses and allocate resources efficiently. However, future advancements in satellite technology, including higher spatial and temporal resolutions from upcoming missions and private constellations, hold the potential to significantly enhance response times. These improvements could enable near-real-time monitoring, critical for reducing casualties and supporting rapid recovery efforts. Additionally, EO techniques contribute to long-term recovery by continuously monitoring landslide-prone regions and informing mitigation strategies.

Despite these advancements, EO-based approaches face limitations. The spatial resolution of Sentinel-2 (10m) restricts the detection of smaller landslides compared to higher-resolution satellites like WorldView or PlanetScope which are available at 1m resolutions. Furthermore, the reliance on vegetation changes as a primary indicator limits the applicability of these

techniques in barren landscapes or densely forested regions. Current methods are also more effective in detecting recent landslides than older or more subtle ones with minimal visible surface changes. Overcoming these challenges requires integrating EO data with complementary technologies, such as radar systems like Sentinel-1, which can detect landslides in non-vegetated or cloud-covered areas, and multi-sensor approaches combining optical, radar, and LiDAR data for enhanced detection.

Looking ahead, the incorporation of AI and machine learning holds promise for improving the accuracy and speed of landslide detection across diverse terrains. Enhanced satellite technology, including near-daily revisit cycles and higher resolutions, will address limitations in response time and the detection of smaller-scale events. Moreover, the wider applicability of EO-based techniques can be achieved by adapting them to different geomorphological conditions and landslide types, reducing reliance on vegetation signals and incorporating multi-temporal analyses to capture older events. These advancements, combined with EO's scalability for large, remote areas, will ensure that landslide mapping continues to play a vital role in disaster preparedness and relief efforts worldwide.

6 Conclusion

This study examined landslide mapping by comparing two automated approaches to rapid landslide mapping: change detection and pixel-based analysis using HazMapper and the SLIP algorithm on Google Earth Engine, complementing these with manual delineation. Each method was assessed to determine its accuracy, efficiency, and effectiveness in identifying and mapping landslide occurrences. The primary goal was to evaluate how these techniques compare when applied to the same study area. The findings show that both HazMapper and GEE offer scalable and efficient solutions for landslide detection, with GEE emerging as the most accurate method overall. GEE's integration of multi-temporal satellite data, combined with the options to add more parameters to detect landscape change, allowed for a more precise identification of landslide-affected areas. Although, HazMapper also provided a robust, user-friendly interface for rapid mapping, though with slightly less accuracy than GEE.

The manual delineation technique, though effective, came with significant drawbacks. It is a labour-intensive process requiring significant time and effort, especially when working with large areas. One of the main limitations observed in the manual approach is its scalability—manual delineation is not practical for large study areas due to the substantial amount of time and effort required which makes it unsuitable for rapid mapping for emergency purposes. Additionally, this method relies heavily on the quality of the imagery and the expertise of the operator, which introduces variability. The use of medium-resolution satellite imagery of 30m in the manual mapping of landslides in this study may result in missing smaller landslides or failing to capture subtle changes in terrain that can indicate landslide activity. Despite this, manual mapping can still provide valuable localized insights and serve as a useful method for cross-validation.

On the other hand, HazMapper and GEE offer more automated and scalable solutions, with GEE showing a distinct advantage in terms of accuracy. As GEE leverages global satellite data archives and cloud computing, it allows for the rapid processing of high volumes of data, making it particularly suitable for large-scale studies. The result of this study also confirms that GEE can be applied to landslide mapping in different terrain conditions and for different landslide types, however, care must be taken to adjust certain parameters according to the landscape features.

In light of these findings, this study highlights the importance of selecting appropriate methods depending on the scale and characteristics of the study area. While manual delineation may be

suitable for small, detailed analyses, HazMapper and GEE provide better options for larger areas where speed and accuracy are essential. Looking ahead, future research will aim to enhance this framework, particularly by developing an automated landslide detection algorithm using GEE. The goal is to integrate higher-resolution satellite data, which can improve detection of smaller or more subtle landslides, and apply machine learning algorithms to further increase accuracy, especially in areas with complex terrain. Such developments could revolutionize landslide mapping, making it faster, more precise, and applicable on a global scale.

7 Future Work

The methods applied in this study successfully achieved the goal of the research in comparing three landslide mapping techniques. However, some limitations could be significantly reduced by considering the following:

1. Using a better resolution satellite imagery for manual delineation. Given that the imagery used in this study was 10m resolution, would the performance of the manual technique be enhanced if better resolution was used in detecting and mapping landslide scar faces?
2. Incorporating other landslide parameters in the GEE code to further refine the result and improve performance of this tool
3. Automatically selecting the best thresholds for the input parameters (e.g. slope angle) for the HazMapper tool to test the sensitivity of this tool in different slopes
4. Developing a code for HazMapper to allow for parametric adjustments rather than using the online tool.
5. Integrating deep learning (DL) algorithms using advanced libraries in python (e.g. TensorFlow or PyTorch) which allows for the deployment of DL models like convolution neural networks (CNN) and offers significant advantage in landslide detection by automatically learning site-specific landslide features. While GEE excels in processing large-scale EO datasets and implementing conventional machine learning techniques, it currently lacks the extensive libraries and frameworks required for this advanced deep learning applications.

Bibliography

- Acharya, G., Cochrane, T. A., Davies, T., & Bowman, E. (2009). The influence of shallow landslides on sediment supply: A flume-based investigation using sandy soil. *Engineering Geology*, 109(3-4), 161-169.
- AFAD 2023: Disaster and Emergency Presidency of Türkiye. https://deprem.afa.d.gov.tr/assets/pdf/Arazi_Onrapor_28022023_surum1_revize.pdf. Last accessed 24 December 2024
- Alexander, D. 1992: On the causes of landslides: human activities, perception, and natural processes. *Environ. Geol. Water Sci.*, 20, 3, 165–179
- Amankwah S.O.Y, Wang G., Gnyawali K., Hagan D. F. T, Sarfo I, Zhen D, Nooni I. K, Ullah W, Duan Z 2022: Landslide detection from bitemporal satellite imagery using attention-based deep neural networks. *Landslides* 19(10):2459-2471. <https://doi.org/10.1007/s10346-022-01915-6>
- Amarasinghe, M. P., Kulathilaka, S. A. S., Robert, D. J., Zhou, A., & Jayathissa, H. A. G. (2024). Risk assessment and management of rainfall-induced landslides in tropical regions: A review. *Natural Hazards*, 120(3), 2179-2231.
- Amatya, P., Kirschbaum, D., Stanley, T., 2019: Use of very high-resolution optical data for landslide mapping and susceptibility analysis along the Karnali highway, Nepal. *Remote Sens.* 11, 2284.
- Amatya, P., Kirschbaum, D., Stanley, T., and Tanyas, H. 2021: Landslide mapping using Object-based image analysis and open-source tools. *Engineering Geology*, 282 (2021) 106000, <https://doi.org/10.1016/j.enggeo.2021.106000>
- Avanzi, G., Galanti, Y., Giannecchini, R., Bartelletti, C. 2015: Shallow landslides triggered by the 25 October 2011 extreme rainfall in Eastern Liguria (Italy). In *Engineering Geology for Society and Territory-Volume 2: Landslide Processes* pp. 515-519
- Ayalew L., Yamagishi, H. 2005: The application of GIS-based logistic regression for landslide susceptibility mapping in the Kakuda-Yahiko Mountains, Central Japan. *Geomorphology* 65:15–31. <https://doi.org/10.1016/j.geomorph.2004.06.010>
- Ballantyne, C. K. 2002: Paraglacial geomorphology. *Quaternary Science Reviews*, 21(18-19), 1935-2017.
- Ballantyne, C. K. 2019: *Scotland's mountain landscapes: a geomorphological perspective*. Liverpool University Press.
- Ballantyne, C. K., & Gordon, J. E. (Eds.). 2021: *Landscapes and Landforms of Scotland*. Springer International Publishing.
- Barbano, M. S., Pappalardo, G., Pirrotta, C., & Mineo, S. 2014: Landslide triggers along volcanic rock slopes in eastern Sicily (Italy). *Natural Hazards*, 73, 1587-1607.

- Barka, A. A., Kadinsky-Cade, K. 1988: Strike-slip fault geometry in Turkey and its influence on earthquake activity. *Tectonics* 7:663–684. <https://doi.org/10.1029/TC007i003p00663>
- Bathrellos, G., Kalivas, D., Skilodimou, H., 2017: Landslide susceptibility assessment mapping: a case study in Central Greece. In: Petropoulos, G.P., Islam, T. (Eds.), *Remote Sensing of Hydrometeorological Hazards*. CRC Press, Taylor & Francis Group, London, U.K, pp. 493–512 (ISBN-13: 978-1498777582).
- Bathrellos, G., Koukouvelas, I., Skilodimou, H., Nikolakopoulos, K., Vgenopoulos, A. 2024: Landslide causative factors evaluation using GIS in the tectonically active Glafkos river area, northwestern Peloponnese, Greece. *Geomorphology* 461 (2024) 109285 <https://doi.org/10.1016/j.geomorph.2024.109285>
- BEAR Scotland available at https://www.bearscot.com/faq_rabt/ last accessed on 25 December 2024
- Bennett, G. L., Miller, S. R., Roering, J. J., and Schmidt, D. A. 2016: Landslides, threshold slopes, and the survival of relict terrain in the wake of the Mendocino Triple Junction, *Geology*, 44, 363–366, <https://doi.org/10.1130/G37530.1>
- Blahůt, J., Balek, J., Klimeš, J., Rowberry, M., Kusák, M., & Kalina, J. (2019). A comprehensive global database of giant landslides on volcanic islands. *Landslides*, 16, 2045-2052.
- Błońska, E., Lasota, J., Piaszczyk, W., Wiecheć, M., & Klamerus-Iwan, A. (2018). The effect of landslide on soil organic carbon stock and biochemical properties of soil. *Journal of Soils and Sediments*, 18, 2727-2737.
- Booth, S., Merritt, J., & Rose, J. (2015). *Quaternary Provinces and Domains – a quantitative and qualitative description of British landscape types. Proceedings of the Geologists' Association*, 126(2), 163–187. doi:10.1016/j.pgeola.2014.11.002
- Brehme, M., Scheytt, T., Çelik, M. *et al.* Hydrochemical characterisation of ground and surface water at Dörtyol/Hatay/Turkey. *Environ Earth Sci* **63**, 1395–1408 (2011). <https://doi.org/10.1007/s12665-010-0810-1>
- British Geological Survey Hazard Research domain page available at <https://www.bgs.ac.uk/geology-projects/shallow-geohazards/landslide-domains/> last accessed 23 December 2024
- Burrows, K., Walters, R.J., Milledge, D., Densmore, A.L., 2020: A systematic exploration of satellite radar coherence methods for rapid landslide detection. *Nat. Hazards Earth Syst. Sci.* 20, 3197–3214. <https://doi.org/10.5194/nhess-20-3197-2020>
- Caine, N. 1982: Toppling failures from Alpine cliffs on Ben Lomond, Tasmania. *Earth Surface Processes and Landforms*, 7, 133–152.
- Calcaterra, D., & Parise, M. (2010). Weathering as a predisposing factor to slope movements: an introduction (Vol. 23, No. 1, pp. 1-4). London: The Geological Society of London.
- Cardinali, M., Ardizzone, F., Galli, M., Guzzetti, F., and Reichenbach, P. 2000: Landslides triggered by rapid snow melting: the December 1996–January 1997 event in Central Italy,

- in: Proceedings 1st Plinius Conference on Mediterranean Storms, 14–16 October 1999, Maratea, Editoriale Bios, Cosenza, 439–448, ISBN 9788877402967
- Case, W. F. 2001: *Landslides: What are they, why they occur*. Utah Geological Survey. Public Information Series, 74
- Çellek, S. (2020). Effect of the slope angle and its classification on landslide. *Natural Hazards and Earth System Sciences Discussions*, 2020, 1-23.
- Cerri, R. I., Rosolen, V., Reis, F. A., Filho, A. J. P., Vemado, F., do Carmo Giordano, L., & Gabelini, B. M. (2020). The assessment of soil chemical, physical, and structural properties as landslide predisposing factors in the Serra do Mar Mountain range (Caraguatatuba, Brazil). *Bulletin of Engineering Geology and the Environment*, 79, 3307-3320.
- Chen, C. Y., & Martin, G. R. (2002). Soil–structure interaction for landslide stabilizing piles. *Computers and Geotechnics*, 29(5), 363-386.
- Chung, J., Rogers, D., Watkins, M. 2014: Estimating severity of seismically induced landslides and lateral spreads using threshold water levels. *Geomorphology*, Vol. 204, pp 31-41, <https://doi.org/10.1016/j.geomorph.2013.07.024>
- Conoscenti C, Ciaccio M, Caraballo-Arias NA, Gómez-Gutiérrez Á, Rotigliano E, Agnesi V (2015) Assessment of susceptibility to earth-flow landslide using logistic regression and multivariate adaptive regression splines: a case of the Belice River basin (western Sicily, Italy). *Geomorphology* 242:49–64. <https://doi.org/10.1016/j.geomorph.2014.09.020>
- Copernicus web browser available at <https://browser.dataspace.copernicus.eu/> last accessed on 19 October 2024
- Daily Mail Online News UK 2019. Available at <https://www.dailymail.co.uk/news/article-7334047/Glengyle-landslide-destroyed-homes-Scottish-village-home-Rob-Roy-MacGregor.html> last accessed 17 September, 2024
- de Freitas, M. H. and Watters, R. J. 1973: Some field examples of toppling failure. *Geotechnique*, 23, 4, 495–514.
- Demir, A., Celebi, E., Ozturk, H., Ozcan, Z., Ozocak, A., Bol, E., ... & Mert, N. (2024). Destructive impact of successive high magnitude earthquakes occurred in Türkiye's Kahramanmaraş on February 6, 2023. *Bulletin of Earthquake Engineering*, 1-27.
- Dieu Tien, B., Shahabi, H., Shirzadi, A., Chapi, K., Alizadeh, M., Chen, W., Mohammadi, A., Bin Ahmad, B., Panahi, M., Hong, H., Tian, Y., 2018: Landslide Detection and Susceptibility Mapping by AIRSAR Data Using Support Vector Machine and Index of Entropy Models in Cameron Highlands, Malaysia. *Remote Sensing* 10 (10) <https://doi.org/10.3390/rs10101527>
- Dou, J., Kuan-Tsung C., Shuisen C., Ali P. Y., Jin-King L., Huan X., Zhu, Z. 2015: Automatic case-based reasoning approach for landslide detection: Integration of object-oriented image analysis and a genetic algorithm. *Remote Sensing* 7, no. 4 (2015): 4318-4342.

- Drusch, M., Del Bello, U., Carlier, S., Colin, O., Fernandez, V., Gascon, F., Marchese & Bargellini, P. (2012). Sentinel-2: ESA's optical high-resolution mission for GMES operational services. *Remote sensing of Environment*, 120, 25-36.
- Duman, T. Y., Emre, Ö. 2013: The East Anatolian Fault: geometry, segmentation and jog characteristics. *Geol Soc* 372:495–529. <https://doi.org/10.1144/SP372.14>
- Durić D, Mladenović A, Pešić-Georgiadis M, Marjanović M, Abolmasov B 2017: Using multiresolution and multitemporal satellite data for post-disaster landslide inventory in the Republic of Serbia. *Landslides* 14:1467-1482. <https://doi.org/10.1007/s10346-017-0847-2>
- Embersson, R., Kirschbaum, D., and Stanley, T.- 2020: New global characterisation of landslide exposure, *Nat. Hazards Earth Syst. Sci.*, 20, 3413–3424, <https://doi.org/10.5194/nhess-20-3413-2020>
- EM-DAT 2023: The International Disaster Database. Centre for Research on the Epidemiology of Disasters. Available at <https://www.emdat.be/>. Accessed 3 March 2024
- Espindola, G.M., Camara, G., Reis, I.A., Bins, L.S., Monteiro, A.M., 2006: Parameter selection for region-growing image segmentation algorithms using spatial autocorrelation. *Int. J. Remote Sens.* 27, 3035–3040.
- European Space Agency, 2020: SAOCOM (SAR Observation and Communications Satellite). <https://directory.eoportal.org/web/eoportal/satellite-missions/s/saocom>
- Fan, J. R., Zhang, X. Y., Su, F. H., Ge, Y. G., Tarolli, P., Yang, Z. Y., Zeng, C., Zeng, Z. 2017: Geometrical feature analysis and disaster assessment of the Xinmo landslide based on remote sensing data. *Journal of Mountain Science*, 14, 9, 1677–1688, doi: 10.1007/s10346-017-0927-3
- Fayne, J. V., Ahamed, A., Roberts-Pierel, J., Rumsey, A., Kirschbaum, D., 2019: Automated Satellite-based Landslide Identification Product for Nepal. *Earth Interactions* Vol 23(3), 1-21
- Fidan, S., Tanyaş, H., Akbaş, A. *et al.* Understanding fatal landslides at global scales: a summary of topographic, climatic, and anthropogenic perspectives. *Nat Hazards* 120, 6437–6455 (2024). <https://doi.org/10.1007/s11069-024-06487-3>
- Fiorucci, F., Ardizzone, F., Mondini, A. C., Viero, A., & Guzzetti, F. 2019: Visual interpretation of stereoscopic NDVI satellite images to map rainfall-induced landslides. *Landslides*, 16, 165-174.
- Foster, C., Pennington, C. V. L., Culshaw, M. G., & Lawrie, K. 2012: The national landslide database of Great Britain: development, evolution and applications. *Environmental earth sciences*, 66, 941-953.
- Froude, M. J., Petley, D. N., 2018: Global fatal landslide occurrence from 2004 to 2016. *Natural Hazards and Earth System Sciences*, 18(8), 2161–2181.
- GADM: GADM maps and data, available at: <https://gadm.org/> last access: 13 October 2024.

- Gariano, S. L., & Guzzetti, F. (2016). Landslides in a changing climate. *Earth-science reviews*, 162, 227-252.
- Gibson, A. D., Culshaw, M. G., Dashwood, C., & Pennington, C. V. L. (2013). Landslide management in the UK—the problem of managing hazards in a ‘low-risk’ environment. *Landslides*, 10, 599-610.
- Gillen, C., 2013: *Geology and Landscapes of Scotland*. Liverpool University Press.
- Giordan, D., Hayakawa, Y., Nex, F., Remondino, F., Tarolli, P., 2018: Review article: the use of remotely piloted aircraft systems (RPASs) for natural hazards monitoring and management. *Nat. Hazards Earth Syst. Sci.* 18, 1079–1096. <https://doi.org/10.5194/nhess-18-1079>
- Goda, K., Kiyota, T., Pokhrel, R. M., Chiaro, G., Katagiri, T., Sharma, K., & Wilkinson, S. (2015). The 2015 Gorkha Nepal earthquake: insights from earthquake damage survey. *Frontiers in Built Environment*, 1, 8.
- Google Earth: available at: <https://earth.google.com/web/> last access: 27 September 2024.
- Google Maps: available at: <https://www.google.co.uk/maps> last access: 15 October 2024.
- Gordon, J.E., Ballantyne, C.K. 2021: Landscapes and Landforms of Scotland: A Geomorphological Odyssey. In: Ballantyne, C.K., Gordon, J.E. (eds) *Landscapes and Landforms of Scotland*. World Geomorphological Landscapes. Springer, Cham. https://doi.org/10.1007/978-3-030-71246-4_1
- Gorelick, N., Hancher, M., Dixon, M., Ilyushchenko, S., Thau, D., & Moore, R. 2017: Google Earth Engine: Planetary-scale geospatial analysis for everyone. *Remote sensing of Environment*, 202, 18-27.
- Guerriero, L., Prinzi, E. P., Calcaterra, D., Ciarcia, S., Di Martire, D., Guadagno, F. M., ... & Revellino, P. (2021). Kinematics and geologic control of the deep-seated landslide affecting the historic center of Buonalbergo, southern Italy. *Geomorphology*, 394, 107961.
- Guha-Sapir, D., Below, R., and Hoyois, P. H.: EM-DAT: International Disaster Database, Université Catholique de Louvain, Brussels, Belgium, available at: <http://www.emdat.be>, last access: 19 December 2024.
- Guzzetti, F., Cardinali, M., & Reichenbach, P. 1996: The influence of structural setting and lithology on landslide type and pattern. *Environmental & Engineering Geoscience*, 2(4), 531-555.
- Guzzetti, F. 2000: Landslide fatalities and the evaluation of landslide risk in Italy. *Engineering geology*, 58(2), 89-107.
- Guzzetti, F., Mondini, A. C., Cardinali, M., Fiorucci, F., Santangelo, M., & Chang, K. T. 2012: Landslide inventory maps: new tools for an old problem. *Earth Sci Rev* 112(1-2):42-66. <https://doi.org/10.1016/j.earscirev.2012.02.001>

- Guzzetti, F., Gariano, S. L., Peruccacci, S., Brunetti, M. T., Marchesini, I., Rossi, M., & Melillo, M. 2020: Geographical landslide early warning systems. *Earth-Science Reviews*, 200, 102973.
- Handwerger, A. L., Huang, M.-H., Jones, S. Y., Amatya, P., Kerner, H. R., Kirschbaum, D. B. 2022: Generating landslide density heatmaps for rapid detection using open-access satellite radar data in Google Earth Engine. *Nat. Hazards Earth Syst. Sci.*, 22, 753–773, <https://doi.org/10.5194/nhess-22-753-2022>
- Harist, M. C., Afif, H. A., Putri, D. N., & Shidiq, I. P. A. (2018). GIS modelling based on slope and morphology for landslide potential area in Wonosobo, Central Java. In *MATEC Web of Conferences* (Vol. 229, p. 03004). EDP Sciences.
- HazMapper online tool. Available at <https://cmscheip.users.earthengine.app/view/hazmapper> last accessed on 15 October 2024
- Herrera, G., Fernandez-Merodo, J., Mulas, J., Pastor, M., Luzi, G., Monserrat, O., 2009: A landslide forecasting model using ground-based SAR data: the Portalet case study. *Engineering Geology* 105, 220–230. <https://doi.org/10.1016/j.enggeo.2009.02.009>
- Highland, L., Bobrowsky, P. 2008: *The Landslide Handbook – A Guide to Understanding Landslides*. US Geological Survey
- Hilton, R. G., Galy, A., and Hovius, N. 2008: Riverine particulate organic carbon from an active mountain belt: Importance of landslides. *Global Biogeochemical Cycles.*, 22, 1–12, <https://doi.org/10.1029/2006GB002905>
- Hölbling, D., Friedl, B., and Eisank, C. 2015: An object-based approach for semi-automated landslide change detection and attribution of changes to landslide classes in northern Taiwan. *Earth Sci. Inform.*, 8, 327–335.
- Hölbling, D., Eisank, C., Albrecht, F., Vecchiotti, F., Friedl, B., Weinke, E., Kociu, A. 2017: Comparing Manual and Semi-Automated Landslide Mapping Based on Optical Satellite Images from Different Sensors. *Geosciences* 2017, 7(2), 37. <https://doi.org/10.3390/geosciences7020037>
- Huang, Q., Wang, C., Meng, Y., Chen, J., and Yue, A. 2020: Landslide Monitoring Using Change Detection in Multitemporal Optical Imagery. *IEEE Geosci. Remote S.*, 17, 312–316, <https://doi.org/10.1109/LGRS.2019.2918254>
- Hungr, O., Leroueil, S., and Picarelli, L. 2014: The Varnes classification of landslide types, an update. *Landslides*, 11, 167–194, <https://doi.org/10.1007/s10346-013-0436-y>
- Iverson, R. M., Reid, M. E., Iverson, N. R., LaHusen, R. G., Logan, M., Mann, J. E., & Brien, D. L. 2000: Acute sensitivity of landslide rates to initial soil porosity. *science*, 290(5491), 513-516.
- Jaafari, A. 2024: An Overview of Triggering and Causing Factors of Landslides. *Landslides in the Himalayan Region: Risk Assessment and Mitigation Strategy for Sustainable Management*, 25-45.

- Kazmi, D., Qasim, S., Harahap, I. S. H., Baharom, S., Imran, M., & Moin, S. 2016: A study on the contributing factors of major landslides in Malaysia. *Civil Engineering Journal*, 2(12), 669-678.
- Keefer, D. K. 1984: Landslides caused by earthquakes, *Geol. Soc. Am. Bull.*, 95, 406–421.
- Keefer, D. K. 2000: Statistical analysis of an earthquake-induced landslide distribution – the 1989 Loma Prieta, California event. *Engineering Geology*, 58, 231–249.
- Keefer, D. K. 2002: Investigating landslides caused by earthquakes—a historical review. *Surveys in geophysics*, 23, 473-510.
- Kirschbaum, D.B.; Adler, R.; Hong, Y.; Hill, S.; Lerner-Lam, A. 2010: A global landslide catalog for hazard applications: method, results, and limitations. *Natural Hazards* 2010, 52, 561–575.
- Kirschbaum, D., Stanley, T., and Zhou, Y. 2015: Spatial and temporal analysis of a global landslide catalog. *Geomorphology*, 249, 4–15, <https://doi.org/10.1016/j.geomorph.2015.03.016>
- Korup, O., Densmore, A. L., Schlunegger, F. 2010: The role of landslides in mountain range evolution. *Geomorphology* 120, 77–90.
- Korup, O., Seidemann, J., & Mohr, C. H. 2019: Increased landslide activity on forested hillslopes following two recent volcanic eruptions in Chile. *Nature Geoscience*, 12(4), 284-289.
- Lacroix, P., Dehecq, A., & Taipei, E. 2020: Irrigation-triggered landslides in a Peruvian desert caused by modern intensive farming. *Nature Geoscience*, 13(1), 56-60.
- Lacroix, P., Gavillon, T., Clément, B., Lavé, J., Jean-Louis, M., Dhungel, S., Vernier, F., 2022: SAR and Optical Images Correlation Illuminates post-seismic Landslide motion after the Mw 7.8 Gorkha earthquake (Nepal). *Scientific reports. Nature* 12:6266
- Lee, S., Chwae, U., & Min, K. 2002: Landslide susceptibility mapping by correlation between topography and geological structure: the Janghung area, Korea. *Geomorphology*, 46(3-4), 149-162.
- Lee, S., Pradhan, B., 2007: Landslide hazard mapping at Selangor, Malaysia using frequency ratio and logistic regression models. *Landslides* 4 (1), 33–41. <https://doi.org/10.1007/s10346-006-0047-y>
- Lenti, L., & Martino, S. 2012: The interaction of seismic waves with step-like slopes and its influence on landslide movements. *Engineering Geology*, 126, 19-36.
- Li, G., West, A. J., Densmore, A. L., Jin, Z., Parker, R. N., and Hilton, R. G. 2014: Seismic Mountain building: Landslides associated with the 2008 Wenchuan earthquake in the context of a generalized model for earthquake volume balance. *Geophysics*, 15, 833–844, 2014.
- Li, Y., Wang, X., & Mao, H. 2020: Influence of human activity on landslide susceptibility development in the Three Gorges area. *Natural Hazards*, 104, 2115-2151.

- Lin Q, Lima P, Steger S, Glade T, Jiang T, Zhang J, Liu T, Wang Y 2021: National-scale data-driven rainfall landslide susceptibility mapping for China by accounting for incomplete landslide data. *Geosci Front* 12:101248. <https://doi.org/10.1016/j.gsf.2021.101248>
- Lindsay, E., Frauenfelder, R., Ruther, D., Nava, L., Rubensdotter, L., Strout, J., Nordal, S. 2022: Multi-temporal satellite image composites in Google Earth Engine for improved landslide visibility: A case study of a Glacial landscape. *Remote Sensing* 2022, 14(10), 2301 <https://doi.org/10.3390/rs14102301>
- Lu, P., Qin, Y., Li, Z., Mondini, A.C., Casagli, N., 2019: Landslide mapping from multi-sensor data through improved change detection-based markov random field. *Remote Sens. Environ.* 231, 111235. <https://doi.org/10.1016/j.rse.2019.111235>
- Lusiana N., Shinohara Y. 2022: The Role of Citrus Groves in Rainfall-Triggered Landslide Hazards in Uwajima. *Japan Water* 14:2113. <https://doi.org/10.3390/w14132113>
- Manconi, A., 2019: Technical note: Limitations on the Use of Space Borne Differential Sar Interferometry for Systematic Monitoring and Failure Forecast of Alpine Landslides. <https://doi.org/10.31223/osf.io/3nmqj>
- Malamud, B., Turcotte, D., Guzzetti, F., Reichenbach, P., 2004: Landslide inventories and their Statistical properties. *Earth Surface Processes and Landforms*. Vol. 29 (6) 687-711
- Martha, T. R., Kerle, N., Jetten, V., van Westen, C. J., Kumar, K. V. 2010: Characterising spectral, spatial and morphometric properties of landslides for semi-automatic detection using object-oriented methods. *Geomorphology*, 116, 24-36, <https://doi.org/10.1016/j.geomorph.2009.10.004>
- Martha, T.R., Kerle, N., van Westen, C.J., Jetten, V., Kumar, K.V., 2012: Object-oriented analysis of multi-temporal panchromatic images for creation of historical landslide inventories. *ISPRS Journal Photogramm. Remote Sens.* 67, 105-119.
- Martha, T.R., Kamala, P., Jose, J., Vinod Kumar, K., Jai Sankar, G., 2016: Identification of new landslides from high resolution satellite data covering a large area using object-based change detection methods. *Indian Society of Remote Sens.* 44, 515-524.
- Matsuura, S., Asano, S., & Okamoto, T. (2008). Relationship between rain and/or meltwater, pore-water pressure and displacement of a reactivated landslide. *Engineering Geology*, 101(1-2), 49-59.
- McKenzie, D. 1972: Active tectonics of the Mediterranean Region. *Geophys J Int* 30:109-185. <https://doi.org/10.1111/j.1365-246X.1972.tb02351.x>
- Meyer, F. J., Ajadi, O. A., Schultz, L., Bell, J., Arnoult, K. M., Gens, R., ... Hogenson, K. 2019: Applications of a SAR-based flood monitoring service during disaster response and recovery. In *IGARSS 2019-2019 IEEE International Geoscience and Remote Sensing Symposium* (pp. 4649-4652). IEEE.
- Milledge, D., Bellugi, D., Watt, J., Densmore, A. 2021: Automated landslide detection outperforms manual mapping for several recent large earthquakes. *Natural Hazards and Earth System Sciences* <https://doi.org/10.5194/nhess-2021-168>

- Mondini, A.C., Guzzetti, F., Reichenbach, P., Rossi, M., Cardinali, M., Ardizzone, F., 2011: Semi-automatic recognition and mapping of rainfall induced shallow landslides using optical satellite images. *Remote Sens. Environ.* 115, 1743–1757.
- Mondini, A.C., Chang, K.-T., Chiang, S.-H., Schlögel, R., Notarnicola, C., Saito, H., 2017: Automatic mapping of event landslides at basin scale in Taiwan using a Montecarlo approach and synthetic land cover fingerprints. *Int. J. Appl. Earth Obs. Geoinf.* 63, 112–121.
- Mondini, C., Guzzetti, F., Chang, K., Monserrat, O., Tapas, R., Manconi, A., 2021: Landslide failures detection and mapping using Synthetic Aperture Radar: Past, present and future. *Earth-Science Reviews* 216 (2021) 103574
- Mondini, A. C., Guzzetti, F., & Melillo, M. 2023: Deep learning forecast of rainfall-induced shallow landslides. *Nature communications*, 14(1), 2466.
- Moreiras, S. M. 2005: Climatic effect of ENSO associated with landslide occurrence in the Central Andes, Mendoza Province, Argentina. *Landslides*, 2, 53–59, <https://doi.org/10.1007/s10346-005-0046-4>
- Moreiras, S., Lisboa, M. S., & Mastrantonio, L. 2012: The role of snow melting upon landslides in the central Argentinean Andes. *Earth Surface Processes and Landforms*, 37(10), 1106–1119.
- Moretto, S., Bozzano, F., & Mazzanti, P. 2021: The role of satellite InSAR for landslide forecasting: Limitations and openings. *Remote sensing*, 13(18), 3735.
- Mugagga, F., Kakembo, V., & Buyinza, M. 2012: A characterisation of the physical properties of soil and the implications for landslide occurrence on the slopes of Mount Elgon, Eastern Uganda. *Natural hazards*, 60, 1113–1131.
- Nettleton I. M., Martin S., Hencher S., Moore R. 2004: Debris flow types and mechanisms. In: Winter MG, Macgregor F, Shackman L (eds) Scottish road network landslide study, pp 45–119
- Nichol, J., Wong, M.S., 2005: Satellite remote sensing for detailed landslide inventories using change detection and image fusion. *Int. J. Remote Sens.* 26, 1913–1926.
- Notti, D., Cignetti, M., Godone, D., Giordan, D. 2023: Semi-automatic mapping of shallow landslides using free Sentinel-2 images and Google Earth Engine. *Nat. Hazards Earth Syst. Sci.*, 23, 2625–2648, <https://doi.org/10.5194/nhess-23-2625-2023>
- Nourani, V., Pradhan, B., Ghaffari, H., and Sharifi, S. S. 2014: Landslide susceptibility mapping at Zonouz Plain, Iran using genetic programming and comparison with frequency ratio, logistic regression and artificial neural network models. *Natural Hazards*, 71, 523–547, doi:10.1007/s11069-013-0932-3
- Novellino, A., Pennington, C., Leeming, K., Taylor, S., Alvarez, I. G., McAllister, E., Arnhardt, C., & Winson, A. (2024). Mapping landslides from space: A review. *Landslides*, 1-12.

- Nowak, B., Marliac, G., Michaud, A. 2021: Estimation of winter soil cover by vegetation before spring-sown crops for mainland France using multispectral satellite imagery. *Environ. Res. Lett.*, 16, 064024, <https://doi.org/10.1088/1748-9326/ac007c>
- Nugroho, F., Danoedoro, P., Arjasakusuma, S., Candra, D. S., Bayanuddin, A., Samodra, G. 2021: Assessment of Sentinel-1 and Sentinel-2 Data for Landslides Identification using Google Earth Engine. *7th Asia-Pacific Conference on Synthetic Aperture Radar (APSAR)*. IEEE, 2021
- Ohlmacher, G. C. 2000: The relationship between geology and landslide hazards of Atchison, Kansas, and vicinity. *Current Research in Earth Sciences*, 1-16.
- Page, R. 1968: Aftershocks and microaftershocks of the great Alaska earthquake of 1964. *Bulletin of the Seismological Society of America*, 58(3), 1131-1168.
- Palamakumbura, R., Finlayson, A., Ciurean, R., Nedumpallile-Vasu, N., Freeborough, K., & Dashwood, C. 2021: Geological and geomorphological influences on a recent debris flow event in the Ice-scoured Mountain Quaternary domain, western Scotland. *Proceedings of the Geologists' Association*, 132(4), 456-468.
- Parise, M. 2001: Landslide hazard zonation of slopes susceptible to rock falls and topples. *Natural Hazards and Earth System Sciences* (2002) 2: 37-49
- Pepe, G., Mandarino, A., Raso, E., Cevasco, A., Firpo, M., Casagli, N. 2019: Extreme Flood and Landslides Triggered in the Arroscia Valley (Liguria Region, Northwestern Italy) During the November 2016 Rainfall Event, in: vol. 1, IAEG/AEG Annual Meeting Proceedings, 17–21 September 2018, San Francisco, California, 171–175, ISBN 978-3-319-93124-1, https://doi.org/10.1007/978-3-319-93124-1_21
- Petley, D. 2012: Global patterns of loss of life from landslides. *Geology*, 40, 927–930, <https://doi.org/10.1130/G33217.1>
- Petley, D. N., Hearn, G. J., Hart, A., Rosser, N. J., Dunning, S. A., Owen, K., and Mitchell, W. A. 2007: Trends in landslide occurrence in Nepal. *Natural Hazards*, 43, 23–44, <https://doi.org/10.1007/s11069-006-9100-3>
- Pistolesi, M., Bertagnini, A., Di Roberto, A., Ripepe, M., & Rosi, M. 2020: Tsunami and tephra deposits record interactions between past eruptive activity and landslides at Stromboli volcano, Italy. *Geology*, 48(5), 436-440.
- Pirasteh, S., & Li, J. (2016). Landslides investigations from geoinformatics perspective: quality, challenges, and recommendations. *Geomatics, Natural Hazards and Risk*, 8(2), 448–465. <https://doi.org/10.1080/19475705.2016.1238850>
- Plafker, G. 1965: Tectonic Deformation Associated with the 1964 Alaska Earthquake: The earthquake of 27 March 1964 resulted in observable crustal deformation of unprecedented areal extent. *Science*, 148(3678), 1675-1687.
- Polemio, M., & Petrucci, O. 2000: Rainfall as a landslide triggering factor an overview of recent international research. *Landslides in research, theory and practice*.

- Pradhan, B., Lee, S. 2007: Utilization of Optical Remote Sensing Data and GIS Tools for Regional Landslide Hazard Analysis Using an Artificial Neural Network Model. *Earth Science Frontiers*, Vol. 14, Issue 6, pp143-151, [https://doi.org/10.1016/S1872-5791\(08\)60008-1](https://doi.org/10.1016/S1872-5791(08)60008-1)
- Prakash N, Manconi A, Loew S. 2020: Mapping landslides on EO data: performance of deep learning models vs. traditional machine learning models. *Remote Sens* 12(3):346. <https://doi.org/10.3390/rs12030346>
- Psomiadis E, Papazachariou A, Soulis KX, Alexiou DS, Charalampopoulos, I. 2020: Landslide mapping and susceptibility assessment using geospatial analysis and earth observation data. *Land* 9(5):133. <https://doi.org/10.3390/land9050133>
- Rau, J. Y., Jhan, J. P., Rau, R. J., 2014: Semiautomatic object-oriented landslide recognition scheme from multisensor optical imagery and DEM. *IEEE Trans. Geosci. Remote Sens.* 52, 1336–1349.
- Roback, K., Clark, M. K., West, A. J., Zekkos, D., Li, G., Gallen, S. F., Chamlagain, D., Godt, J. W. 2018: The size, distribution, and mobility of landslides caused by the 2015 *Mw* 7.8 Gorkha earthquake, Nepal, *Geomorphology*, 301, 121–138, 2018.
- Robinson, T. R., Rosser, N., Walters, R. J. 2019: The Spatial and Temporal Influence of Cloud Cover on Satellite-Based Emergency Mapping of Earthquake Disasters. *Sci. Rep.*, vol. 9, no. 1, p. 12455, Dec. 2019, doi: 10.1038/s41598-019-49008-0
- Rodriguez, K.M., Weissel, J.K., Kim, Y., 2002: Classification of landslide surfaces using fully polarimetric SAR: examples from Taiwan. In: *IEEE International Geoscience and Remote Sensing Symposium*, 5, pp. 2918–2920. <https://doi.org/10.1109/IGARSS.2002.1026821>
- Rosly, M. H., Mohamad, H. M., Bolong, N., & Harith, N. S. H. 2022: An overview: relationship of geological condition and rainfall with landslide events at East Malaysia. *Trends in Sciences*, 19(8), 3464-3464.
- Roush, A. G. 2024: *Continuous Monitoring of High Risk Disaster Areas by Applying Change Detection to Free Satellite Imagery* (Doctoral dissertation, Virginia Tech).
- Salmi, E. F., Nazem, M., & Karakus, M. 2017: Numerical analysis of a large landslide induced by coal mining subsidence. *Engineering Geology*, 217, 141-152.
- Samia, J., Temme, A., Bregt, A., Wallinga, J., Guzzetti, F., Ardizzone, F., Rossi, M. 2017: Do landslides follow landslides? Insights in path dependency from a multi-temporal landslide inventory. *Landslides* 2017) 14:547–558 DOI 10.1007/s10346-016-0739-x
- Santangelo, M., Cardinali, M., Rossi, M., Mondini, A. C., and Guzzetti, F. 2010: Remote landslide mapping using a laser rangefinder binocular and GPS, *Nat. Hazards Earth Syst. Sci.*, 10, 2539–2546, <https://doi.org/10.5194/nhess-10-2539-2010>
- Scaioni, M.; Longoni, L.; Melillo, V.; Papini, M. 2014: Remote Sensing for Landslide Investigations: An Overview of Recent Achievements and Perspectives. *Remote Sens.* 2014, 6, 9600–9652.

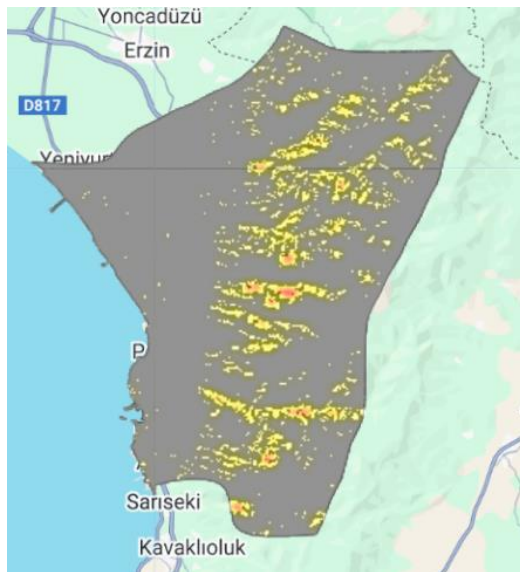
- Scheip, C.M., Wegmann, K.W. 2021: HazMapper: A global open-source natural hazard mapping application in Google Earth Engine. *Nat. Hazards Earth Syst. Sci.* 2021, 21, 1495–1511.
- Schlogl M., Gutjahr K., & Fuchs, S. 2022: The challenge to use multi-temporal InSAR for landslide early warning. *Nat Hazards* 1-7. <https://doi.org/10.1007/s11069-022-05289-9>
- Şengör A. M. C., & Yilmaz Y. 1981: Tethyan evolution of Turkey: a plate tectonic approach. *Tectonophysics* 75:181–241. [https://doi.org/10.1016/0040-1951\(81\)90275-4](https://doi.org/10.1016/0040-1951(81)90275-4)
- Shano, L., Gisila, B., Jerene, W., Ekaso, D., Baye, T., Degife, T., Chameno, G., Dosa, Z., Jothimani, M. 2024: Fatal landslides in Kencho, Shacha & Gozdi villages, Gofa zone, Ethiopia: A detailed investigation (Geological, Geotechnical, geophysical & geospatial) of the July 22, 2024 catastrophe and its socioeconomic repercussions. *Quaternary Science Advances* 16 (2024) 100241 <https://doi.org/10.1016/j.qsa.2024.100241>
- Sim, J., & Wright, C. C. 2005: The kappa statistic in reliability studies: use, interpretation, and sample size requirements. *Physical therapy*, 85(3), 257-268.
- Sim, K.B., Lee, M.L., Wong, S.Y., 2022: A review of landslide acceptable risk and tolerable risk. *Geoenvironmental Disasters* 9, 3. <https://doi.org/10.1186/s40677-022-00205-6>.
- Sparkes, B., Dunning, S., Lim, M., & Winter, M. G. 2017: Characterisation of recent debris flow activity at the Rest and be Thankful, Scotland. In *Advancing Culture of Living with Landslides: Volume 5 Landslides in Different Environments* (pp. 51-58). Springer International Publishing.
- Spiker, E. C. and Gori, P. 2003: National landslide hazards mitigation strategy, a framework for loss reduction, 1244, US Geological Survey
- Stead, D. 2015: The influence of shales on slope instability. In *ISRM Congress* (pp. ISRM-13CONGRESS). ISRM.
- Stead, D., & Wolter, A. 2015: A critical review of rock slope failure mechanisms: The importance of structural geology. *Journal of Structural Geology*, 74, 1-23.
- Stumpf, A., Kerle, N., 2011: Object-oriented mapping of landslides using random forests. *Remote Sens. Environ.* 115, 2564–2577.
- Stumpf, A. 2013: Landslide recognition and monitoring with remotely sensed data from passive optical sensors. PhD Thesis submitted to the University of Strasbourg, France
- Sun, W., Tian, Y., Mu, X., Zhai, J., Gao, P., Zhao, G., 2017: Loess landslide inventory map based on GF-1 satellite imagery. *Remote Sens.* 9, 314.
- Sun, L., Ma, B., Pei, L., Zhang, X., & Zhou, J. L. 2021: The relationship of human activities and rainfall-induced landslide and debris flow hazards in Central China. *Natural hazards*, 107, 147-169.
- Sunbul, F., Haner, B., Mungan, H., Akarsu, V., Sunbul Guner, A. B., & Temiz, C. 2021: Stability analysis of a landslide: a view with implications of microstructural soil characters. *Indian Geotechnical Journal*, 51, 647-660.

- Tan O, Pabuçcu Z, Tapırdamaz MC et al 2011: Aftershock study and seismotectonic implications of the 8 March 2010 Kovancılar (Elazığ, Turkey) earthquake (mw=6.1). *Geophys Res Lett* 38: L11304. [https:// doi.org/10.1029/2011GL047702](https://doi.org/10.1029/2011GL047702)
- Temme, A. J. 2021: Relations between soil development and landslides. *Hydrogeology, chemical weathering, and soil formation*, 177-185.
- Travelletti, J., Delacourt, C., Allemand, P., Malet, J. P., Schmittbuhl, J., Toussaint, R., & Bastard, M. 2012: Correlation of multi-temporal ground-based optical images for landslide monitoring: Application, potential and limitations. *ISPRS Journal of Photogrammetry and Remote Sensing*, 70, 39-55.
- Tsai, F., Hwang, J.-H., Chen, L.-C., Lin, T.-H. 2010: Post-disaster assessment of landslides in southern Taiwan after 2009 Typhoon Morakot using remote sensing and spatial analysis. *Nat. Hazards Earth Syst. Sci.*, 10, 2179–2190, <https://doi.org/10.5194/nhess10-2179-2010>
- Turel, M., & Frost, J. D. 2011: Delineation of slope profiles from digital elevation models for landslide hazard analysis. In *Geo-Risk 2011: Risk Assessment and Management* (pp. 829-836).
- Türkmen G., Ertürk A., & Türkman M. 1974: Dörtüol and Erzin plain hydrogeological investigation report. Report No. 1904/6. Devlet Su İşleri
- UNESCO 1973: Annual summary of information on natural disasters, no. 6: 1971, United Nations Educational, Scientific and Cultural Organization, Paris, France, pp. 82
- Vasantha Kumar, S., & Bhagavanulu, D. V. S. 2008: Effect of deforestation on landslides in Nilgiris district—A case study. *Journal of the Indian Society of Remote Sensing*, 36, 105-108.
- Wang, J. J., Liang, Y., Zhang, H. P., Wu, Y., & Lin, X. 2014: A loess landslide induced by excavation and rainfall. *Landslides*, 11, 141-152.
- Wang, F., Fan, X., Yunus, A.P. et al. Coseismic landslides triggered by the 2018 Hokkaido, Japan (M_w 6.6), earthquake: spatial distribution, controlling factors, and possible failure mechanism. *Landslides* 16, 1551–1566 2019: <https://doi.org/10.1007/s10346-019-01187-7>
- Wang, K., Xu, H., Zhang, S., Wei, F., & Xie, W. 2020: Identification and extraction of geomorphological features of landslides using slope units for landslide analysis. *ISPRS International Journal of Geo-Information*, 9(4), 274.
- Warburton, J., Milledge, D. G., Johnson, R. 2008: Assessment of shallow landslide activity following the January 2005 storm, Northern Cumbria, Cumberland. *Geological Society proceedings*, 7, 263–283
- Whiteley, J. S., Chambers, J. E., Uhlemann, S., Wilkinson, P. B., & Kendall, J. M. (2019). Geophysical monitoring of moisture-induced landslides: A review. *Reviews of Geophysics*, 57(1), 106-145.

- Wicki, A., Lehmann, P., Hauck, C., Seneviratne, S. I., Waldner, P., & Stähli, M. (2020). Assessing the potential of soil moisture measurements for regional landslide early warning. *Landslides*, 17, 1881-1896.
- Winter, M.G., Heald, A.P., Parsons, J.A., Macgregor F., Shackman, L. 2006: Scottish debris flow events of August 2004. *Quarterly Journal of Engineering Geology & Hydrogeology* 39(1), 73-78.
- Winter, M.G., McInnes, R.G., Bromhead, E.N. 2008: Landslide risk management in the United Kingdom. *Proceedings, 2007 International Forum on Landslide Disaster Management* (Eds: Ho, K., Li, V.), Volume I, 343-374. The Hong Kong Institution of Engineers, Hong Kong.
- Winter, M. G., Waaser, T., & Fiddes, G. 2024: The A83 Loch Shira landslide, Scotland. In *Geotechnical Engineering Challenges to Meet Current and Emerging Needs of Society* (pp. 1398-1401). CRC Press.
- Xie, J., Uchimura, T., Wang, G., Selvarajah, H., Maqsood, Z., Shen, Q., Mei, G., Qiao, S. 2020: Predicting the sliding behavior of rotational landslides based on the tilting measurement of the slope surface. *Engineering Geology*, Vol. 269, 105554, <https://doi.org/10.1016/j.enggeo.2020.105554>
- Yalcin, A. 2007: The effects of clay on landslides: A case study. *Applied Clay Science*, 38(1-2), 77-85.
- Yang, W., Wang, M., and Shi, P. 2013: Using MODIS NDVI time series to identify geographic patterns of landslides in vegetated regions. *IEEE Geosci. Remote. S*, 10, 707–710, <https://doi.org/10.1109/LGRS.2012.2219576>
- Zhang, C., Yin, Y., Dai, Z., Huang, B., Zhang, Z., Jiang, X., & Wang, L. 2021. Reactivation mechanism of a large-scale ancient landslide. *Landslides*, 18, 397-407.
- Zhang, C., Yin, Y., Yan, H., Li, H., Dai, Z., & Zhang, N. 2021: Reactivation characteristics and hydrological inducing factors of a massive ancient landslide in the three Gorges Reservoir, China. *Engineering Geology*, 292, 106273.
- Zhang, Y., Ren, S., Liu, X., Guo, C., Li, J., Bi, J., & Ran, L. 2023: Reactivation mechanism of old landslide triggered by coupling of fault creep and water infiltration: A case study from the east Tibetan Plateau. *Bulletin of Engineering Geology and the Environment*, 82(8), 291.
- Zhang, Z., Liu, M., Tan, Y. J., Walter, F., He, S., Chmiel, M., Su, J. 2024: Landslide hazard cascades can trigger earthquakes. *Nature Communications* (2024) 15:2878 <https://doi.org/10.1038/s41467-024-47130-w>
- Zhong, C., Liu, Y., Gao, P., Chen, W., Li, H., Hou, Y., Nuremanguli, T., Ma, H. 2019: Landslide mapping with remote sensing: challenges and opportunities. *International Journal of Remote Sensing* vol. 41, 2020 issue 4 pp. 1555-1581
- Zhong, C., Liu, Y., Gao, P., Chen, W., Li, H., Hou, Y., ... & Ma, H. 2020: Landslide mapping with remote sensing: challenges and opportunities. *International Journal of Remote Sensing*, 41(4), 1555-1581.

- Zhu, Z., Yuan, X., Gan, S., Zhang, J., Zhang, X. 2023: A Research on a new mapping method for landslide susceptibility based on SBAS-InSAR technology. *The Egyptian Journal of Remote Sensing and Space Sciences* 26 (2023) 1046-1056
<https://doi.org/10.1016/j.ejrs.2023.11.009>
- Zhuang, J., Peng, J., Xu, Y., Xu, Q., Zhu, X., & Li, W. 2016: Assessment and mapping of slope stability based on slope units: A case study in Yan'an, China. *Journal of Earth System Science*, 125(7), 1439-1450.

Appendix I - Screenshot anomalous layer of Dortyol showing landslides.



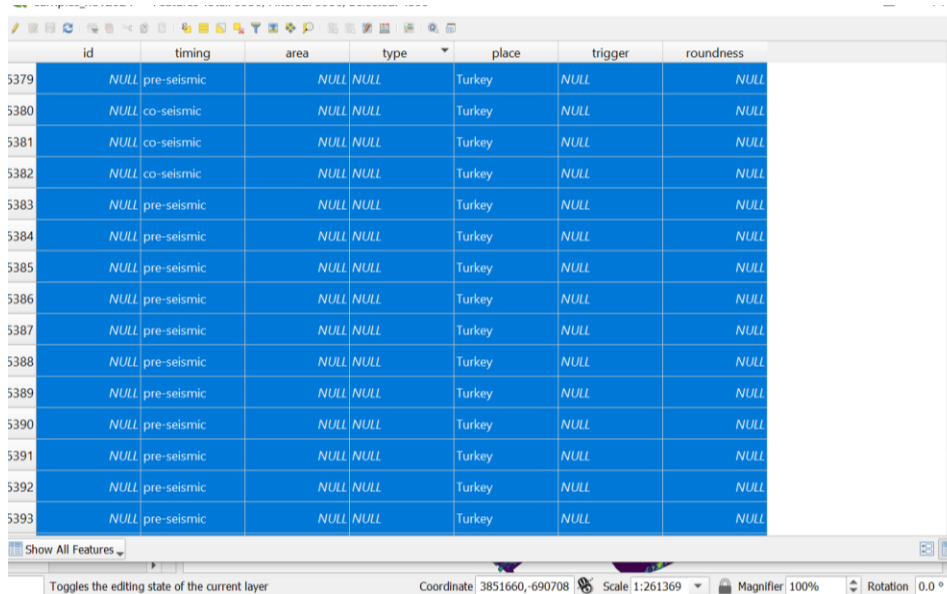
This anomalous layer of Dörtöyl generated using the GEE code shows the occurrence of landslides on the East of Dörtöyl where elevation is greater than 80m above sea level, compared to the West, along the coast with lower elevation.

Appendix II – Satellite imagery from Copernicus



Screenshot of satellite imagery for Glengyle downloaded from Copernicus website used in the manual mapping of landslides in the study location.

Appendix III - Screenshot of Dortyol landslide inventory



id	timing	area	type	place	trigger	roundness
5379	NULL pre-seismic	NULL	NULL	Turkey	NULL	NULL
5380	NULL co-seismic	NULL	NULL	Turkey	NULL	NULL
5381	NULL co-seismic	NULL	NULL	Turkey	NULL	NULL
5382	NULL co-seismic	NULL	NULL	Turkey	NULL	NULL
5383	NULL pre-seismic	NULL	NULL	Turkey	NULL	NULL
5384	NULL pre-seismic	NULL	NULL	Turkey	NULL	NULL
5385	NULL pre-seismic	NULL	NULL	Turkey	NULL	NULL
5386	NULL pre-seismic	NULL	NULL	Turkey	NULL	NULL
5387	NULL pre-seismic	NULL	NULL	Turkey	NULL	NULL
5388	NULL pre-seismic	NULL	NULL	Turkey	NULL	NULL
5389	NULL pre-seismic	NULL	NULL	Turkey	NULL	NULL
5390	NULL pre-seismic	NULL	NULL	Turkey	NULL	NULL
5391	NULL pre-seismic	NULL	NULL	Turkey	NULL	NULL
5392	NULL pre-seismic	NULL	NULL	Turkey	NULL	NULL
5393	NULL pre-seismic	NULL	NULL	Turkey	NULL	NULL

Screenshot of Dörtöyl landslide inventory in QGIS showing landslide types classified as only pre- and co-seismic landslides. This minimal classification limited the further analysis in this area to assess the performance of the optimal method in identifying each specific type of landslide in this location. Hence, the generalisation of the methods performance in identifying landslides prevalent in this location.

Appendix IV – Satellite imagery for Rest and Be Thankful



The satellite imagery from Copernicus website showing actual landslides in Rest and Be Thankful, confirming GEE's efficiency in identifying more landslides in the area more than BGS manually mapped landslides based on reported cases.